To the Graduate Council:

I am submitting herewith a dissertation written by Yan-Ming Zheng entitled "A Numerical Study of Strongly Nonlinear Baroclinic Instability." I have examined the final copy of this dissertation for form and content and recommend that it be accepted in partial fulfillment of the requirements for the degree of Doctor of Philosophy with a major in Aerospace Engineering.

Basil N. Antar

Basil N. Antar, Major Professor

We have read this dissertation
and recommend its acceptance:

Frank G. Collins

K R Kimble

Accepted for the Council:

Vice Provost
and Dean of the Graduate School

A NUMERICAL STUDY OF

STRONGLY NONLINEAR BAROCLINIC INSTABILITY

A Dissertation

Presented for the

Doctor of Philosophy

Degree

The University of Tennessee, Knoxville

Yan-Ming Zheng

August 1990

ACKNOWLEDGMENTS

The author gratefully acknowledges the help, encouragement and guidance she received over the years from Dr. B. N. Antar, supervisor and chairman of the doctoral committee. The author expresses his gratitude for the help and advice received from the other members of the committee, Drs. T.H. Moulden, K. Kimble, F. Collins, and J. M. Wu.

Sincere thanks are also expressed to the UTSI administration for their financial support and for permission to use the computer facilities and to the UTSI library personnel of their help towards finding numerous technical literature.

Thanks are extended to the author's son, Jack P. Mo, his birth and growth is a great encouragement.

Special thanks also goes to the author's husband, Dr. J. D. Mo, for his constant support, encouragement and great sacrifices throughout this effort.

ABSTRACT

Inviscid and viscous stability analysis has been conducted numerically for the strongly nonlinear baroclinic flow in an annulus. An Eady model, modified by two Ekman layers of different strengths, is employed and by using a truncated spectral expansion, the model is reduced to a nonlinear automomous system of equations which describes the dynamics of several zonal wave number disturbances with its lower two meridional y-modes, and of the mean flow correction with its lowest four meridional y-modes. Each y-mode consists of a baroclinic and a barotropic pattern.

Linear instability of the flow in the annulus is discussed for the stratification parameter S and dissipation δ. In the strongly unstable inviscid case, for different initial perturbation, the wave goes through an amplitude vacillation cycle for different time length, and finally, develops into irregular motion. In the viscous nonlinear analysis, axisymmetric flow, traveling steady waves and amplitude vacillation are found in the model. The difference between the solutions of several zonal wave number and that of single zonal wave number are checked. With S decreasing, i.e., radial temperature difference decreases if the rotation rate is fixed, the zonal wave number transition occurs, and this transition phenomena does not depend on the initial perturbation but is determined by the characteristics of the flow. The meridional mode number transition occurs while the supercriticality increases. The higher Ekman dissipation damps the flow faster than that of the lower one. The large dissipation damps the disturbance more effectively than the larger stratification does.

The comparison of the present numerical results with experiments and existing analytical result shows good agreement.

TABLE OF CONTENTS

LIST OF FIGURES

LIST OF SYMBOLS

a	annulus inner radius
b	annulus outer radius
C_p	specific heat at constant pressure
d	annulus height
D	dissipative energy by viscosity
e	internal energy
E	Ekman number
$\vec{f_b}$	body force
$\vec{f_f}$	frictional force
g	gravitational acceleration
h	step length
k	thermal conductivity
L	horizontal scale of motion
N	Brunt-Vaisala frequency
p	static pressure
p_s, ρ_s, T_s	basic pressure, density and temperature
Q	rate of heat addition fer unit mass
R	gas constant.
R_{OT}	thermal Rossby number
r, θ, ϕ	spherical coordinate
S	stratification parameter
t	time
t_b	time at which the irregular solution starts
T	static temperature

$\vec{v}$	velocity vector.
x, y, z	Cartisian coordinates
ν	kinematic viscosity
ρ	fluid density
γ	asymmetry parameter between the upper and lower Ekman layers.
δ	Ekman layer dissipation parameter
Φ	Perturbation stream function
ψ	stream function
ζ_o	vorticity
Ω	rotating rate of annulus.
∇	nabla operator
σ	Prandtl number
α	thermal expansion coefficient
$\top$	Taylor number
ϵ	truncation error
	<u>Subscripts</u>
k, l	index for zonal wave number and meridional mode number

CHAPTER I

INTRODUCTION

§1.1 Technical Background

In an attempt to understand the general circulation of the atmosphere and the origin of the earth's magnetic field, a series of experiments[1−5] have been performed in the past. Basically, there were two kind of experimental settings in use. Either a "dishpan" or an annulus was filled with fluid and mounted on a rotating table. The dishpan was differentially heated at the bottom in an axially symmetric manner, whereas the differential heating of the annulus was achieved by holding the vertical walls at different uniform temperatures, the outer wall normally being warmer than the inner one. The experiments made with the annulus proved to be easier to control and to reproduce. As shown in Figure 1-1, an incompressible, viscous, heat-conducting fluid was filled in the annulus of rectangular cross section with a rigid upper lid. The annulus was constrained to rotate about a vertical axis at a constant angular velocity. The rotation vector coincides with the axis of the annulus and is opposite to the direction of the gravitational acceleration. The annulus represents a hemisphere of the earth, the fluid represents the atmosphere, and the motion of the fluid is intended to represent the atmospheric circulation. The characteristics of the observed flow in the annulus[5] depend mainly on the dimensionless parameters, R_{OT} and T, where R_{OT} is a measure of the impressed horizontal temperature contrast and T is a measure of the fluid viscosity.

These two principal dimensionless parameters are known as the thermal Rossby number and the Taylor number. They are defined by

$$R_{OT} = \frac{\alpha g d \Delta \mathsf{T}}{\Omega^2 (b-a)^2}$$

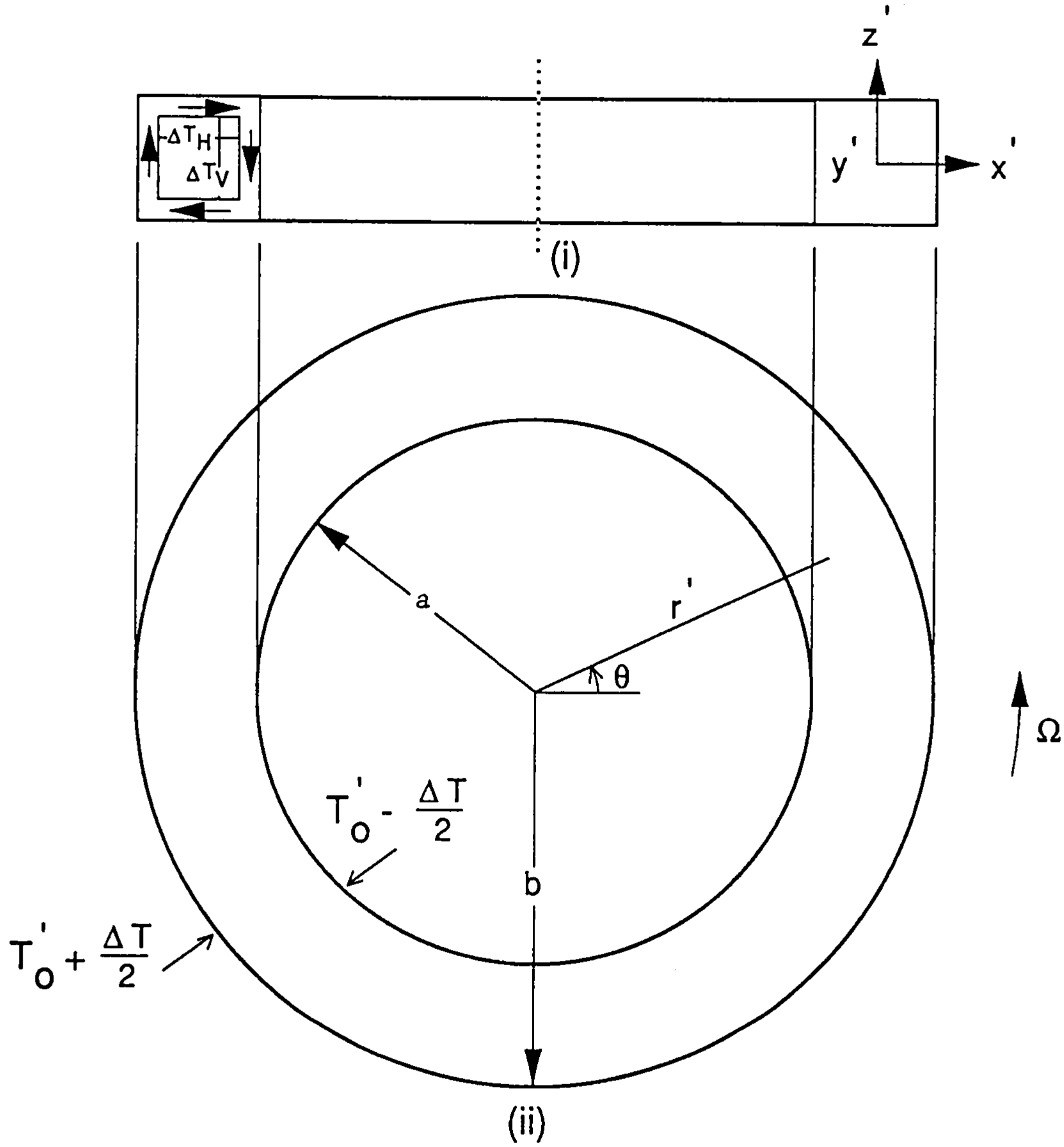

Fig. 1-1. Schematic of annulus test model

$$\mathsf{T} = \frac{4\Omega^2(b-a)^5}{\nu^2 d}$$

where b, a, and d are the outer radius, inner radius and depth of the annulus, respectively, α is the thermal expansion coefficient, $\Delta\mathsf{T}$ is the impressed temperature difference between outer and inner walls, and ν is the kinematic viscosity, g is the gravitational acceleration, and Ω is the rotation rate.

Experimentally, it was found that there is a value of the Taylor number, T namely the critical Taylor number, T^*, below which axisymmetric zonal flow arises irrespective of the value of Rossby number, R_{OT}. However, when $\mathsf{T} > \mathsf{T}^*$, axisymmetric flow occurs only at sufficiently high values of R_{OT}, namely $R_{OT} > R^*_{OT}$, i.e. in the upper axisymmetric regime. In this regime, the axisymmetric flow is stable because of the high static stability set up by the convective motion. At sufficiently low values of R_{OT}, namely $R_{OT} < R^{**}_{OT}$, i.e. in the lower symmetric regime. In this region, the flow is stable because of viscosity and conductive dissipation. R^*_{OT} and R^{**}_{OT} depend on T and also on the Prandtl number, σ. Within the range $R^{**}_{OT} < R_{OT} < R^*_{OT}$, the flow is nonaxisymmetric. Three regimes of nonaxisymmetric flow have been identified. They are: a. The flow pattern has the form of steady horizontal waves. These waves drift slowly, and with very uniform angular velocity, relative to the rotating apparatus; b. the flow is irregular in the sense that although vestiges of a wave-like pattern are present, rapid and complicated fluctuations occur; c. "vacillation" has properties somewhat intermediate between those of the steady wave regime and the irregular regime, and in its most pronounced form represents a transitional phenomenon between the other two regimes. This last region is referred to as vacillation in the sense of implying regular fluctuation. Vacillation observed in annulus experiments has been divided into three categories[6-9]: amplitude vacillation, structural (or tilted-trough) vacillation, and wave number vacillation. These vacillations are characterized by periodic variation in wave amplitude, in wave structure and in the dominant zonal wavenumber, respectively. The characteristics of some of these flow regimes as well as their location in the R_{OT}, T plane are shown in Figure 1-2 and Figure 1-3, respectively.

There are a number of atmospheric features which are observed in the middle and high altitudes on daily weather maps or in the data pertaining to these atmospheric regions. The simplest one is the presence of a quasi-axisymmetric zonal flow, the prevailing westerlies. This flow contains cyclones and planetary waves which alter its zonal symmetry. Another important feature of atmospheric dynamics of the middle and high latitudes is the presence of quasi-periodic fluctuations in the quantities which describe these flows. For example, the data analyzed by Webster and Keller [12] showed a fairly regular variation, with a 20 day period, in the ratio of eddy to zonal kinetic energy at 200mb and over a mid-latitude belt in the southern Hemisphere. This regular fluctuation, called vacillation, is sometimes characterized by quasi-periodic variations in wave shape, with troughs titillating from the North-East to the South-West or from the North-west to the South-East, or by the meridional distribution of the wave energy which may result in a situation of blocking the high or polar vortex. For example, Van Loon et al.[13] found oscillations which were out of phase between the middle and the high latitudes in the winter stratosphere indicating that appreciable fluctuations in the meridional energy distribution existed.

Comparing vacillations in the atmosphere and in the annulus experiments, it can be seen that the vacillation in the atmosphere seems to be a mixture of amplitude vacillation and structural vacillation, in which amplitude vacillation is characterized by large periodic growth and decay of wave energy. On the other

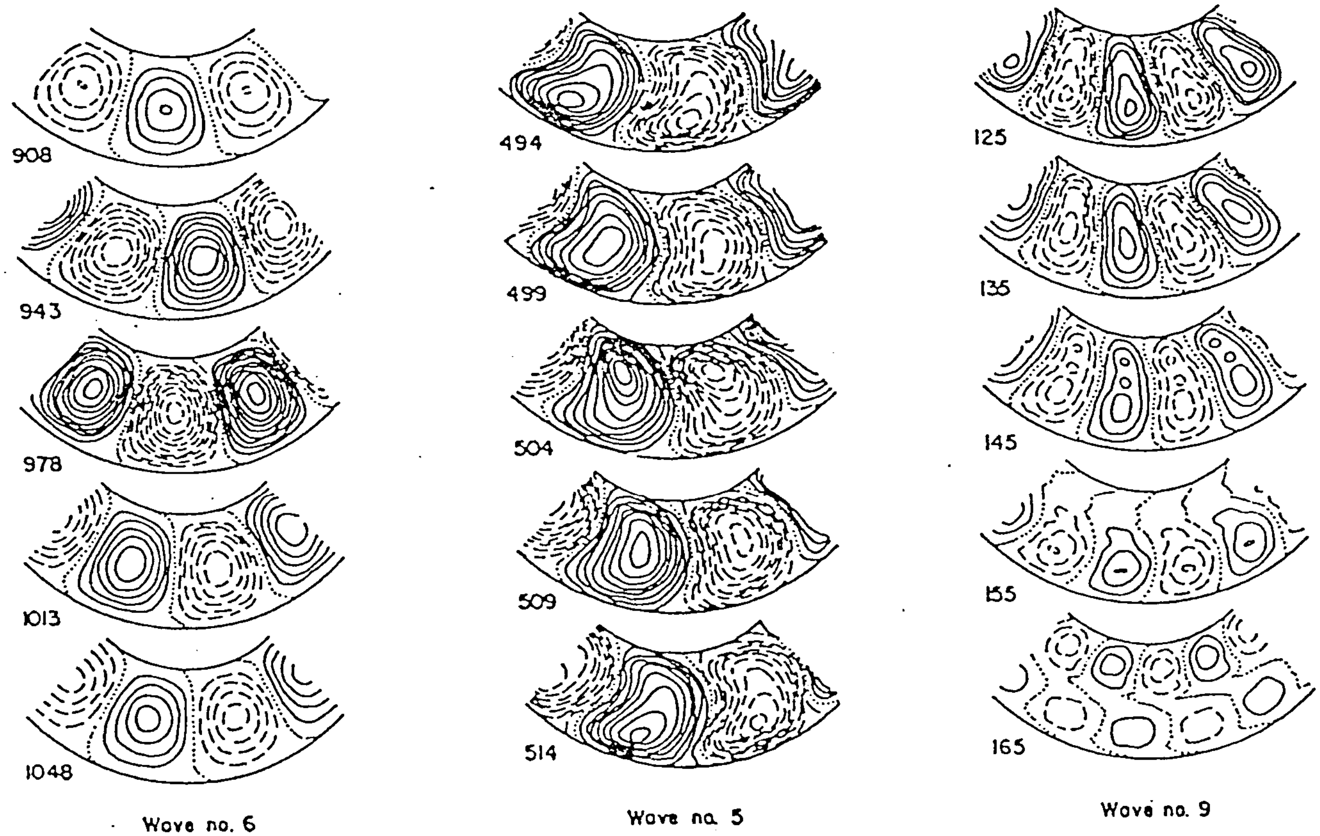

(a) amplitude vacillation (b) structural vacillation (c) geostrophic turbulence

Fig. 1-2. Sequences of synoptic temperature patterns[10]

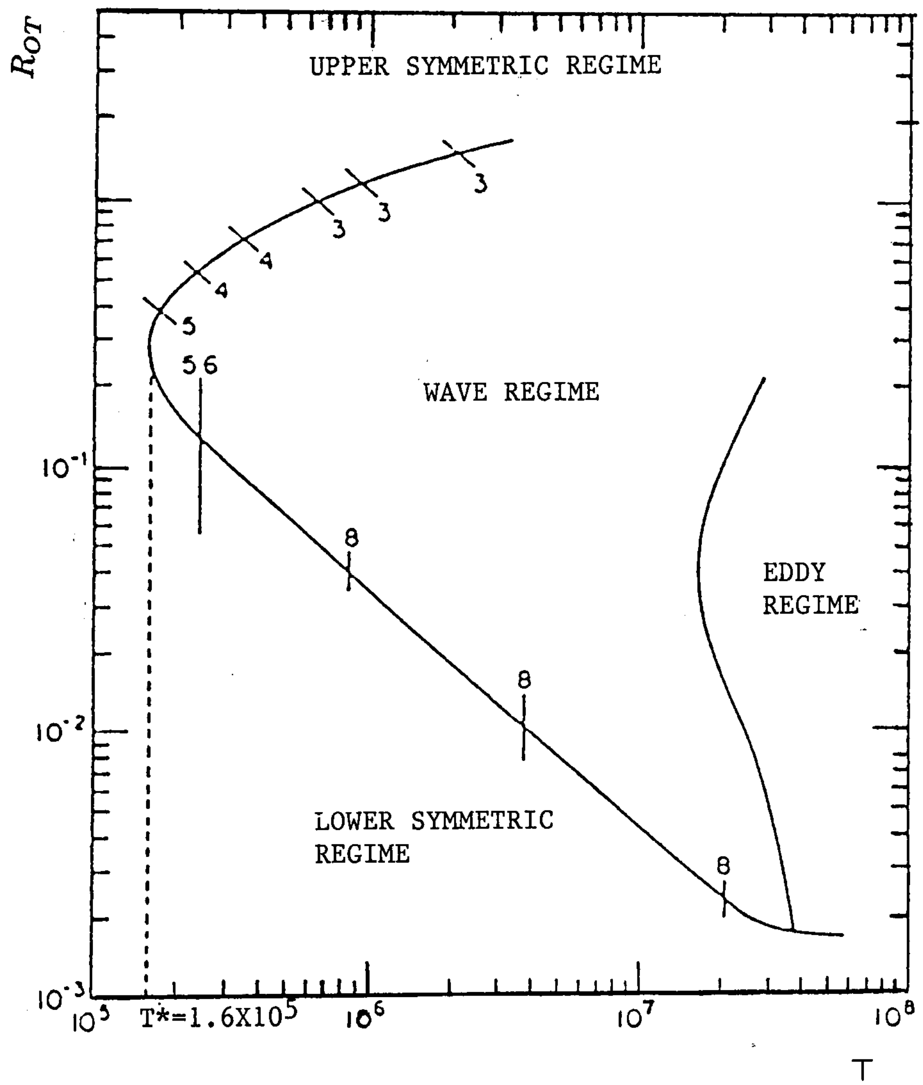

Fig. 1-3. Schematic of regimes in annulus experiments[11]

hand, structural vacillation denotes fluctuations of the wave shape and energy distribution in the radial direction with time, with comparatively small variations in the total wave energy[10].

Thus, although the geometry of the annulus and the nature of the fluid are quite different from those of the atmosphere, annulus experiments, when viewed as efficient generators of baroclinic eddies, can be used effectively to study quasi-geostrophic, nonlinear, baroclinic instabilities and to learn some of the fundamental features of these nonlinear flows.

§1.2 Objectives of the Present Work

As discussed in the last section, baroclinic instability has been observed in the laboratory experiments on the rotating annulus. So called baroclinic instability is the instability which hinges on the noncoincidence of the constant density and the constant pressure surfaces. It is also the most important form of instability in the large scale flow of the atmosphere which has the feature of being nearly hydrostatic, nearly geostrophic, and wave-like in appearance. In fact, annulus experiments have not only guided studies concerning the predictability or periodicity of the atmosphere, but also have become the subject of numerous theoretical and numerical studies.

The previous theoretical and numerical studies on the baroclinic instability can be classified as linear, weakly-nonlinear and strongly nonlinear. The pioneering work of Charney [14] and Eddy [15] demonstrated that the existence of large-scale cyclone waves in the atmosphere could be explained in terms of the instability of a baroclinic zonal current to infinitesimal wave disturbances. Since that time the original theoretical problem has been considerably extended, usually by considering the effects of more realistic basic states (e.g., the effects of horizontal shear, viscosity, or departures from geostrophic balance[16]). In such elaborations of the problem the wave disturbance is still considered to be an infinitesimal disturbance on the basic flow. The subsequent results of the linear instability theory are only valid while the growing amplitude of the wave remains sufficiently small for nonlinear effects to be ignored.

Some effects of nonlinearity have been computed by Phillips [17]. Starting with an unstable wave of small but finite amplitude which exhibited exponential growth, he computed the second-order changes in the basic current in which the wave was embedded. An unavoidable defect in such a straightforward expansion is that each succeeding term in the amplitude expansion grows more rapidly than the previous term and therefore severely restricts the time for which the expansion remains valid. Nevertheless, the results of Phillips' calculations should be correct initially and it only remains to find a method to embed them in a perturbation theory which remains uniformly valid in time.

In addition to seeking a theory which adequately predicts the nonlinear wave effects on the mean flow, the evolution of the wave itself to finite amplitude is of importance.

Stuart [18] and Watson [19], in their discussion of the stability of homogeneous shear flows, showed that when nonlinear processes were considered in that problem, the squared modules of the amplitude A satisfies

$$\frac{d}{dt}|A|^2 = |A|^2(\kappa c_i - N|A|^2). \tag{1.1}$$

This is known as the Landau equation, and in which κ is the wavenumber in the direction of the basic flow, c_i the imaginary part of the phase speed of the wave as calculated by linear theory, while N is the real part of a complex number calculated according to a recipe given by their nonlinear theory. If $\kappa c_i > 0$ (linearly unstable wave) and $N > 0$ (finite-amplitude stability), the amplitude tends monotonically (Figure 1-4) to a steady final value given by

$$|A|^2 = \kappa c_i / N. \tag{1.2}$$

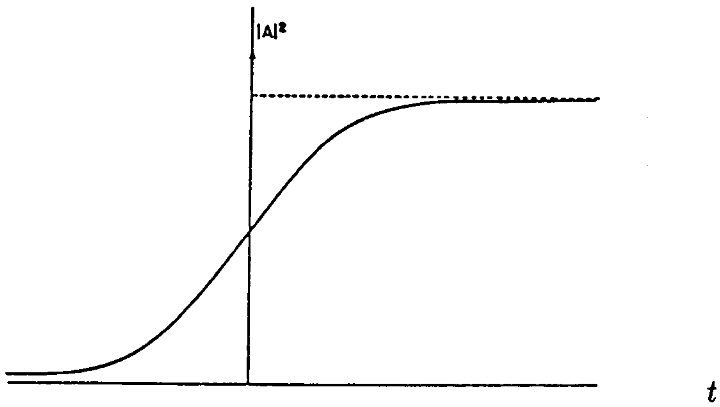

Fig. 1-4. Amplitude growth as a function of time

Indeed, it has frequently been hypothesized that an equation of the form (1.1) must hold as a description of the amplitude evolution in a large variety of stability problems.

The results of previous theoretical studies of the hydrodynamics instability in the quasi-geostrophic flow fall into two categories: weakly nonlinear theory, and strongly nonlinear theory. In the first category, the points representing the system under investigation lie within the unstable region and near the marginal curve. The marginal curve (or neutral stability curve) is the knee-shaped curve in Figure 1-3 which separates the axisymmetric flow region from the wave-like flow (non-axisymmetric region). In the second category, general studies with different modes in the unstable region and away from the marginal curve have been conducted.

A fairly complete weakly nonlinear theory of amplitude vacillation on the two layer f-plane has been developed by Pedlosky [20][21][22] using asymptotic expansions near the neutral curve for a single unstable wave. Pedlosky suggested that vacillation may be understood through the long time evolution of a nonlinearly unstable baroclinic wave. For his analysis he used a two-level, quasi-geostrophic model and accounted for only weak nonlinearity. By weakly nonlinear, it is meant here that the analysis was confined to waves with parameters in the neighborhood of the neutral stability curve in the regime diagram. He studied the inviscid, viscous and the weakly viscous cases. He found for the inviscid case, that the wave went through an amplititude vacillation cycle which depended for all time on the initial conditions. While for the viscous case, the disturbance evolved monotonically towards a steady state. Only when the dissipation was very small, did long term unsteadiness or amplitude vacillation appear. In all of these analyses, only the interaction of single zonal and meridional waves with the basic state was considered. Allowance was made for wave-wave interaction. Also by its nature such an analysis is restricted to small supercriticality whereby the wave-mean flow interaction was very modest. In a later work, Pedlosky [23] combined both dissipation and the β-effect and found, again for the two-level model, that vacillation may occur when both effects are small at fixed supercriticality. However, upon increasing either of these effects only steady solutions existed.

In a related study Drazin [24] [25] considered the evolution of a weakly nonlinear unstable baroclinic wave in a continuously stratified fluid. His results were to a certain degree similar to those found for the two level model. He again found a steady state equilibration for large dissipation and periodic oscillation for the inviscid case.

Barcilon and Drazin[26] used a weakly nonlinear theory to study the baroclinic instability in the quasi-geostrophic flow of a slightly viscous fluid in a rectangular channel. The basic states differ slightly from Eady's model. Owing to these differences, the critical layers lead to weak instabilities. The weak dissipation is allowed to overcome exactly the growth on a marginal curve different from Eady's.

They found that in some regions of the parameter space amplitude vacillation occurred.

Chou and Loesch[27][28] used the asymptotic approach, the ad hoc approach, and the spectral numerical approach to study the Eddy model modified by Ekman dissipation on the lower boundary and a free upper boundary. The time evolution of the disturbance is generally characterized by a single bump pattern, a growth stage to a maximum amplitude followed by a decay stage. During the decay stage, the spectral solution develops an amplitude vacillation. The asymptotic and the ad hoc solutions qualitatively capture the growth and decay of the disturbance, but fail to predict vacillation. They also employed both asymptotic and spectral numerical methods to study finite-amplitude dynamics of baroclinic disturbance in the presence of asymmetric Ekman pumping at the lower and upper boundaries. The results exhibit that eventual equilibration, regular vacillation, and chaotic vacillation depend on the actual values of supercriticality, dissipation, stratification parameters, and fundamental zonal wave number.

Boville [29] [30] [31] working with the two-level model of Pedlosky studied the effects of strong nonlinearity on the evolution of a baroclinic wave. Thus, he was able to perform calculations in which the parameters settings were fairly close to those found in the atmosphere and the annulus experiments. His analysis admitted any degree of supercriticality and also full interaction was allowed between the original basic state and the unstable wave. However, the analysis permitted only the interaction between the harmonics of one unstable wave. Boville found that considerable difference existed in the dynamics of vacillation between the $\beta-$ and f-plane analysis. The inclusion of a single zonal harmonic gave a good approximation to the full solution for the latter while it did not in the former. He found that the interaction between waves of different zonal scales to be of crucial importance to the vacillation cycle on the β-plane. He also showed that vacillation will occur in a system fairly closely related to the atmosphere at mid latitude when the parameter values were close to those in the atmosphere.

Weng[32] used a modified Eddy model to study analytically and numerically the behavior of strongly nonlinear, baroclinic waves in her dissertation. By means of a truncated spectral expansion, the model is reduced to a nonlinear automous system of equation which describes the dynamics of a single zonal wave number disturbance with its lowest two meridional modes, and of the mean flow correction with its lowest four meridional modes. Each meridional mode consists of a baroclinic and a barotropic pattern. She gave a unified picture that described the four regimes observed in the rotating annulus experiments, i.e. axisymmetric zonal flow, traveling steady waves, amplitude vacillation and structural vacillation.

The transition from symmetric flow to steady wave flow is due to baroclinic instability of the symmetric flow with respect to a lowest meridional mode, i.e. sinπy-perturbation. Steady waves are stable when the flow is energetically balanced between baroclinicity and the Ekman dissipation through nonlinearity.

The transition from traveling steady waves to amplitude vacillation is due to the baroclinic instability of the traveling, steady, sinπy-wavy flow with respect to a sinπy-perturbation. A typical amplitude vacillation is the vacillation of wave potential energy with time, via interference of nonlinear barotropic and baroclinic patterns of the lowest meridional mode of the wave.

The transition from amplitude vacillation to structural vacillation is due to both the baroclinic instability of the vacillating, sinπy-wavy flow with respect to a sin2πy-perturbation and the nonlinear mode-mode interaction. This transition occurs gradually in a parameter region. A typical structural vacillation is the vacillation of the redisturbance of wave kinetic energy in the meridional direction with time, via interference of the lowest two nonlinear meriodinal-modes of the wave.

The Ekman dissipation seems to play two roles: large amounts of dissipation are stabilizing, and small amounts of dissipation are destabilizing.

However, the results presented in Weng's dissertation are those of highly truncated model and only for single zonal wave number. Those results can be amplified and may be modified if a system with a large number of zonal and meridional modes is considered.

The numerical study of the baroclinic instability associated with the annulus experiment constitutes the objective of the present work. We try to study this problem by means of a spectral expansion. Unlike the analytical approach in this case, the length of the spectral expansion solution can be defined based on practical requirements. Then the shortcoming of Weng's highly truncated model can be overcome. Further, this work can be viewed as an extension of Weng's model to include any numbers of modes in both the meridional and zonal directions, thus, the possibility of wave number transition can be also investigated.

After the model is developed, the model is used to study the long term evolution of baroclinic waves, the manner in which flow transits from one regime to another, and the phenomena of wave number transitions. The setup of such a model and subsequent numerical simulation are the main content of this work. From the literature search, it appears that this is the first time such a multi-wave number model is used to study the inviscid and viscous instability of the flow in the annulus as well as the wave number transition phenomenon numerically.

§1.3 Outline of the Approaches

In chapter II, a general mathematical formulation and the perturbation equation under some simplification condition for the atmospherical flows and rotating flow in annulus are derived. The numerical procedure is given in Chapter III. In the last two chapters, the computed results are presented and discussed, and the conclusion and existing problems are pointed out.

CHAPTER II

MATHEMATICAL FORMULATION

§2.1 Mathematical Formulation of Atmosphere Flow

2.1.1 General Full Equation Formulation

For fluid motion in the atmosphere, the governing equations of motion can be derived from the three basic physical conservation laws in the traditional way. These physical laws state the mass, momentum, and energy conservation of fluid system, from which the continuity, momentum and energy equations can be derived respectively.

The continuity equation can be written in the following general form

$$\frac{\partial \rho}{\partial t} + \nabla \bullet (\rho \vec{v}) = 0 \tag{2.1}$$

where ρ is the density and $\vec{v}$ is the velocity vector. t is the time variable. ∇ is the gradient operator.

The momentum equation, formulated in a inertial coordinate system, takes the following form

$$\frac{\partial \vec{v}}{\partial t} + \vec{v} \bullet \nabla \vec{v} = -\frac{1}{\rho}\nabla p + \vec{f_b} + \vec{f_f} \tag{2.2}$$

in which p is the static pressure, $\vec{f_b}$ is the body force and $\vec{f_f}$ is the frictional force.

The energy equation is written in the following form

$$\frac{\partial e}{\partial t} + \vec{v} \bullet \nabla e + p\frac{\partial}{\partial t}(\frac{1}{\rho}) = \frac{k}{\rho}\nabla^2 T + Q + D \tag{2.3}$$

where e is the internal energy per unit mass, k is the thermal conductivity, T is the absolute temperature. Q is the rate of heat aguementation per unit mass, and D is the dissipative energy by viscosity.

To close the set of the governing equations for the unknowns, the thermodynamic equation of state is introduced, which is

$$p = f(\rho, R, T) \tag{2.4}$$

where R is the gas constant. f represents a function, which needs to be defined based on the fluid and the state under consideration.

It is known that the above stated four equations are the basic set of the governing equations for the fluid dynamic problems. For our concrete problem in hand, the governing equations for solution are the adaptation of these basic equations. Below we give a summarized version of the derivation[33].

2.1.2 Quasi-geostrophic Potential Vorticity Equation

2.1.2.1 Coordinate transformation

The equations given in §2.1.1 are valid for an inertial coordinate system . Conventionally, the coordinate system is chosen to be fixed to the earth for a general fluid problems including atmospheric flow. However, the earth has a rotation about its axis. So the momentum equation needs to be modified as, referring to a earth oriented coordinate system,

$$\frac{\partial \vec{v}}{\partial t} + \vec{v} \bullet \nabla \vec{v} + 2\vec{\Omega} \times \vec{v} = -\frac{1}{\rho}\nabla p + \vec{f_b} + \vec{f_f} \tag{2.5}$$

where $\vec{\Omega}$ is the earth's angular velocity, and $2\vec{\Omega} \times \vec{v}$ is the Coriolis force.

When solving the momentum equation (2.5), the vector form of the equation is replaced by its three scalar component equations in the chosen coordinate system. A natural choice is a spherical coordinate (r, θ, ϕ), with the earth's center of gravity as origin. Coordinate r is the radial distance from the earth's center, θ is the latitude angle, and ϕ is the longitude angle. The velocity components in the eastward, northward and vertical directions are u, v, and w, as shown in Figure 2-1,

The continuity equation in the spherical coordinate is

$$\frac{d\rho}{dt} + \rho\{\frac{\partial w}{\partial r} + \frac{2w}{r} + \frac{1}{rcos\theta}\frac{\partial(vcos\theta)}{\partial\theta} + \frac{1}{rcos\theta}\frac{\partial u}{\partial\phi}\} = 0 \tag{2.6}$$

The momentum equations are

$$\frac{du}{dt} + \frac{uw}{r} - \frac{uv}{r}tan\theta - 2\Omega sin\theta v + 2\Omega cos\theta w = -\frac{1}{\rho rcos\theta}\frac{\partial p}{\partial\phi} + \frac{f_\phi}{\rho} \tag{2.7a}$$

$$\frac{dv}{dt} + \frac{wv}{r} + \frac{u^2}{r}tan\theta + 2\Omega sin\theta u = -\frac{1}{\rho r}\frac{\partial p}{\partial\theta} + \frac{f_\theta}{\rho} \tag{2.7b}$$

$$\frac{dw}{dt} - \frac{u^2 + v^2}{r} - 2\Omega cos\theta u = -\frac{1}{\rho}\frac{\partial p}{\partial r} - g + \frac{f_r}{\rho} \tag{2.7c}$$

where f_ϕ, f_θ, f_r are the three components of the frictional forces acting on the fluid, and the material derivative is:

$$\frac{d}{dt} = \frac{\partial}{\partial t} + \frac{u}{rcos\theta}\frac{\partial}{\partial\phi} + \frac{v}{r}\frac{\partial}{\partial\theta} + w\frac{\partial}{\partial r}$$

The equations of motion must be completed with the addition of a thermodynamic equation:

$$\frac{d\Theta}{dt} = \frac{\Theta}{C_pT}\left(\frac{k}{\rho}\nabla^2 T + Q\right) \tag{2.8}$$

Where Θ is the potential temperature, i.e.,

$$\Theta = T\left(\frac{p_0}{p}\right)^{R/C_p}$$

We suppose that the motion occurs in the mid-latitude region. For simplicity, as shown in the Figure 2-1, a local orthogonal coordinate system (x,y,z) is introduced with its origin in the point O on the earth's surface [34].

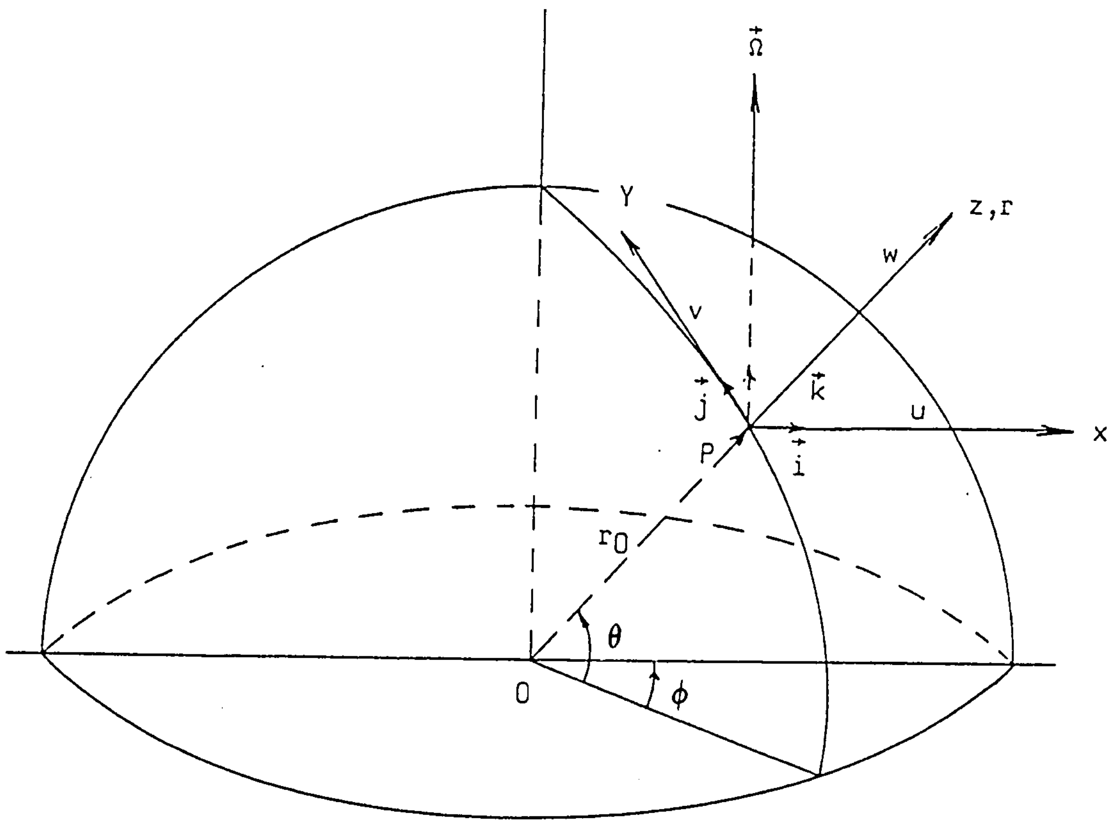

Fig. 2-1. Spherical coordinate and local orthogonal coordinate systems

Let $\vec{i}, \vec{j}, \vec{k}$ stand for the unit vectors in the x, y and z directions, respectively. The relationship between spherical and local coordinates system is given by

$$x = \phi r_0 cos\theta_0 \tag{2.9a}$$

$$y = (\theta - \theta_0) r_0 \tag{2.9b}$$

$$z = r - r_0 \tag{2.9c}$$

where θ_0 is central latitude, r_0 is the earth's radius.

Therefore, the corresponding momentum equations in a rectangular coordinate system with origin at the earth surface take the form

$$\frac{du}{dt} = -\frac{1}{\rho}\frac{\partial p}{\partial x} + 2\Omega(vsin\theta - wcos\theta) + \frac{f_x}{\rho} \tag{2.10a}$$

$$\frac{dv}{dt} = -\frac{1}{\rho}\frac{\partial p}{\partial y} - 2\Omega usin\theta + \frac{f_y}{\rho} \tag{2.10b}$$

$$\frac{dw}{dt} = -\frac{1}{\rho}\frac{\partial p}{\partial z} + 2\Omega ucos\theta - g + \frac{f_z}{\rho} \tag{2.10c}$$

In the above, we denote $\vec{g} = (0, 0, -g)$, $\vec{F} = (f_x, f_y, f_z)$, $\vec{\Omega} = (0, \Omega cos\theta, \Omega sin\theta)$.

2.1.2.2 Nondimensionalization of the governing equations

Before nondimensionlizing the governing equations, a scale discussion about the atmospherical flow problems is helpful for reducing the complexity and understanding more physics. In the atmosphere, the circulatory motions are important. Atmospheric circulations are described by sorting out events according to size and time. Small whirlwinds that carry dust skyward are far too small to show up, while cyclones and anti-cyclones reveal large-scale wind patterns. A small eddy, like a dust devil, lasts only a few moments; whereas, a large vortex, like a hurricane, may persist for days.

The present study emphasizes the large-scale motions. This does not mean that the motion systems of smaller scale are unimportant, but that the microscale and medium-scale circulations are, to a large extent, controlled by the large-scale motion system. Only large-scale motion can be observed and analyzed over a large portion of the globe.

To proceed systematically it is essential to introduce nondimensional variables. The existence of characteristic scales is exploited by the introduction of nondimensional variables denoted by primes, i.e.,

$$x = Lx' \tag{2.11a}$$

$$y = Ly' \tag{2.11b}$$

and

$$z = Dz' \tag{2.12}$$

$$r = r_0 + z = r_0 + DZ' \tag{2.13}$$

while the time is scaled by the advective time L/U, i.e.,

$$t = \frac{L}{U}t' \tag{2.14}$$

For the velocity components

$$u = Uu'$$

$$v = Uv' \tag{2.15}$$

and

$$w = \frac{D}{L}Uw' \tag{2.16}$$

Where D is the vertical scale of motion and L is the horizontal scale of motion. U is a characteristic horizontal speed. Since the atmosphere is very shallow compared with the earth's radius, r_0, r may be replaced by r_0 when r is undifferentiated.

The scaling for density, pressure and potential temperature is more subtle. If the relative velocity is small (i.e., for small Rossby number), the pressure will be only slightly disturbed from the value it would have in the absence of motion, $p_s(z)$, defined by the relation

$$\frac{\partial p_s(z)}{\partial z} = -\rho_s(z)g, \tag{2.17}$$

which is what (2.7a,b,c) reduce to if u,v,and w are zero. We can think of $p_s(z)$ and $\rho_s(z)$ as defining a "standard" atmosphere, i.e., a basic state upon which fluctuations due to the motion occur. The basic state is assumed known, although in fact its determination from first principles requires the consideration of mechanisms such as radiative transfer in the atmosphere, etc. Alternatively, p_s and ρ_s may be defined as the global average of p and ρ at each level z. We then write

$$p = p_s(z) + \tilde{p}(x, y, z, t),$$

$$\rho = \rho_s(z) + \tilde{\rho}(x, y, z, t)$$

where $\tilde{p}$ and $\tilde{\rho}$ are spatially and temporally varying departures from the standard values p_s and ρ_s. How shall $\tilde{p}$ and $\tilde{\rho}$ be scaled? We anticipate that for the motions of interest to us the horizontal pressure gradient will be of the same order as the Coriolis acceleration. The order of the Coriolis acceleration at the latitude θ_0 is given by

$$\rho 2\Omega u sin\theta_0 = O(2\Omega sin\theta_0 U \rho_s),$$

while the magnitude of the pressure gradient is $\tilde{p}/L$. thus we anticipate that $\tilde{p} = O(\rho_s U f_0 L)$, where

$$f_0 = 2\Omega sin\theta_0 \tag{2.18}$$

is the Coriolis parameter at the central latitude θ_0. These considerations imply that the pressure should be written

$$p = p_s(z) + \rho_s U f_0 L p' \tag{2.19}$$

with the expectation that p' is an O(1) quantity with an O(1) variation over distances of O(L). Note that ρ_s in the above formula is a function of z alone.

Similarly we may anticipate that the buoyancy force per unit mass due to $\tilde{\rho}$ will be of the same order as the vertical pressure gradient, since an observed feature of large-scale motions is the excellence of the hydrostatic approximation. The vertical pressure gradient associated with $\tilde{p}$ is

$$\frac{\partial \tilde{p}}{\partial z} = O(\frac{\tilde{p}}{D}) = O(\frac{\rho_s U f_0 L}{D})$$

and hence if $\tilde{\rho} g$ is to be of this order,

$$\tilde{\rho} = O(\rho_s U \frac{f_0 L}{gD})$$

so that the density should be written as

$$\rho = \rho_s(z)(1 + \varepsilon F \rho') \tag{2.20}$$

and for the potential temperature, we have

$$\Theta = \Theta_s(z)(1 + \varepsilon F \theta') \tag{2.21}$$

where

$$\varepsilon = \frac{U}{f_0 L} = Rossby\ \ Number \tag{2.22}$$

$$F = \frac{f_0^2 L^2}{gD} = Froude\ \ number \tag{2.23}$$

$$p_s = -g\int_0^z \rho_s(z)dz. \tag{2.24}$$

in which p_s, ρ_s and Θ_s are functions of z in the basic state, s. Another dimensionless quantity is the Ekman number defined as $E = \mu/(2\Omega L^2)$.

If equations (2.11)-(2.17), (2.19) and (2.20) are substituted into equations (2.7a,b,c), we obtain, after division by the constants multiplying the pressure terms,

$$\varepsilon\{\frac{du}{dt} + \frac{L}{r_*}(\delta_r uw - uvtan\theta)\} - v\frac{sin\theta}{sin\theta_0} + \delta_r w\frac{cos\theta}{sin\theta_0}$$
$$= -\frac{cos\theta_0}{cos\theta}\frac{r_0}{r_*}\frac{\partial p}{\partial x}\frac{1}{1+\varepsilon F\rho} + \frac{f_{*\phi}}{\rho_* U f_0} \tag{2.25a}$$

$$\varepsilon\{\frac{dv}{dt} + \frac{L}{r_*}(\delta vw + u^2 tan\theta)\} + u\frac{sin\theta}{sin\theta_0}$$
$$= -\frac{r_0}{r_*}\frac{\partial p}{\partial y}\frac{1}{1+\varepsilon F\rho} + \frac{f_{*\theta}}{\rho_* U f_0} \tag{2.25b}$$

$$(1+\varepsilon F\rho)\{\frac{\varepsilon\delta_r^2 dw}{dt} - \frac{\varepsilon\delta_r}{r_*}(u^2+v^2) - \frac{\delta_r u cos\theta}{sin\theta_0}\}$$
$$= -\frac{1}{\rho_s}\frac{\partial(p\rho_s)}{\partial z} - \rho + \frac{f_{*z}}{\rho_s U f_0}\delta_r \tag{2.25c}$$

and the continuity equation becomes

$$\varepsilon F\frac{d\rho}{dt} + (1+\varepsilon F\rho)$$
$$\times\{\frac{w}{\rho_s}\frac{\partial\rho_s}{\partial z} + \frac{\partial w}{\partial z} + 2\frac{D}{r_*}w + \frac{r_0}{r_*}\frac{\partial v}{\partial y} - \frac{L}{r_*}vtan\theta + \frac{r_0}{r_*}\frac{cos\theta_0}{cos\theta}\frac{\partial u}{\partial x}\} = 0 \tag{2.26}$$

where

$$\frac{d}{dt} = \frac{\partial}{\partial t} + u\frac{cos\theta_0}{cos\theta}\frac{r_0}{r_*}\frac{\partial}{\partial x} + v\frac{r_0}{r_*}\frac{\partial}{\partial y} + w\frac{\partial}{\partial z}$$

and

$$\delta_r = \frac{D}{L} \tag{2.27}$$

Unprimed variables are nondimensional, while dimensional variables are denoted by asterisks.

To this point, no approximations have been made. It is now possible to systematically exploit the smallness of the parameters ε, δ_r, L/r_0, and F. The parameters ε, δ_r,L/r_0 and F are all independent, and their relative orders will vary somewhat from phenomenon to phenomenon. In the following, we will give the scaling of the parameters for the case we consider and get the corresponding approximate equations.

2.1.2.3 Geostrophic motion

For the large-scale atmospheric motion at mid-latitudes, the ordering relationships are as follows:

$$\begin{aligned} \varepsilon &= \frac{U}{f_0 L} \ll 1. \\ \delta_r &= \frac{D}{L} = O(\varepsilon^2) \\ \frac{L}{r_0} &= O(\varepsilon) \\ \frac{r}{r_0} - 1 &\leq O(\varepsilon^2) \\ E &< O(\varepsilon) \end{aligned} \tag{2.28}$$

Once the ordering relationships are chosen in this way, each variable may be considered as a function of ε with the other parameters directly related to ε by the preceding considerations. Since ε is small, we write, for example:

$$u(x,y,z,t,\varepsilon) = u_0(x,y,z,t) + \varepsilon u_1(x,y,z,t) + \dots \tag{2.29}$$

where the u_k are independent of ε and O(1). If the expansion (2.29) is applied to each dependent variable and that expansion is substituted into the equations of motion, i.e. terms of like order in ε which result must balance, since ε, while small, is also arbitrary, and the equations must hold for all orders in ε. In this way equations (2.25-26) are simplified as

$$v_0 = \frac{\partial p_0}{\partial x} \tag{2.30a}$$

$$u_0 = -\frac{\partial p_0}{\partial y} \tag{2.30b}$$

$$\rho_0 = -\frac{1}{\rho_s}\frac{\partial}{\partial z}(\rho_s p_0) \tag{2.30c}$$

$$\frac{1}{\rho_s}\frac{\partial}{\partial z}(w_0 \rho_s) + \frac{\partial u_0}{\partial x} + \frac{\partial v_0}{\partial y} = 0 \tag{2.31}$$

and

$$\Theta_0 = \frac{\partial p_0}{\partial z} \tag{2.32}$$

The β-plane approximation first emerges at this point. The β-plane is defined as a plane where the Coriolis parameter, f, is approximated by $f = f_0 + \beta y$, in which $\beta = df/dy$.

Equation (2.30c) is the hydrostatic approximation in the vertical direction. Equations (2.30a,b) are the geostrophic approximations. Under the conditions of the geostrophic approximation, the large scale atmospheric motion is called the geostrophic motion. The wind with velocity of the geostrophic wind is the thermal wind. By the geostrophic and hydrostatic approximation with aid of the equation of state, the thermal wind equations are presented as[35]

$$\frac{\partial u}{\partial z} = -\frac{g}{fT}\frac{\partial T}{\partial y} + \frac{u}{T}\frac{\partial T}{\partial z} \tag{2.33a}$$

$$\frac{\partial v}{\partial z} = \frac{g}{fT}\frac{\partial T}{\partial x} + \frac{v}{T}\frac{\partial T}{\partial z} \tag{2.33b}$$

So, it can be shown that in a barotropic atmosphere there can be no increase of geostrophic wind with height due to $\partial u/\partial z = \partial v/\partial z = 0$. However, in a baroclinic atmosphere, the vertical wind shear depends mainly upon the horizontal temperature gradients.

2.1.2.4 Quasi-geostrophic potential vorticity equation

The quasi-geostrophic motion is a particular class of motions, i.e. the large-scale, essentially geostrophic motion.

Equations (2.30a) and (2.30b) further imply that the horizontal, O(1) geostrophic velocities, are horizontally non-divergent, since from (2.30a,b),

$$\frac{\partial v_0}{\partial y} + \frac{\partial u_0}{\partial x} = 0$$

So that (2.31) implies

$$\frac{\partial}{\partial z}(\rho_s(z) w_0) = 0$$

Hence, $\rho_s w_0$ must be independent of z. If w_0 vanishes for any z it will be zero for all z. If the region under consideration is bounded above or below by a horizontal solid surface, then the O(1) vertical velocity on that surface must vanish, i.e.

$$w_0 = 0 \tag{2.34}$$

and so:

$$w = \varepsilon w_1 + \varepsilon^2 w_2 ..... \tag{2.35}$$

If the vorticity equation is denoted by

$$\zeta_0 = \frac{\partial v_0}{\partial x} - \frac{\partial u_0}{\partial y} \tag{2.36}$$

the conserved vorticity equation in the quasi-geostrophic motion can be obtained by[33]

$$\frac{d_0}{dt}\left(\zeta_0 + \beta y + \frac{1}{\rho_s}\frac{\partial}{\partial z}(\frac{\rho_s \theta_0}{S})\right) = 0 \tag{2.37}$$

where

$$\frac{d_0}{dt} = \frac{\partial}{\partial t} + u_0\frac{\partial}{\partial x} + v_0\frac{\partial}{\partial y}$$

S is the stratification parameter, as the fluid is stratified by a heavier fluid underlying a lighter one. It is defined as

$$S = \frac{N^2 D^2}{f_0^2 L^2} \tag{2.38}$$

in which N is the Brunt-Vaisala frequency. This frequency is also referred to as the buoyancy frequency[36]. It is defined as

$$N^2 = \frac{g}{\Theta}\frac{d\Theta}{dz} \tag{2.39}$$

and is a measure of the static stability of the environment[37].

The geostrophic and hydrostatic approximations allows us to express each dependent variable in (2.37) in terms of

$$\psi = p_0 \tag{2.40}$$

So that (2.37) becomes the governing equation of motion, i.e.

$$\{\frac{\partial}{\partial t} + \frac{\partial\psi}{\partial x}\frac{\partial}{\partial y} - \frac{\partial\psi}{\partial y}\frac{\partial}{\partial x}\}\{\frac{\partial^2\psi}{\partial x^2} + \frac{\partial^2\psi}{\partial y^2} + \frac{1}{\rho_0}\frac{\partial}{\partial z}\left(\frac{\rho_s}{S}\frac{\partial\psi}{\partial z}\right) + \beta y\} = 0 \tag{2.41}$$

This is the quasi-geostrophic potential vorticity equation.

2.1.2.5 Boundary conditions for the potential vorticity equation

The boundary conditions for Equation (2.41) are determined by the vertical velocity, the vorticity and the bottom topography as well as the upper-surface status.

For atmosphere flow, the lower-boundary condition depends on the Ekman layer and is presented as

$$w_1(x,y,0) = \frac{E_v^{\frac{1}{2}}}{2\varepsilon}\zeta_0(x,y) + \vec{V}_0 \bullet \nabla\left(\frac{h_B}{\varepsilon D}\right) \tag{2.42}$$

where E_v is the vertical Ekman number defined as $2A_v/(fD^2)$, in which A_v is called the vertical turbulent viscosity coefficient[33], and h_B is the elevation of the lower boundary above the reference level z=0. In quasi-geostrophic scaling and ordering, we have

$$\frac{h_B}{D} = \varepsilon\eta_B(x,y) \tag{2.43}$$

$$w_1 = -\frac{1}{S}\frac{d\Theta_0}{dt} \tag{2.44}$$

Substituting Equations (2.43), (2.44) into (2.42) yields

$$\frac{1}{S}[\frac{d\Theta_0}{dt}]_{z=0} = -\frac{E_v^{1/2}}{2\varepsilon}\zeta_0(x,y) - \vec{V}_0 \bullet \nabla\eta_B(x,y) \tag{2.45}$$

The upper boundary condition is a more difficult problem[33]. The atmosphere is not bounded above, although the most energetic "weather"-related motions of synoptic scale are to a great extent confined to the troposphere. In physical terms, it can be stated as follows, either the amplitude of the energy of the motion must decay to zero for large z, or if it remains finite but nonzero, the flux of motion energy must be directed upwards.

The mathematical formulation of the upper boundary condition is

$$w_1(x,y,1) = \frac{E_v^{1/2}}{2\varepsilon}[\zeta_T(x,y) - \zeta_0(x,y)] \tag{2.46}$$

where ζ_T is the upper vorticity at the level z=1. If the fluid flow is bounded above by a free or rigid horizontal surface, then Equation (2.46) is expressed in the following two boundary conditions:

$$\frac{1}{S}\frac{d\Theta_0}{dt} = 0 \qquad (free) \qquad at \quad z = 1 \tag{2.47a}$$

$$\frac{1}{S}\frac{d\Theta_0}{dt} = \frac{E_v^{1/2}}{2\varepsilon}\zeta_0(x,y) \qquad (rigid) \qquad at \ \ z=1 \tag{2.47b}$$

Substituting Equations (2.30a,b), (2.32), and (2.36) into (2.45), (2.47a,b) with the aid of the equality $\psi = p_0$, the equation for the lower boundary becomes

$$\frac{d}{dt}[\frac{\partial\psi}{\partial z}] + S[\frac{\partial\psi}{\partial x}\frac{\partial\eta_B}{\partial y} - \frac{\partial\psi}{\partial y}\frac{\partial\eta_B}{\partial x}] = -\frac{SE_v^{1/2}}{2\varepsilon}\nabla^2\psi \tag{2.48}$$

and, the upper boundary,

$$\frac{d}{dt}[\frac{\partial\psi}{\partial z}] = 0 \qquad\qquad (free) \tag{2.49a}$$

$$\frac{d}{dt}[\frac{\partial\psi}{\partial z}] = \frac{SE_v^{1/2}}{2\varepsilon}\nabla^2\psi \quad (rigid) \tag{2.49b}$$

where

$$\frac{d}{dt} = \frac{\partial}{\partial t} + \frac{\partial\psi}{\partial x}\frac{\partial}{\partial y} - \frac{\partial\psi}{\partial y}\frac{\partial}{\partial x}$$

§2.2 Mathematical Formulation of Flow in Annulus

In the above section, the full governing equations for the atmospherical flows have been derived. However, in practice, flows in the atmosphere are very complicated. A direct numerical simulation of these flows in the atmosphere is still not practical and too expansive. As introduced in the chapter I, the flow in an annulus is proposed to model the flow in the real atmosphere and is studied in this work.

2.2.1 Basic Assumptions

Since the very similarity of the phenomenon in the atmosphere and in the annulus experiment, the dynamics of baroclinic waves in an annulus is dealt with instead of in the real atmosphere in this work.

We consider a viscous, incompressible, non-conductive fluid flow in an annulus. Although the entire fluid is viscous, the Ekman layers are assumed to be the seat of the largest viscous dissipation.

Basically, there are three key effects which control the main charateristics of these flows: the imposed temperature difference or the zonal-mean vertical shear which constitutes the energy source of the system, the Ekman dissipation which constituted the energy sink of the system, and the rotation rate. Other effects may modify quantitatively each flow regime, but do not affect qualitatively the properties of these flows. In the following work, the main assumptions are listed:

A1: A Boussinesq fluid. By the Boussinesq approximation the variation of the density of the fluid is neglected in each term of the equation of the motion except when coupled with gravity to produce bouyancy forces.

A2: The flow is taken as quasi-geostrophic.

A3: The basic flow is purely baroclinic.

A4: A constant Coriolis parameter is assumed.

A5: The Brunt-Vaisala frequency is taken to be a constant.

A6: The flow is confined in the vertical direction by two rigid horizontal boundaries, and in the lateral direction by two vertical walls. Dissipation is found at the top and bottom Ekman layers, which are of unequal strengths. There is no flow normal to the lateral boundaries and the boundary layer dynamics at these sidewalls is not considered, and since the gap between outer and inner cylinders is much smaller than the mean radius of these two cylinders, the flow in the annulus can be recognized as an infinite channel.

A7: Heat conduction is neglected because heat convection is dominant in the main flow region.

2.2.2. Governing Equations

A viscous incompressible, non-conducting fluid contained in a channel is considered. The coordinate system is the Cartisian system, where x, y, and z measure distance along the channel, across the channel and vertically, respectively. The corresponding velocity components are u, v and w. The whole system is viewed from a reference frame, rotating with angular velocity $\Omega\vec{k}$ about the z-direction. The equations of motion, continuity and heat transport are[38]

$$\frac{\partial\vec{v}}{\partial t} + (\vec{v}\bullet\nabla)\vec{v} + 2\Omega\vec{k}\times\vec{v} = -\frac{1}{\rho_0}\nabla p + \alpha g(T - T_0)\vec{k}, \tag{2.50a}$$

$$\nabla\bullet\vec{v} = 0, \tag{2.50b}$$

$$\frac{\partial T}{\partial t} + (\vec{v}\bullet\nabla)T = 0, \tag{2.50c}$$

where ρ_0 is the density at the reference temperature T_0.

Finally p is a modified pressure representing the departure of the total pressure field from the value necessary to balance the steady centrifugal term $\Omega\vec{k}\times(\Omega\vec{k}\times\vec{r})$ and the hydrostatic term $g\rho_0\vec{k}$. We have of course assumed an equation of state of the form

$$\rho = \rho_0[1 - \alpha(T - T_0)] \tag{2.51}$$

We shall be concerned with the instability (to wave-like disturbances) of a basic state that is a zonal flow, varying linearly with height, and in particular we consider a zonal flow with linear vertical shear. Thus, taking the depth of the annulus, d, as a vertical length scale and U as a horizontal velocity scale, we can write

$$\vec{U} = (U/d)z\vec{i}, \tag{2.52}$$

which is in geostrophic and hydrostatic balance with the basic temperature and pressure fields

$$T_s = T_0 + \frac{\Delta T}{d}z - \frac{2\Omega U}{\alpha g d}y, \tag{2.53a}$$

$$P_s = \rho_0 \left(\frac{\alpha g \Delta T}{2d}z^2 - \frac{2\Omega U}{d}yz \right), \tag{2.53b}$$

It is convenient to non-dimensionalize the variables, denoting dimensionless quantities by tildes, so that we have

$$(x, y) = (b-a)(\tilde{x}, \tilde{y}), \quad z = d\tilde{z}$$

$$(u, v) = U(\tilde{u}, \tilde{v}), \quad w = (Ud/(b-a))\varepsilon\tilde{w}$$

$$t = \frac{(b-a)}{U}\tilde{t}, \quad T = T_0 + \frac{\Delta T}{d}z + \frac{2\Omega U(b-a)}{\alpha g d}\tilde{T},$$

$$p = (\alpha g \rho_0 / 2d)\Delta T z^2 + 2\Omega U(b-a)\rho_0 \tilde{p} \tag{2.54}$$

here $\varepsilon = U/(2(b-a)\Omega)$ is the Rossby number and we define the dimensionless parameter $R_{OT} = g\alpha d\Delta T/4\Omega^2(b-a)^2$ as the thermal Rossby number which gives a measure of the stratification of the flow. The crucial importance of such a parameter has been recognized since the earliest experiments of Hide [3][4]. We shall assume $R_{OT} = O(1)$, d≪(b-a) and $\varepsilon \ll 1$ so that the baroclinic instability will occur when $\tilde{w}$ is O(1) in the limit of small ε.

We now drop the tildes and work with dimensionless quantities throughout. The basic flow is therefore

$$\vec{U} = z\vec{i}$$

corresponding to temperature and pressure fields

$$T_s = -y, \quad P_s = -yz.$$

To examine its stability we write

$$\vec{v} = \vec{U} + \vec{v}', \quad T = T_s + T', \quad p = p_s + p'$$

where primes denote perturbed quantities, and substitute these into the equations of motion, continuity and heat conduction.

After a little algebra we obtain the quasi-geostrophic equation for p', namely the perturbation stream function Φ, which becomes,

$$[\frac{\partial}{\partial t} + z\frac{\partial}{\partial x} + J_{(x,y)}(\Phi;\ )]\nabla^2_{R_{OT}}\Phi = 0 \tag{2.55}$$

Where

$$\nabla^2_{R_{OT}} = [\frac{\partial^2}{\partial z^2} + R_{OT}\left(\frac{\partial^2}{\partial x^2} + \frac{\partial^2}{\partial y^2}\right)]$$

$$J_{(x,y)}(f,g) = \frac{\partial f}{\partial x}\frac{\partial g}{\partial y} - \frac{\partial f}{\partial y}\frac{\partial g}{\partial x} \tag{2.56}$$

As a result of assumptions A1, A3 and A5, the potential vorticity gradient in the basic state vanishes, and the potential vorticity of the perturbation is conserved. If we assume that initially the potential vorticity is zero, it then remains zero for all $t > 0$. Under the assumptions A4 and A5, the stratification factor, S, which is approximately equal to the thermal Rossby number R_{OT} (see section 2.2.3), is a constant. Thus, the governing equation for the flow in the annulus becomes

$$\frac{\partial^2\Phi}{\partial x^2} + \frac{\partial^2\Phi}{\partial y^2} + \frac{1}{S}\frac{\partial^2\Phi}{\partial z^2} = 0 \tag{2.57}$$

For the boundary condition in the y direction, we assume that the rigid walls exists at $y = \pm 1$ containing the region of the flow and the perturbations. Under this condition it follows that for v_0 to vanish on $y = \pm 1$, i.e.,

$$\frac{\partial\Phi}{\partial x} = 0 \qquad at \quad y = \pm 1, \tag{2.58}$$

If the zonal momentum equation is integrated in x from $-\infty$ to ∞ (which is equivalent to integration around a complete latitude circle), it follows that

$$\frac{\partial \bar{u}_0}{\partial t} = \bar{v}_1 - \frac{\partial}{\partial y}(\overline{v_0 u_0}) \tag{2.59}$$

where an overbar represents the averaging process

$$\overline{(.)} = \lim_{x\to\infty} \frac{1}{2x} \int_x^x (.)dx$$

Note that $\bar{v}_0$ must be zero, since v_0 is geostrophic. Since both v_1 and v_0 must vanish on $y = \pm 1$, it in turn follows that, in addition to (2.58), Φ must satisfy

$$\frac{\partial^2}{\partial t \partial y}\bar{\Phi} = 0, \qquad y = \pm 1 \tag{2.60}$$

But in the z direction, according to assumption A6, the boundary conditions are

$$\frac{\partial}{\partial t}[\frac{\partial \Phi}{\partial z}] = \frac{\partial F}{\partial x} - \frac{\partial G}{\partial y} + 2zr_{\pm}\delta\nabla^2\Phi \qquad at \quad z = -\frac{1}{2},\ \frac{1}{2} \tag{2.61}$$

where

$$F = \Phi - z\frac{\partial \Phi}{\partial z} + \frac{\partial \Phi}{\partial y}\frac{\partial \Phi}{\partial z} \tag{2.62a}$$

$$G = \frac{\partial \Phi}{\partial x}\frac{\partial \Phi}{\partial z} \tag{2.62b}$$

and

$$\delta = \frac{E^{1/2}}{2\,\varepsilon}S, \tag{2.63}$$

the tracer r is defined as

$$r_{\pm} = \begin{cases} \gamma, & \text{at } z{=}\frac{1}{2},\ 0 < \gamma < 1, \\ 1, & \text{at } z{=}{-}\frac{1}{2}. \end{cases} \tag{2.64}$$

where γ is the measure of the asymmetry between the upper and lower Ekman layers. For $\gamma = 1$, equal strength Ekman layers are found at the top and bottom boundaries. In most of the our experiments we consider $\gamma \sim O(0.1)$.

2.2.3. Relevant Parameters

For a given Prandtl number, some of the key parameters used to describe a given experiment are the imposed thermal Rossby number,

$$R_{OT} = \frac{g\alpha d\Delta T}{4\Omega^2(b-a)^2}, \tag{2.65}$$

and the Taylor number,

$$\mathsf{T} = \frac{4\Omega^2 d^2}{\nu}, \tag{2.66}$$

the meaning of these terms can be inferred from Chapter I, but, we use a different length scale for Taylor number.

When the intensities of the two Ekman layers are specified and kept fixed, it is more convenient to select the following two parameters in our model to describe a given experiment: the stratification parameter,

$$S = \frac{N^2 H^2}{f^2 L^2} = \frac{g\alpha d\Delta T_v}{4\Omega^2(b-a)^2}, \tag{2.67}$$

and a measure of the Ekman layer dissipation at the lower boundary,

$$\delta = \frac{E^{1/2}}{2\varepsilon} S, \tag{2.68}$$

where ΔT_v is the interior vertical temperature difference, E is the Ekman number, $E = \nu/2\Omega H^2$, and ε is the Rossby number, $\varepsilon = U/2\Omega(b-a)$.

If we use the thermal wind as the scale of the basic flow, i.e., take

$$U = \frac{g\alpha d\Delta T_H}{2\Omega(b-a)}, \tag{2.69}$$

where ΔT_H is the interior horizontal temperature contrast, then

$$\varepsilon = \frac{g\alpha H \Delta T_H}{4\Omega^2(b-a)^2}, \tag{2.70}$$

Thus, ΔT_v and ΔT_H, which characterize the theoretical basic state, are set-up by intricate, and sometimes poorly understood, physical processes in these experiments. We will assume ΔT_v and ΔT_H to be known.

Observations show that $\Delta T_v \sim \Delta T$ and $\Delta T_H/\Delta T_v = \varepsilon_T << 1$. For the upper symmetric regime, ε_T does not vary too much as ΔT and Ω change (Peffer et al.[10], Barcilon[11]). We will treat this ratio ε_T as a constant; thus,

$$S = \frac{\varepsilon}{\varepsilon_T} \approx R_{0T} \tag{2.71}$$

and

$$\delta = \frac{E^{\frac{1}{2}}}{2\varepsilon_T} = \frac{\mathsf{T}^{-\frac{1}{4}}}{\varepsilon_T}, \tag{2.72}$$

Therefore, the two important parameters in our model, S and δ, are proportional to the two key parameters, R_{0T} and $\mathsf{T}^{-\frac{1}{4}}$, found in the annulus experiments.

CHAPTER III

NUMERICAL PROCEDURE AND PROGRAMMING

§3.1 Eiganfunction Expansion

The formulation of the nonlinear problem for this study has been derivated and discussed in the previous chapters. Because of the nonlinearity of the problem, it is impossible to find an analytical solution, and a computer aid solution is necessary. A spectral method was used in our study.

Spectral methods involves seeking the solution to a differential equation in terms of a series of known, smooth functions. They have recently emerged as a viable alternative to finite difference and finite element methods for the numerical solution of partial differential equations. The key recent advance was the development of transform methods for the efficient implementation of the spectral equations. Spectral methods have proved particularly useful in numerical fluid dynamics where large spectral hydrodynamics codes are now regularly used to study turbulence and transition, numerical weather prediction, and ocean dynamics[39].

In chapter II, the nonlinear problem was shown to consist of the following equations: the linear equation for the perturbation problem,

$$\frac{\partial^2\Phi}{\partial x^2} + \frac{\partial^2\Phi}{\partial y^2} + \frac{1}{S}\frac{\partial^2\Phi}{\partial z^2} = 0 \tag{3.1}$$

For the boundary condition in the y direction,

$$\frac{\partial\Phi}{\partial x} = 0 \qquad at \;\; y = \pm 1, \tag{3.2a}$$

$$\frac{\partial^2}{\partial t\partial y}\bar{\Phi} = 0, \qquad at \;\; y = \pm 1, \tag{3.2b}$$

where an overbar represents the averaging process

$$\overline{(\cdot)} = \lim_{x\to\infty} \frac{1}{2x} \int_x^x (.)dx$$

In the z direction,

$$\frac{\partial}{\partial t}[\frac{\partial \Phi}{\partial z}] = \frac{\partial F}{\partial x} - \frac{\partial G}{\partial y} + 2zr_{\pm}\delta\nabla^2\Phi \qquad at \quad z = -\frac{1}{2},\ \frac{1}{2} \tag{3.3}$$

where

$$F = \Phi - z\frac{\partial \Phi}{\partial z} + \frac{\partial \Phi}{\partial y}\frac{\partial \Phi}{\partial z}$$

$$G = \frac{\partial \Phi}{\partial x}\frac{\partial \Phi}{\partial z} \tag{3.4}$$

Viewing the above equations, we can see that the whole problem is a nonlinear problem. But equations (3.1) and(3.2) consistes of a linear problem, so, by separation of variables, we can get the corresponding eigenfunction. Then,by means of an eigenfunction expansion, the trunctated solution to the whole original nonlinear problem can be described as

$$\Phi = \sum_{\substack{k=k1 \\ k\neq 0}}^{k1} \sum_{l=1}^{L1} \{A_{k,l}(t)ch2\mu_{k,l}z + B_{k,l}(t)sh2\mu_{k,l}z\}\, e^{ikx} sin l\pi y$$

$$+ \sum_{l=1}^{L2} \{A_{0,l}(t)ch2\mu_{0,l}z + B_{0,l}(t)sh2\mu_{0,l}z\}\, \frac{cos l\pi y}{l\pi} \tag{3.5}$$

where $\mu_{k,l} = \{(k^2 + l^2\pi^2)s\}^{1/2}/2$, and the coefficients $(A_{-k,l}, B_{-k,l})$ are equal to $(A^*_{k,l}, B^*_{k,l})$ to insure that Φ is real, where the star * denotes the complex conjugate. The vertical structure of each component depends on the horizontal wavenumber, $(k^2 + l^2\pi^2)^{1/2}$, and on the stability parameter, S.

The time-dependent coefficients $A_{k,l}$ and $B_{k,l}$ are determined by use of the boundary conditions at $z = \pm\frac{1}{2}$.

Differentiating Φ with respect to x, y, z, and t, respectively,

$$\Phi_x = \frac{\partial\Phi}{\partial x} = \sum_{\substack{k=k1 \\ k\neq 0}}^{k1} \sum_{l=1}^{L1} a_1(k,l,t,z)e^{ikx} sin(l\pi y)ik \tag{3.6}$$

$$\Phi_{xx} = \frac{\partial^2\Phi}{\partial x^2} = \sum_{\substack{k=k1 \\ k\neq 0}}^{k1} \sum_{l=1}^{L1} a_1(k,l,t,z)e^{ikx} sin(l\pi y)(-k^2) \tag{3.7}$$

$$\Phi_y = \frac{\partial\Phi}{\partial y} = \sum_{\substack{k=k1 \\ k\neq 0}}^{k1} \sum_{l=1}^{L1} a_1(k,l,t,z)e^{ikx} cos(l\pi y)l\pi$$

$$+\sum_{l=1}^{L2} a_2(l,t,z)(-sin(l\pi y))l\pi \tag{3.8}$$

$$\Phi_{yy} = \frac{\partial^2\Phi}{\partial y^2} = \sum_{\substack{k=k1 \\ k\neq 0}}^{k1} \sum_{l=1}^{L1} a_1(k,l,t,z)e^{ikx} sin(l\pi y)(-l^2\pi^2)$$

$$+\sum_{l=1}^{L2} a_2(l,t,z)cos(l\pi y))(-l^2\pi^2) \tag{3.9}$$

$$\Phi_z = \frac{\partial\Phi}{\partial z} = \sum_{\substack{k=k1 \\ k\neq 0}}^{k1} \sum_{l=1}^{L1} a_5(k,l,t,z)e^{ikx} sin(l\pi y)$$

$$+\sum_{l=1}^{L2} a_6(l,t,z)cos(l\pi y) \tag{3.10}$$

$$\Phi_{zz} = \frac{\partial^2\Phi}{\partial z^2} = \sum_{\substack{k=k1 \\ k\neq 0}}^{k1} \sum_{l=1}^{L1} a_1(k,l,t,z)e^{ikx} sin(l\pi y)(4\mu_{k,l}^2) + \sum_{l=1}^{L2} a_2(l,t,z)cos(l\pi y)(4\mu_{0,l}^2) \tag{3.11}$$

in which

$$a_1(k,l,t,z) \equiv A_{k,l}(t)cosh(2\mu_{k,l}z) + B_{k,l}(t)sinh(2\mu_{k,l}z)$$

$$a_2(l,t,z) \equiv [A_{0,l}(t)cosh(2\mu_{0,l}z) + B_{0,l}(t)sinh(2\mu_{0,l}z)]/l\pi$$

$$a_3(k,l,t,z) \equiv \frac{dA_{k,l}(t)}{dt}cosh(2\mu_{k,l}z) + \frac{dB_{k,l}(t)}{dt}sinh(2\mu_{k,l}z)$$

$$a_4(l,t,z) \equiv [\frac{dA_{0,l}(t)}{dt}cosh(2\mu_{0,l}z) + \frac{dB_{0,l}(t)}{dt}sinh(2\mu_{0,l}z)]/l\pi$$

$$a_5(k,l,t,z) \equiv [A_{k,l}(t)sinh(2\mu_{k,l}z) + B_{k,l}(t)cosh(2\mu_{k,l}z)]2\mu_{k,l}$$

$$a_6(l,t,z) \equiv [A_{0,l}(t)sinh(2\mu_{0,l}z) + B_{0,l}(t)cosh(2\mu_{0,l}z)]2\mu_{0,l}/l\pi$$

and

$$\frac{\partial\Phi_z}{\partial t} = \sum_{\substack{k=k1\\k\neq 0}}^{k1}\sum_{l=1}^{L1}[\frac{dA_{k,l}(t)}{dt}sinh(2\mu_{k,l}z) + \frac{dB_{k,l}(t)}{dt}cosh(2\mu_{k,l}z)]e^{ikx}sin(l\pi y)2\mu_{k,l}$$

$$+\sum_{l=1}^{L2}[\frac{dA_{0,l}(t)}{dt}sinh(2\mu_{0,l}z) + \frac{dB_{0,l}(t)}{dt}cosh(2\mu_{0,l}z)]\frac{cos(l\pi y)}{l\pi}2\mu_{0,l} \qquad (3.12)$$

Substituting equations (3.5) through (3.12) into equation (3.3) gives

$$\sum_{\substack{k=k1\\k\neq 0}}^{k1}\sum_{l=1}^{L1}[\frac{dA_{k,l}(t)}{dt}sinh(2\mu_{k,l}z) + \frac{dB_{k,l}(t)}{dt}cosh(2\mu_{k,l}z)]e^{ikx}sin(l\pi y)2\mu_{k,l}$$

$$+\sum_{l=1}^{L2}[\frac{dA_{0,l}(t)}{dt}sinh(2\mu_{0,l}z) + \frac{dB_{0,l}(t)}{dt}cosh(2\mu_{0,l}z)]\frac{cos(l\pi y)}{l\pi}2\mu_{0,l}$$

$$= \frac{\partial F}{\partial x} - \frac{\partial G}{\partial y} + 2zr_{\pm}\delta[\sum_{\substack{k=k1\\k\neq 0}}^{k1}\sum_{l=1}^{L1}a_1(k,l,t,z)e^{ikx}sin(l\pi y)(-k^2 - l^2\pi^2)$$

$$+\sum_{l=1}^{L2}a_2(l,t,z)cos(l\pi y))(-l^2\pi^2)] \quad at \;\; z = \pm\frac{1}{2} \qquad (3.13)$$

Multiplying both sides of the equation (3.13) by $e^{-ikx}sin(l\pi y)$ and integrating by parts with respect to x and y, the following expression are obtained:

$$\frac{\pm dA_{k,l}(t)}{dt}sinh(\mu_{k,l}) + \frac{dB_{k,l}(t)}{dt}cosh(\mu_{k,l})$$

$$= \frac{1}{2\pi\mu_{k,l}} \int_{-\pi}^{\pi} \int_{0}^{1} (\frac{\partial F}{\partial x} - \frac{\partial G}{\partial y})|_{z=\pm\frac{1}{2}} e^{ikx} sin(l\pi y) dx dy$$

$$+ \frac{2\mu_{k,l}\delta r_\pm}{S} [\mp A_{k,l}(t) cosh(\mu_{k,l}) - B_{k,l}(t) sinh(\mu_{k,l})], \qquad at \;\; z = \pm\frac{1}{2}$$

Solving these two equations yields

$$\frac{dA_{k,l}(t)}{dt} = \frac{\theta_{i+}(k,l) - \theta_{i-}(k,l)}{2sinh(\mu_{k,l})} + \theta_{vA}(k,l) \tag{3.14}$$

$$\frac{dB_{k,l}(t)}{dt} = \frac{\theta_{i+}(k,l) + \theta_{i-}(k,l)}{2cosh(\mu_{k,l})} + \theta_{vB}(k,l) \tag{3.15}$$

where

$$\theta_{i\pm}(k,l) \equiv \frac{1}{2\pi\mu_{k,l}} \int_{-\pi}^{\pi} \int_{0}^{1} (\frac{\partial F}{\partial x} - \frac{\partial G}{\partial y})|_{z=\pm\frac{1}{2}} e^{ikx} sin(l\pi y) dx dy \qquad (k \neq 0) \tag{3.16}$$

$$\theta_{vA}(k,l) \equiv -\frac{\mu_{k,l}\delta}{Ssinh(\mu_{k,l})} [(r_+ + r_-) cosh(\mu_{k,l}) A_{k,l}(t)$$

$$+ (r_+ - r_-) sinh(\mu_{k,l}) B_{k,l}(t)] \quad (k \neq 0) \tag{3.17a}$$

$$\theta_{vB}(k,l) \equiv -\frac{\mu_{k,l}\delta}{Scosh(\mu_{k,l})} [(r_+ - r_-) cosh(\mu_{k,l}) A_{k,l}(t)$$

$$+ (r_+ + r_-) sinh(\mu_{k,l}) B_{k,l}(t)] \quad (k \neq 0) \tag{3.17b}$$

To deal with the situation for the wave number $k = 0$, i.e. the mean flow correction, multiply both sides of the equation (3.13) by $cos(l\pi y)$ and integrate by parts with respect to x and y. The following expressions are obtained:

$$\frac{\pm dA_{0,l}(t)}{dt} sinh(\mu_{0,l}) + \frac{dB_{0,l}(t)}{dt} cosh(\mu_{0,l})$$

$$= \frac{l}{2\mu_{0,l}} \int_{-\pi}^{\pi} \int_{0}^{1} (\frac{\partial F}{\partial x} - \frac{\partial G}{\partial y})|_{z=\pm\frac{1}{2}} cos(l\pi y) dx dy$$

$$\mp \frac{2\mu_{0,l}\delta r_\pm}{S} [A_{0,l}(t) cosh(\mu_{0,l}) \pm B_{0,l}(t) sinh(\mu_{0,l})]$$

Solving the above two equations yields, similarly to the case for $k \neq 0$,

$$\frac{dA_{0,l}(t)}{dt} = \frac{\theta_{i+}(0,l) - \theta_{i-}(0,l)}{2sinh(\mu_{0,l})} + \theta_{vA}(0,l) \tag{3.18}$$

$$\frac{dB_{0,l}(t)}{dt} = \frac{\theta_{i+}(0,l) + \theta_{i-}(0,l)}{2cosh(\mu_{0,l})} + \theta_{vB}(0,l) \tag{3.19}$$

where

$$\theta_{i\pm}(0,l) \equiv \frac{l}{2\mu_{0,l}} \int_{-\pi}^{\pi} \int_{0}^{1} (\frac{\partial F}{\partial x} - \frac{\partial G}{\partial y})|_{z=\pm\frac{1}{2}} cos(l\pi y) dx dy \tag{3.20}$$

$$\theta_{vA}(0,l) \equiv -\frac{\mu_{0,l}\delta}{Ssinh(\mu_{0,l})}[(r_+ + r_-)cosh(\mu_{0,l})A_{0,l}(t)$$

$$+(r_+ - r_-)sinh(\mu_{0,l})B_{0,l}(t)] \tag{3.21a}$$

$$\theta_{vB}(0,l) \equiv -\frac{\mu_{0,l}\delta}{Scosh(\mu_{0,l})}[(r_+ - r_-)cosh(\mu_{0,l})A_{0,l}(t)$$

$$+(r_+ + r_-)sinh(\mu_{0,l})B_{0,l}(t)] \tag{3.21b}$$

Therefore, the final equations for all coefficients in the eiganfunction expansion solution have been created. They are a set of simultaneous ordinary differential equations. All coefficients $A_{k,l}(t)$ and $B_{k,l}(t)$ are function of time and can be obtained by time integrating Equations (3.14) through (3.21).

§ 3.2 Numerical procedure

After applying the eiganvalue expansion and the subsequent manipulation as discussed in the last section, a set of coupled ordinary differential equations are obtained. In this section, the numerical procedure for integrating this set of equations is discussed.

3.2.1 Discretization

Applying the Discrete Fourier Transformation (DFT) technique[40][41] to Equation (3.5), and the following expressions are obtained

$$\Phi(m,n) = \sum_{\substack{k=k1\\k\neq 0}}^{k1}\sum_{l=1}^{L1}[A_{k,l}(t)Cosh(2\mu_{k,l}z) + B_{k,l}(t)Sinh(2\mu_{k,l}z)]e^{ik\frac{2\pi}{M}m}sin(l\pi\frac{n}{N})$$

$$+\sum_{l=1}^{L2}[A_{0,l}(t)Cosh(2\mu_{0,l}z) + B_{0,l}(t)Sinh(2\mu_{0,l}z)]\frac{cos(l\pi\frac{n}{N})}{l\pi} \tag{3.22}$$

$$m = 1,2,.....M \qquad\qquad n = 1,2,.....N$$

where M and N are the number of grid points in x and y direction, respectively.

Similarly, the DFTs for Φ_x, Φ_y and Φ_z are given by

$$\Phi_x(m,n) = \sum_{\substack{k=k1\\k\neq 0}}^{k1}\sum_{l=1}^{L1}a_1(k,l,t,z)e^{ik\frac{2\pi}{M}m}sin(l\pi\frac{n}{N})\bullet ik \tag{3.23}$$

$$\Phi_y(m,n) = \sum_{\substack{k=k1\\k\neq 0}}^{k1}\sum_{l=1}^{L1}a_1(k,l,t,z)e^{ik\frac{2\pi}{M}m}cos(l\pi\frac{n}{N})\bullet l\pi$$

$$+\sum_{l=1}^{L2}a_2(l,t,z)(-sinl\pi\frac{n}{N})\bullet l\pi \tag{3.24}$$

$$\Phi_z(m,n) = \sum_{\substack{k=k1\\k\neq 0}}^{k1}\sum_{l=1}^{L1}a_5(k,l,t,z)e^{ik\frac{2\pi}{M}m}sin(l\pi\frac{n}{N})$$

$$+\sum_{l=1}^{L2}a_6(l,t,z)cos(l\pi\frac{n}{N}) \tag{3.25}$$

For the numerical calculation, Equation (3.4) with the aid of Equation (3.22)-(3.25) are used to compute the DFT of F and G. Thus

$$F(n,m) = \Phi(n,m) - [z - \Phi_y(n,m)]\Phi_z(n,m) \tag{3.26}$$

$$G(n,m) = \Phi_x(n,m)\Phi_z(n,m). \tag{3.27}$$

According to Equations (3.14)-(3.21), the inverse DFTs of F(n,m) and G(n,m) for the double integral Equations (3.16) and (3.20)are given by

$$\theta_{\pm}(k,l) = \frac{1}{MN\mu_{k,l}} \sum_{\substack{k=k1 \\ k\neq 0}}^{k1} \sum_{l=1}^{L1} ikF(m,n)sin(l\pi\frac{n}{N})$$

$$+l\pi\sum_{l=1}^{L2} G(m,n)cos(l\pi\frac{n}{N})\}e^{-ik\frac{2\pi}{M}m} \quad k \neq 0 \tag{3.28}$$

$$\theta_{\pm}(0,l) = -\frac{l^2\pi^2}{MN\mu_{0,l}}\{\sum_{\substack{k=k1 \\ k\neq 0}}^{k1} \sum_{l=1}^{L1} G(m,n)sin(l\pi\frac{n}{N})\} \tag{3.29}$$

Once $\theta_{\pm}(k,l)$ has been determined, dA/dt and dB/dt can be found from Equations (3.14) to (3.21). Up to here, we can use Merson scheme to integrate the ordinary differential equations to get $A_{k,l}(t)$ and $B_{k,l}(t)$.

3.2.2. Merson Scheme

In practice, there is no single numerical method which is applicable to every differential equation, or which is best possible for every member of even the much smaller class of ordinary linear equations. The field is very large, and for the most economic use of the computing machine, coupled with the necessity for producing accurate answers, a variety of methods, each appropriate to its particular and rather small class of problems are used. Usually, the speed, convenience and accuracy are three points for comparing the merits and demerits of the numerical methods.

By accuracy, it means the difference between the true solution of the problem and the computed approximation, and the aim is to limit the discrepancy to the amount justified in the particular context, and to know that this has been achieved. Speed and convenience are more difficult to define. They include both the human programming time and the machine computing time, and the latter will also depend upon the size of its storage.

We should select the available numerical procedure which is believed to be best for this problem. Here we select the Merson scheme [42–44] to be our integrating scheme which may varies time step automatically to ensure a given accuracy (see appendix A).

§3.3 Computer Program

In order to visualize the numerical calculation process more clearly, the flow diagram is shown in Figure 3-1, which is written in a form valid for the general purpose. The program is written in FORTRAN language.

Step 1. Call system to assign one INPUT file and one OUTPUT file. It is more convenient to adjust the input parameters instead of changing the original source program. Output file is used for a systematic data plot and analysis after the computer run for each conditions.

Step 2. Call subroutine INPUT. All required parameters in the calculation are stored in the INPUT, which includes the maximum time interval, total time length, meridional mode and zonal wave number, Ekman layer dissipation, Ekman layer asymmetry tracer and stratification factor.

Step 3. Calculate the coefficients in the linear relationship by using Equation(1-6) in appendix B.

Step 4. Giving initial conditions. As a time-dependent problem, a initial condition is necessary. In this work, we give different initial conditions for the

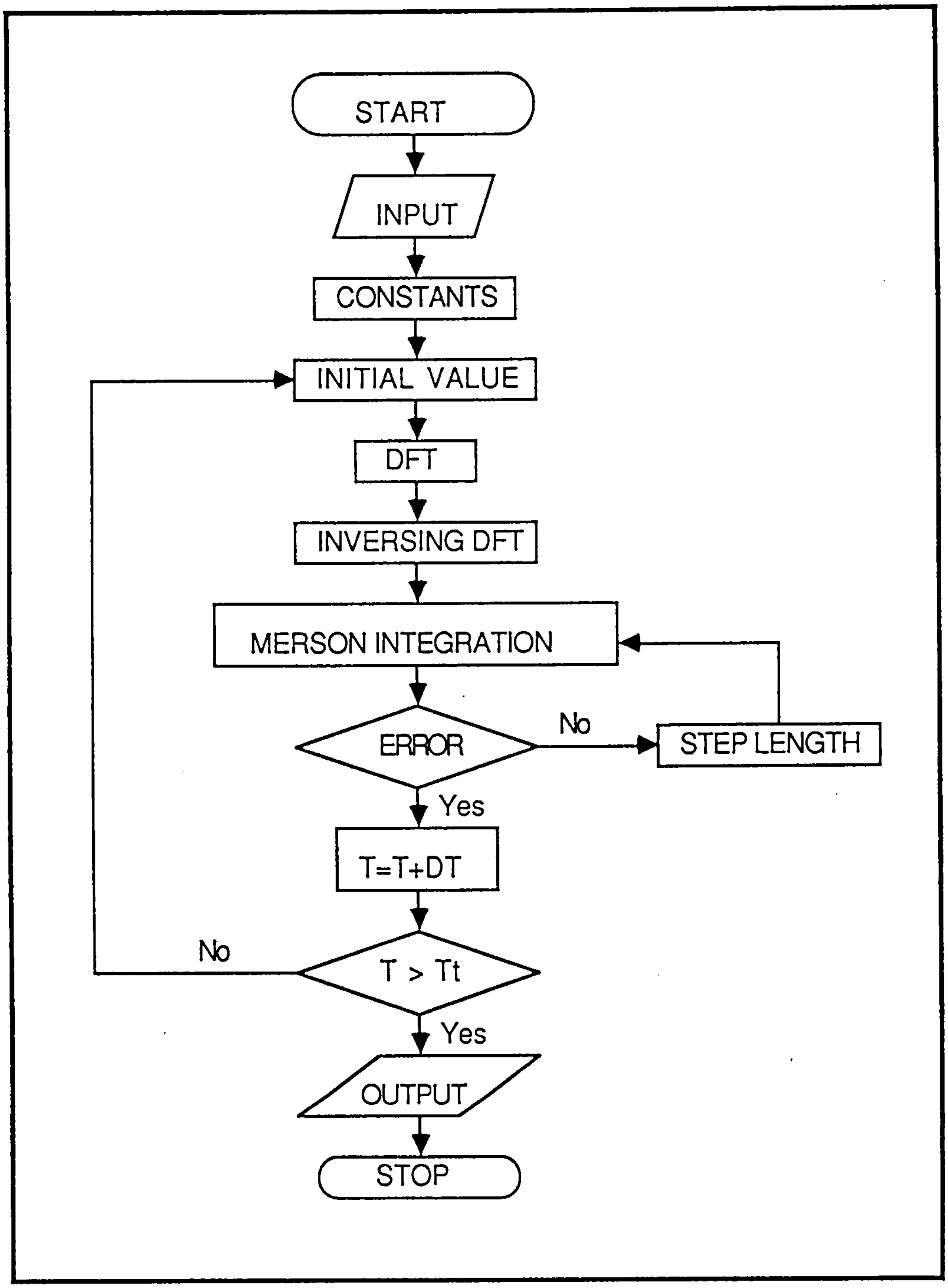

Fig. 3-1. Flow diagram of computational process

$A_{k,l}(0)$, and the $B_{k,l}(0)$ are calculated from the linear relation, i.e., equation (4.2) and (4.3) (see chapter II), so that the initial wave state can be described by the linear dynamics.

In addition, to avoid repeat calculation of the eiganfunction values at the grid point or zonal wave number and meridional mode number, a common matrix is used and prevalued in this subroutine.

Step 5. Look for the streamfunction from the above initial value by using DFT technique, from which F(M,N) and G(M,N) are found.

Step 6. Find the right hand side term of the differential equation from the inverse DFT of F and G.

Step 7. Use the Merson scheme to integrate one time step, a updated time step solution is obtained.

Step 8. Estimate errors by a general trunction error formula.

Step 9. Error criterion:

If the error falls into the given error margin, start a new time step solution by going back to step 5 and using the previous step solution as the new step initial value and keeping the same time step length;

If the error is greater than the upper limit of the given margin, the time step length will be reduced to half of the previously used one and go back to step 7;

If the error is smaller than the lower limit of the given margin, the time step length will be doubled and go back to step 7.

For the later two cases, the process will continue until the error falls into the given margin. Otherwise, a given maximum and minimum time step length will be adopted.

Step 10. Look for the time change rate of wave components, together with corresponding wave components, to plot the phase diagrams.

Step 11. Check the total time. If a given time length is reached, the program will stop; otherwise continue the integrating process.

Step 12. Output the results for each time step, which include wave components, the time rate change of the wave components and streamfunction used for the final display of the results.

CHAPTER IV

COMPUTATIONAL RESULTS AND DISCUSSION

All the calculations for the results of this section were performed partially on a VAX-11/785 computer at the University of Tennessee Space Institute (UTSI) and partially on the NASA/MSFC-Cray XMP Computer at Huntsville, Alabama. The computations are divided into three parts. The first part deals with the linear analysis; the second and the third parts discuss the inviscid nonlinear and viscous nonlinear analysis, respectively.

§4.1. Linear Analysis of the Stability

Before examining the nonlinear system, a linear approximation is made to provide a low accuracy solution and to gain some physical guide to further numerical experiments.

In the linear analysis, the instability of the basic, baroclinic flow is discussed when a small perturbation with single zonal wavenumber and single meridional mode is introduced. The effects of stratification, S, and dissipation, δ, on the wave selection are discussed separately.

The baroclinic stability of the basic zonal flow, $\bar{\psi} = -yz$, can be tested directly. If a perturbation with a wavenumber equal to k and a mode number equal to l is applied to this basic state, the linear stability problem obtained from Equations (3.14) through (3.21) becomes

$$\begin{aligned}\frac{dA_{k,l}(t)}{dt} &= -\alpha_1 A_{k,l}(t) + (\alpha_2 + i\alpha_3)B_{k,l}(t) \\ \frac{dB_{k,l}(t)}{dt} &= -\alpha_4 B_{k,l}(t) + (\alpha_5 + i\alpha_6)A_{k,l}(t)\end{aligned} \tag{4.1}$$

where the coefficients α_k are defined in appendix B.

Let

$$B_{k,l}(t) = \Lambda A_{k,l}(t) \tag{4.2}$$

and solving for Λ, it can be shown that

$$\Lambda = \frac{1}{2(\alpha_2 + i\alpha_3)}\{\alpha_1 - \alpha_4 \pm [(\alpha_1 - \alpha_4)^2 + 4(\alpha_5 + i\alpha_6)(\alpha_2 + i\alpha_3)]^{1/2}\}, \tag{4.3}$$

and upon substituting (4.2) and (4.3) into (4.1), we obtain

$$\frac{dA_{k,l}(t)}{dt} = \sigma_{k,l}A_{k,l}(t) = (kc_i - ikc_r)A_{k,l}(t) \tag{4.4}$$

where

$$\sigma_{k,l} = -\alpha_1 + \Lambda(\alpha_2 + i\alpha_3) \tag{4.5}$$

and kc_i, ikc_r are the linear growth rate and phase speed, respectively.

From Equation (4.5), the real part of sigma equals zero, i.e. $\sigma_r = 0$ is the marginal stability criterion. By manipulation, the neutral curve can be obtained in the following form:

$$\delta = \frac{k}{k^2 + l^2\pi^2}\{\frac{Y(\mu(k,l,S)}{\gamma}\}^{1/2} \tag{4.6}$$

where

$$Y(\mu(k,l,S)) = \frac{[1 - \mu(k,l,S)th(\mu(k,l,S))][\mu(k,l,S) - th(\mu(k,l,S))]}{th(\mu(k,l,S))}$$
$$+ \left(\frac{1-\gamma}{1+\gamma}\right)^2 [\frac{2th(\mu(k,l,S)}{1 + th(\mu(k,l,S))} - \mu(k,l,S)] \tag{4.7}$$

while the linear growth rate and phase speed are:

$$kc_i = Re\{-\frac{1}{2}(\alpha_1 + \alpha_4) \pm \frac{1}{2}\sqrt{(\alpha_1 - \alpha_4)^2 + 4(\alpha_2 + i\alpha_3)(\alpha_5 + i\alpha_6)}\} \tag{4.8}$$

$$ikc_r = Im\{-\frac{1}{2}(\alpha_1 + \alpha_4) \pm \frac{1}{2}\sqrt{(\alpha_1 - \alpha_4)^2 + 4(\alpha_2 + i\alpha_3)(\alpha_5 + i\alpha_6)}\} \tag{4.9}$$

Since the problem is treated as linear, there is no coupling between the different wave numbers and mode numbers and each can be considered separately.

There are five parameters, namely k, l μ(or S), γ, and δ in Equation (4.6). Whenever four of these parameters are prescribed, the remaining value is the critical one given by equation (4.6). Thus, if we fix k, l, and γ Equation (4.6) gives the relationship between S and δ for the marginal curve.

Figure 4-1 shows two set of marginal curves for the modes 1 and 2, in the δ-S plane, when γ is fixed and k=1, 2, 3, 4, 5 and 6. Some of the two sets of curves cross; but, at least in the physical space, there is no parameter setting for which both modes with the same k are marginally unstable.

For fixed k, l, and γ, we find that $Y(\mu)$ has a maximum (see Figure 4-2) and so does δ_c. Only when $\delta < \delta_{c_{max}}$, are there two critical values of S that correspond to two points on the upper and lower marginal curves, respectively. When $\delta < \delta_{c_{max}}$, the flow is stable. Equation (4.6) shows that $\delta_{c_{max}}$ increases when γ decreases. Figure 4.3(a,b) shows different marginal curves for the case of $\gamma = 0.5$ and $\gamma = 1.0$. These suggest that the Ekman layer asymmetry has a destablizing effect, for it extends the range of the unstable waves and increases the growth rate of these waves by modifying the marginal curves in the parameter space.

In what follows we let $\gamma = 0.1$. Then, the most unstable wavenumber depends on the location of the representative point in the δ-S plane. Figure 4-4 shows the linear growth rates and phase speeds for different zonal wavenumbers, k, and for meridional wavenumbers l=1,2 and for S=0.1 and $\delta = 0.01$. For this parameter setting, the most unstable zonal wavenumber for the $sin\pi y$-mode is k=5. The abscissa represents the observed wavenumbers which are necessarily integers. To investigate the effects of S and δ on the wave selection, we consider representative points along two perpendicular lines crossing at the point S=0.1 and $\delta = 0.01$ in

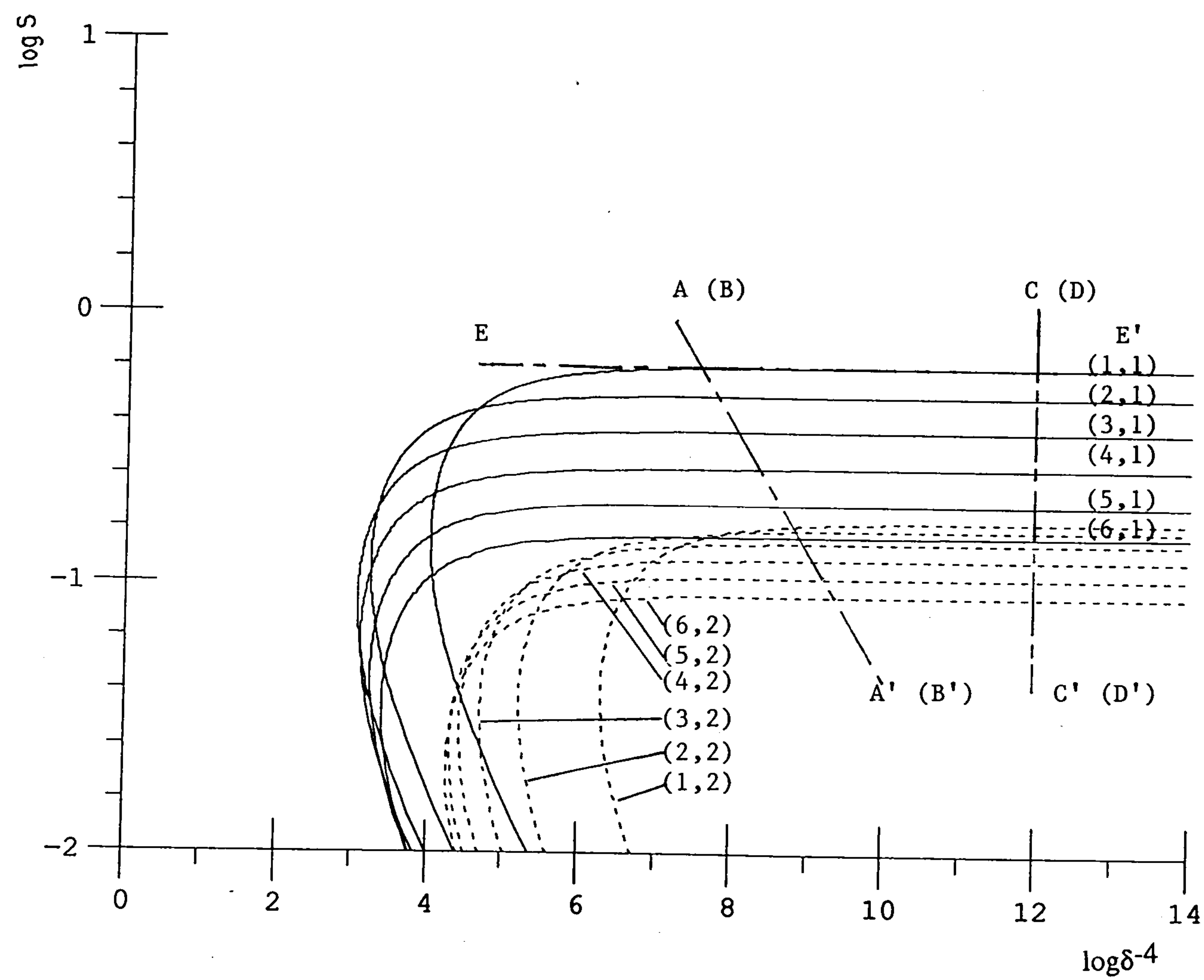

Fig. 4-1. Marginal curves on S-δ plane for $\gamma = 0.1$.

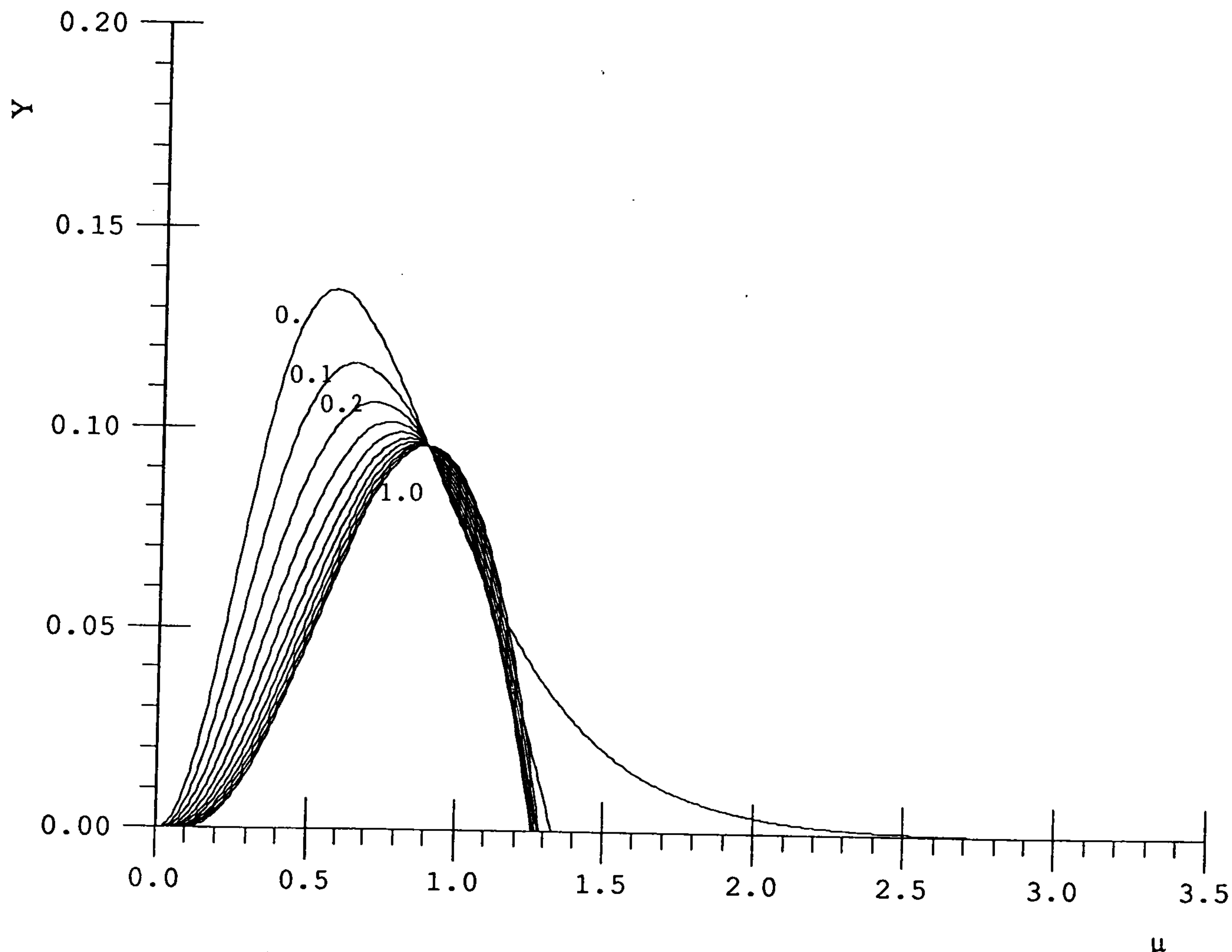

Fig. 4-2. $Y(\mu)$ vs μ for different γ with an increment 0.1.

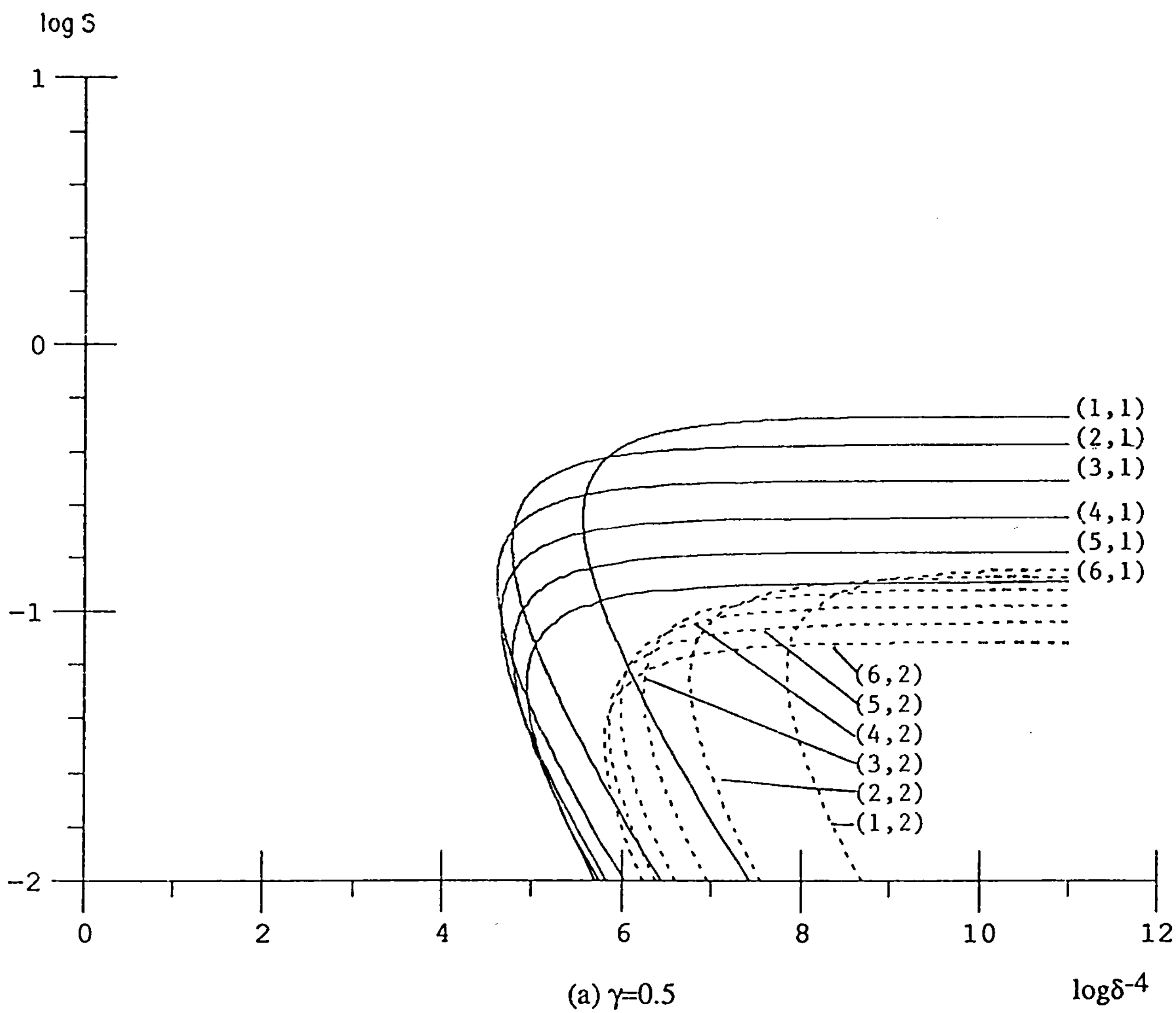

(a) γ=0.5

Fig. 4-3. Marginal curves

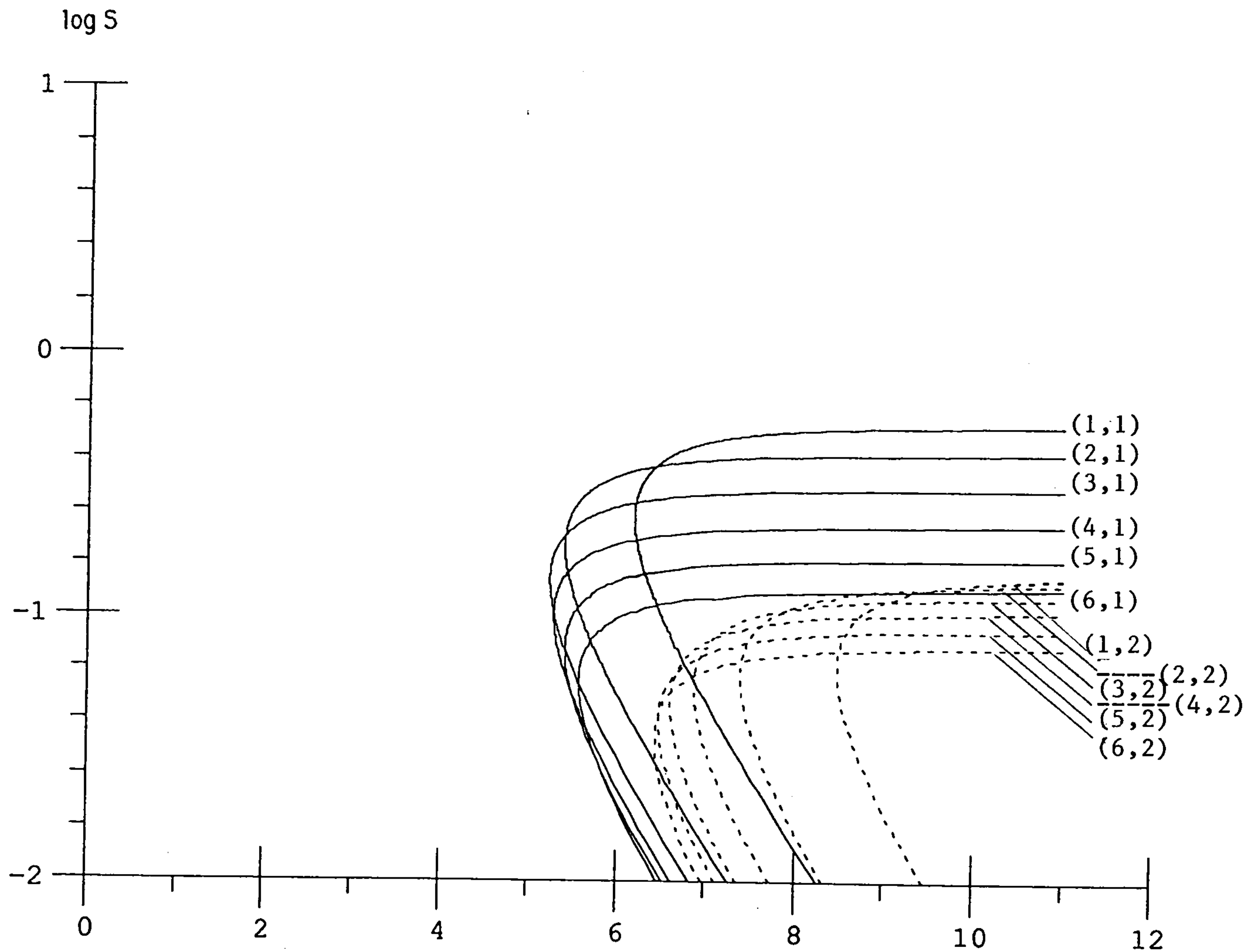

(b) γ=1.0

Fig. 4-3. Continue

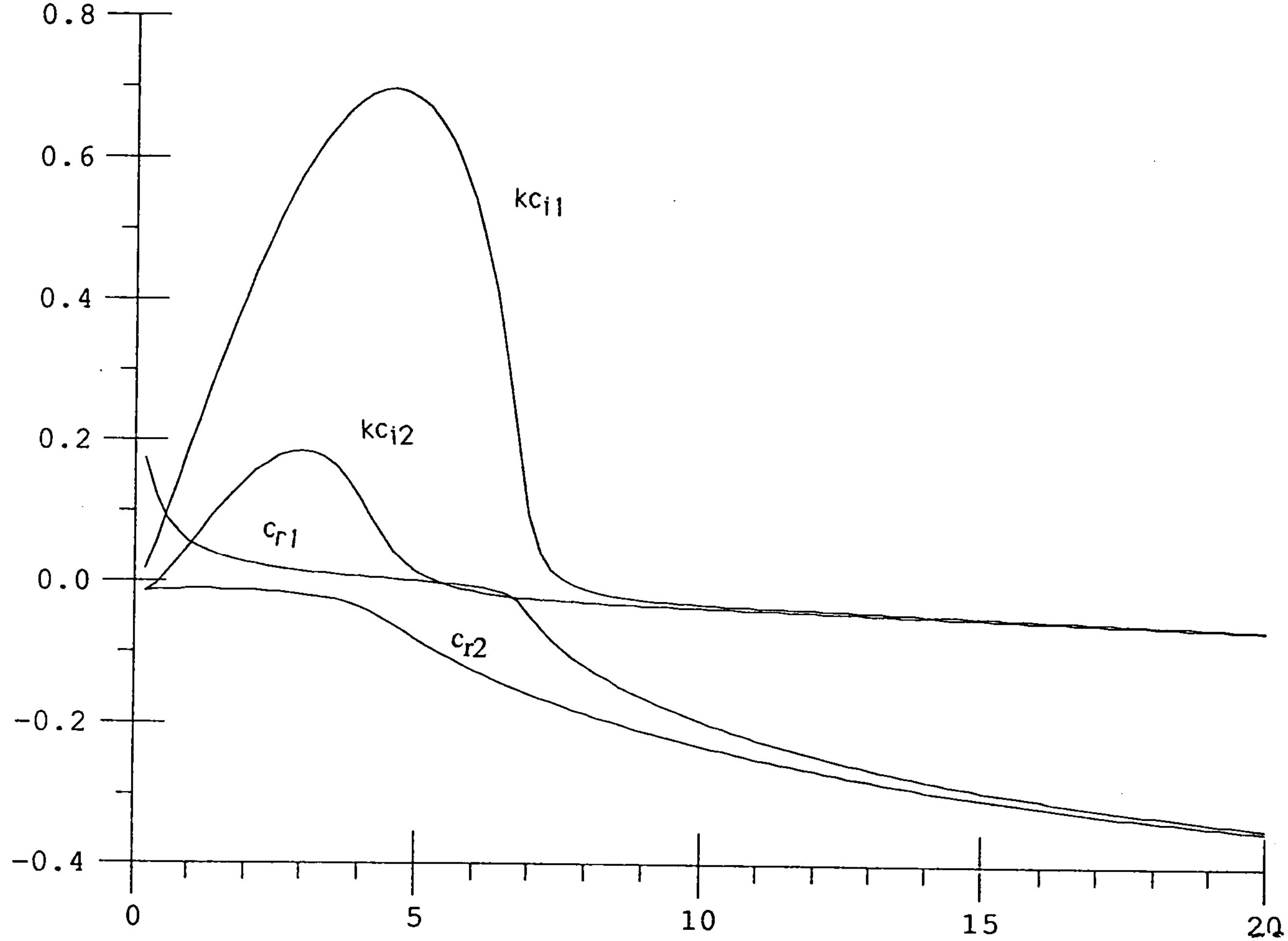

Fig. 4-4. Linear growth rates and phase speed of $\sin\pi y$ and $\sin 2\pi y$-mode,

$S=0.1$, $\delta=0.01$, $\gamma=0.1$

the δ-S plane. We then calculate the linear growth rates for wavenumber from 1 to 10 along these lines, respectively.

As shown in Figure 4-5 for a fixed S, as δ changes, the most unstable wavenumber will not change significantly. The most unstable wavenumber is still k=5 in most of the region where $\delta < \delta_c$, except in a small region near δ_c where the most unstable wavenumber is k=4. This means that the most unstable wavenumber is almost the same for fluids with different viscosity when the imposed temperature difference and rotation rate are fixed. Basically, the Ekman dissipation does not affect the wave selection, but it does affect the growth rates of all the unstable modes. Figure 4-6 shows that the most unstable wavenumber becomes larger and larger as S decreases, implying that the higher wavenumbers form more readily in a wide annulus than in a narrow annulus when the fluid depth, rotation rate, dissipation and the imposed temperature difference are fixed, since S $\propto (b-a)^{-2}$. When the rotation rate is fixed, higher wavenumbers will occur at the lower imposed temperature difference for the same annulus geometry with the same fluid, since $S \propto \Delta T$.

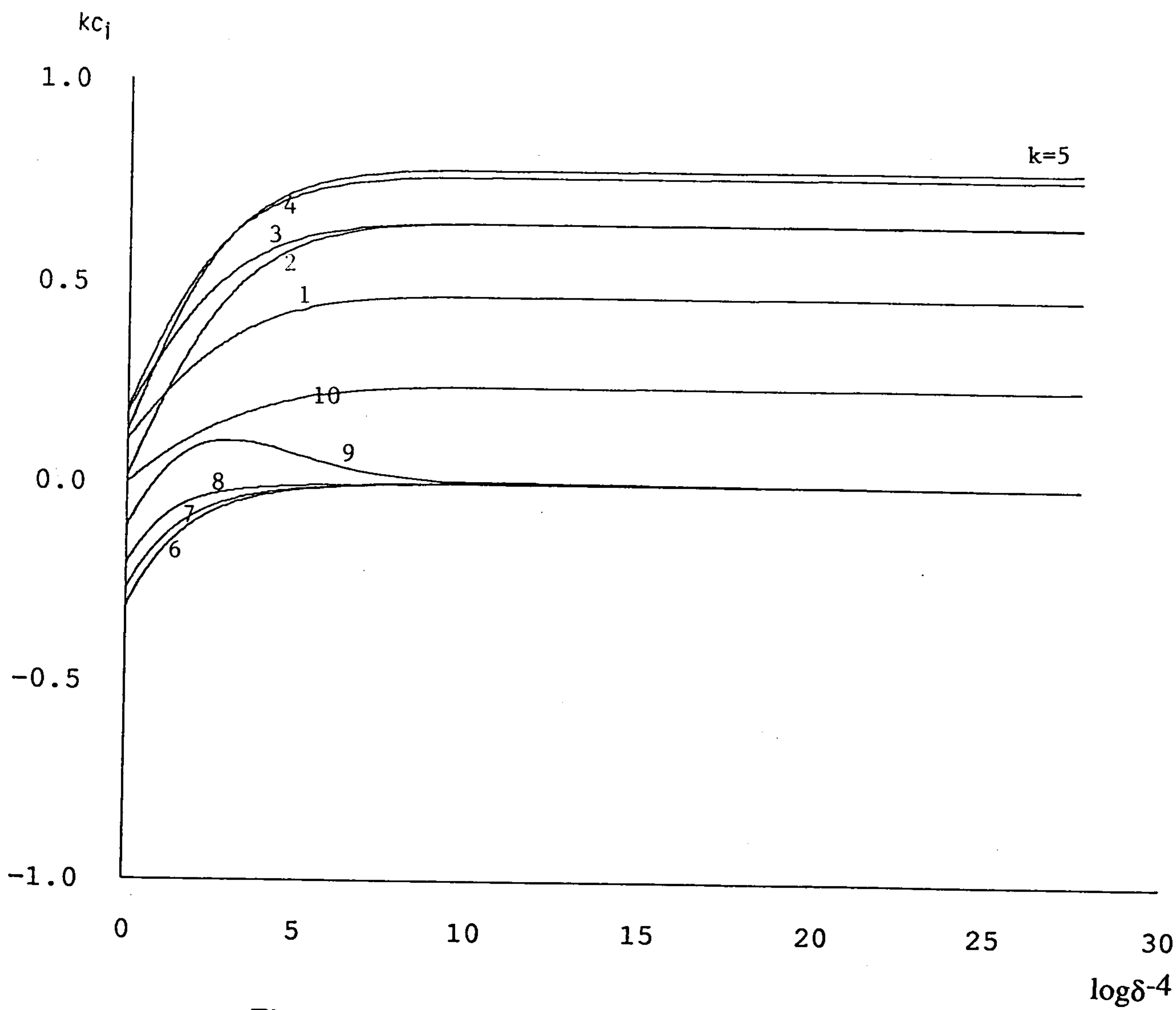

Fig. 4-5. Linear growth rates of the $\sin\pi y$-mode vs $\log\delta^{-4}$

$S=0.1, \gamma = 0.1.$

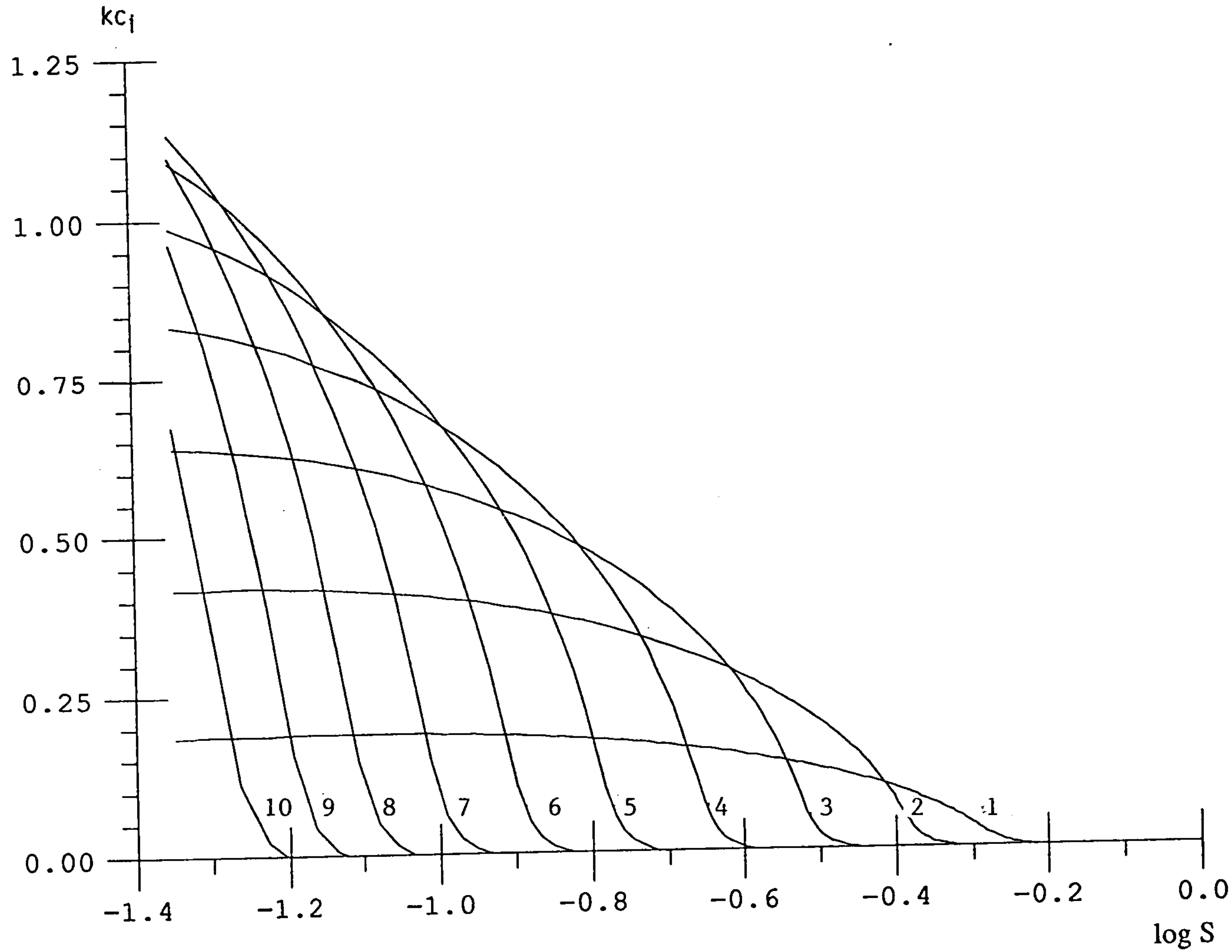

Fig. 4-6. Linear growth rates of the $\sin\pi y$-mode vs logS,

δ=0.01, $\gamma = 0.1$.

§4.2. Nonlinear analysis

For the initial value integration, Merson scheme was used in the numerical calculations with an initial time step t=0.02. The practical step length can vary automatically to ensure a given accuracy. All the results presented in this work has an absolute truncation error of 1.0×10^{-7}. This error value was obtained by testing several values and finding no significant change in the numerical solution if the error goes down further. The initial values for $A_{k,1}(t)$ and $A_{k,2}(t)$ were specified, and $B_{k.1}(0)$ and $B_{k,2}(0)$ are calculated by using Equations (4.2), (4.3) so that the initial wave state is described by the linear dynamics. In the viscous flow analysis, the parameter which reflect the asymmetry between the two Ekman layers is chosen such that $\gamma = 0.1$ for all cases, i.e. the dissipation in the upper layer is ten times weaker than that in the lower layer. This value was chosen so as to bring the model closer to atmospheric dynamics.

4.2.1 Analysis of inviscid nonlinear instability

For the physical model described in chapter II, a linear analytical study has been persuade in section 4.1. In this section the nonlinear stability characteristics are first examined without the effects of dissipation, i.e., for a completely inviscid problem. The model employed here consists of an inviscid homogeneous incompressible fluid with variable density where the lighter fluid is above and rotating with an angular velocity, Ω.

Under the above approximation, the governing equations are reduced to:

$$\frac{\partial^2 \Phi}{\partial z^2} + S[\frac{\partial^2 \Phi}{\partial x^2} + \frac{\partial^2 \Phi}{\partial y^2}] = 0 \tag{4.10}$$

$$\frac{\partial \Phi}{\partial x} = \frac{\partial^2 \Phi}{\partial y \partial t} = 0 \qquad at \quad y = 0, \;\; 1. \tag{4.11}$$

$$\frac{\partial}{\partial t}\left[\frac{\partial \Phi}{\partial z}\right] = \frac{\partial F}{\partial x} - \frac{\partial G}{\partial y} \qquad at \quad z = -\frac{1}{2}, \ \frac{1}{2} \tag{4.12}$$

It can be seen that the only difference between this set of governing equations and the one for the full equations is in the boundary condition in the z-direction. Even though an inviscid fluid is taken into consideration, the formulation is still nonlinear, so the solution can only be found by numerical integration.

In a series of numerical experiments, the three lowest wave numbers, i.e., wave number k=1, 2, 3, with two meridional modes for the perturbations $\sin\pi y$ and $\sin 2\pi y$ and four meridional modes for the mean flow correction are considered. Only the initial values for the principal mode amplitudes $A_{3,1}(0)$ and $A_{3,2}(0)$ are varied, while the other modes are set at zero amplitude initially. In these numerical experiments, we fix the stratification parameter, S at S=0.65.

Figure 4-7 shows the time development of the wave for different initial conditions for $A_{3,1}(0)$ and $A_{3,2}(0)$ and in Figure 4-7(a) $A_{3,1}(0)$=0.01, $A_{3,2}(0)$=0.01i, and in Figure 4-7(b) $A_{3,1}(0)$=0.02, $A_{3,2}(0)$=0.01i. It can be seen that the wave goes through an amplitude vacillation cycle, and finally, the wave reaches an irregular state. The structure of the wave and the time at which the irregular solution sets in, t_b, depends on the specified initial conditions. The phase diagram for the wave amplitude evolution for the same initial conditions as in Figure 4-7 (a) (b) are presented in Figure 4-8 (a) (b). It is clearly seen that the phase diagram has good periodicity up to t_b, but a random state is found for time greater than t_b. Strictly speaking, Figure 4-8 shows a broadening of the amplitude period with time for $t < t_b$ indicating that the wave is not exactly periodic. Thus the amplitude undergoes a slight variation in periodicity with time for the time period t: $t < t_b$.

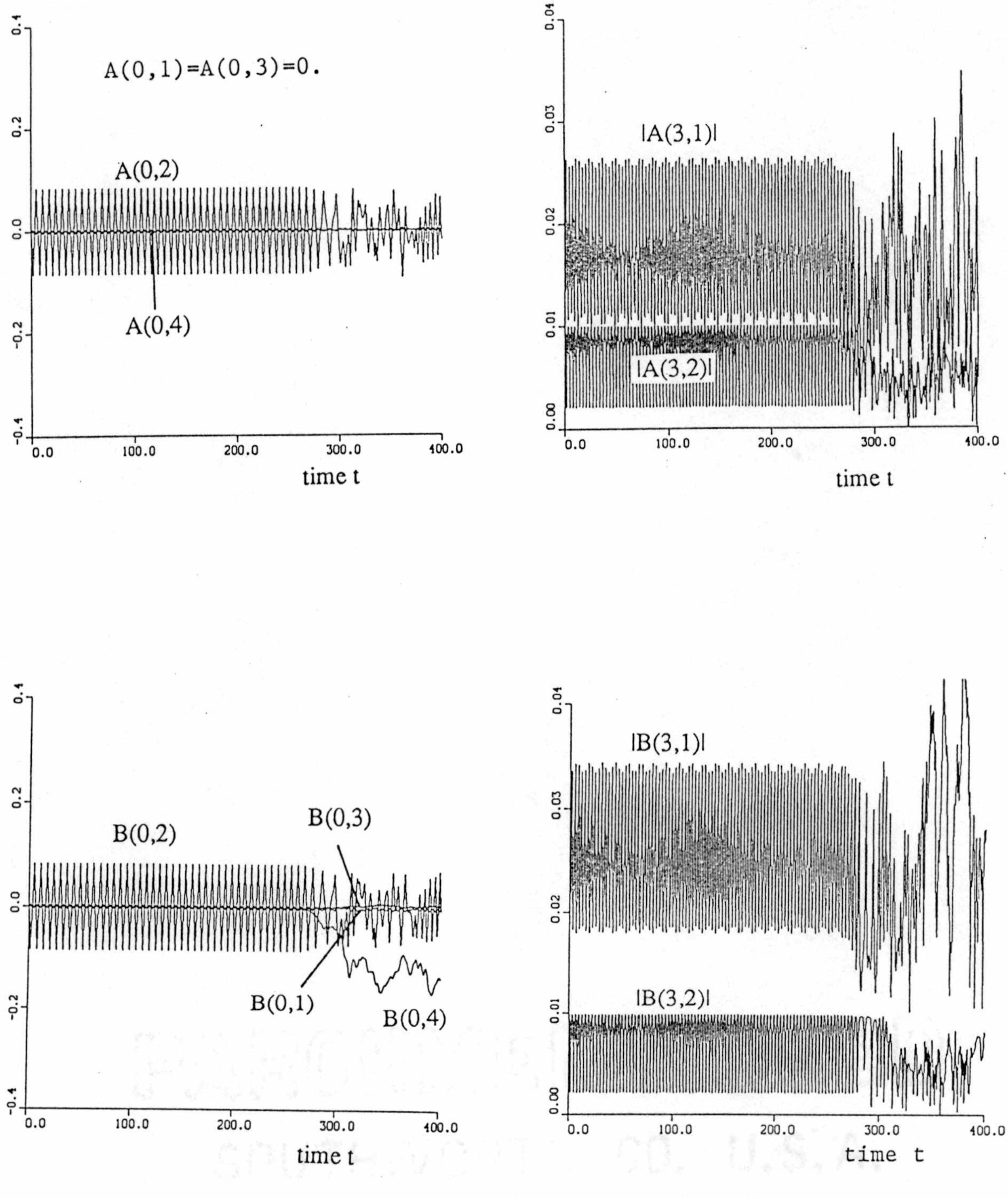

(a) S=0.65, δ=0.0, $A_{3,1}(0)=0.01$, $A_{3,2}(0)=0.01i$

Fig. 4-7. The evolution of the wave components for different initial values

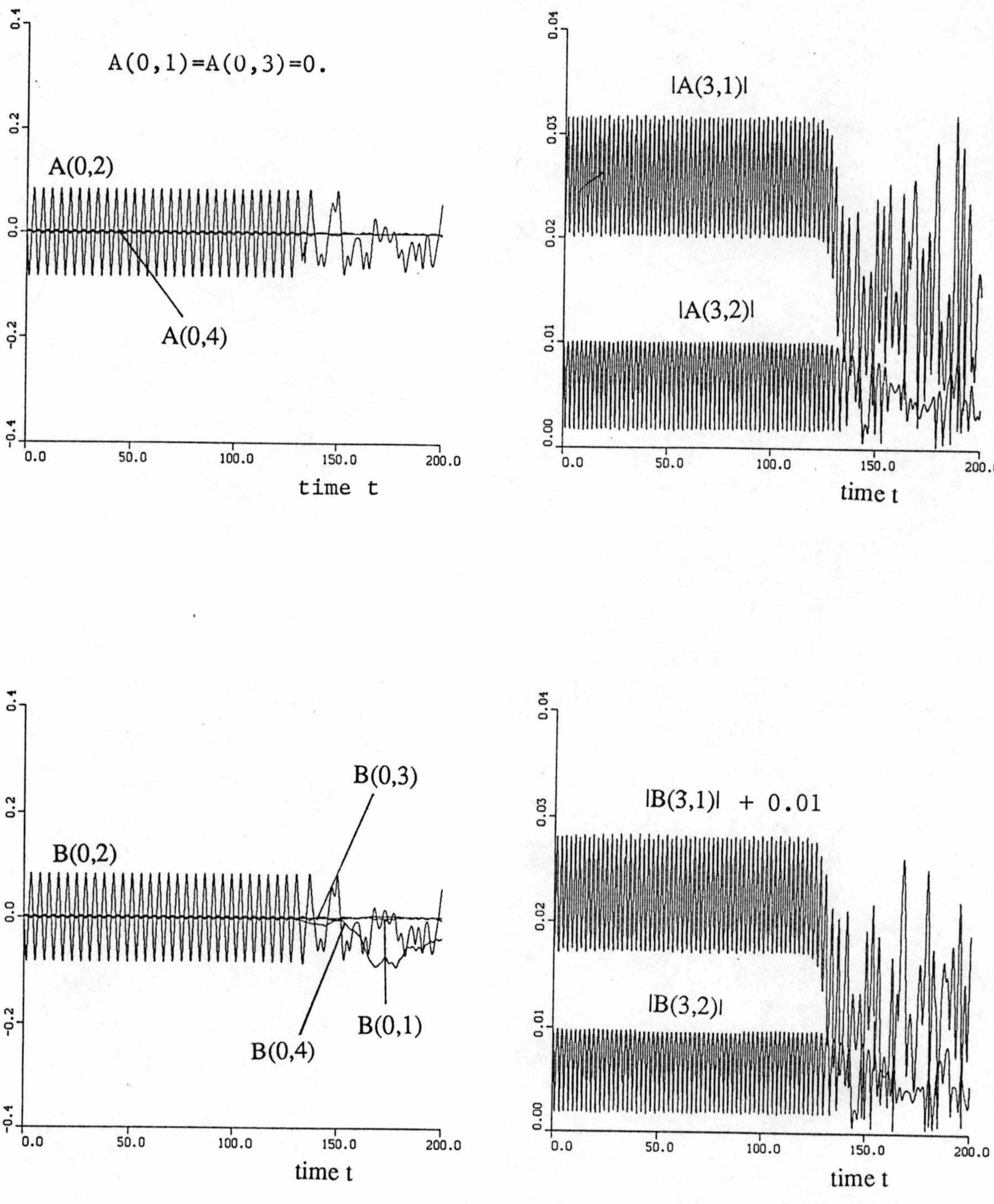

(b) S=0.65, δ=0.0, $A_{3,1}(0)$=0.02, $A_{3,2}(0)$=0.01i

Fig. 4-7. Continue

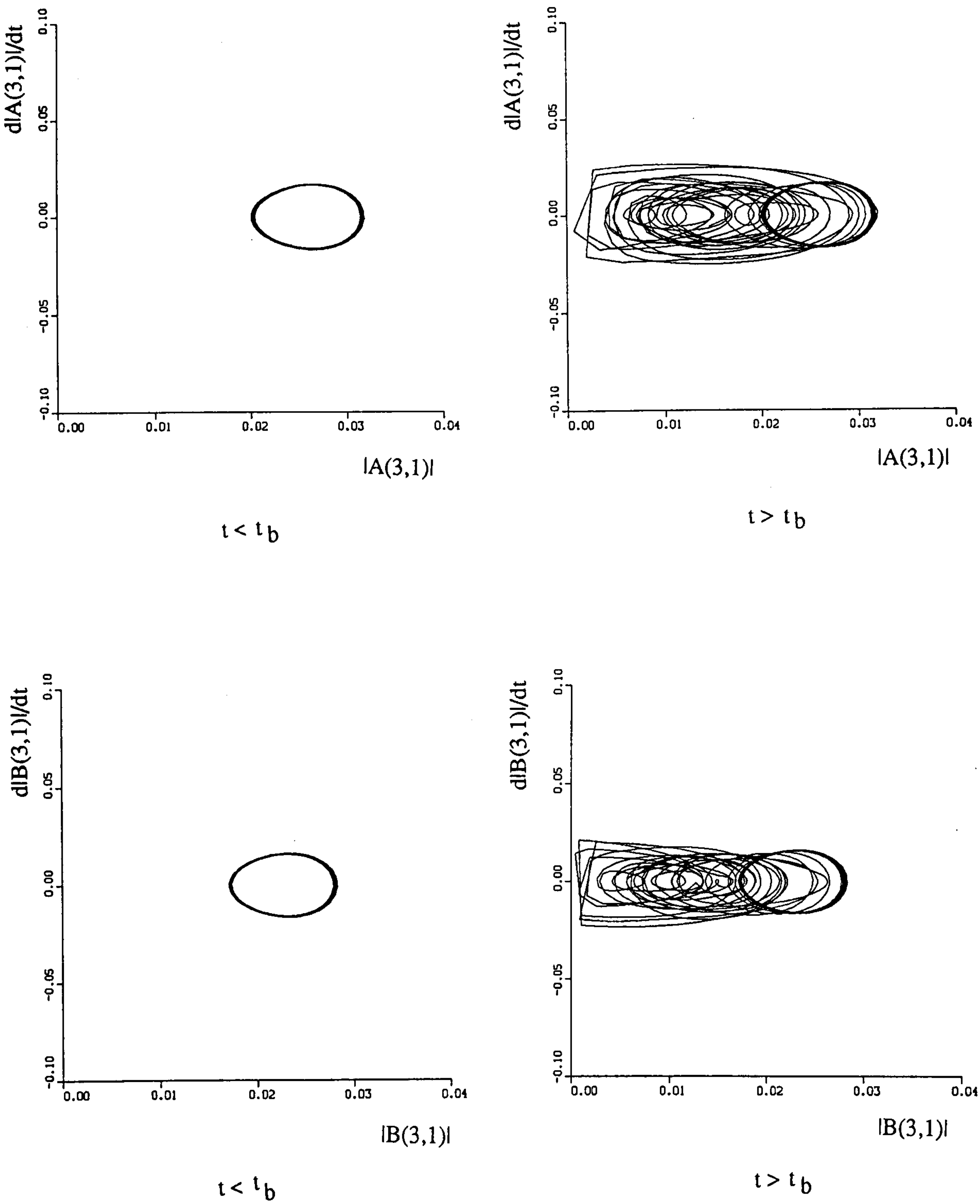

(a) for the case of Fig. 4-7(a)

Fig. 4-8. Phase diagram

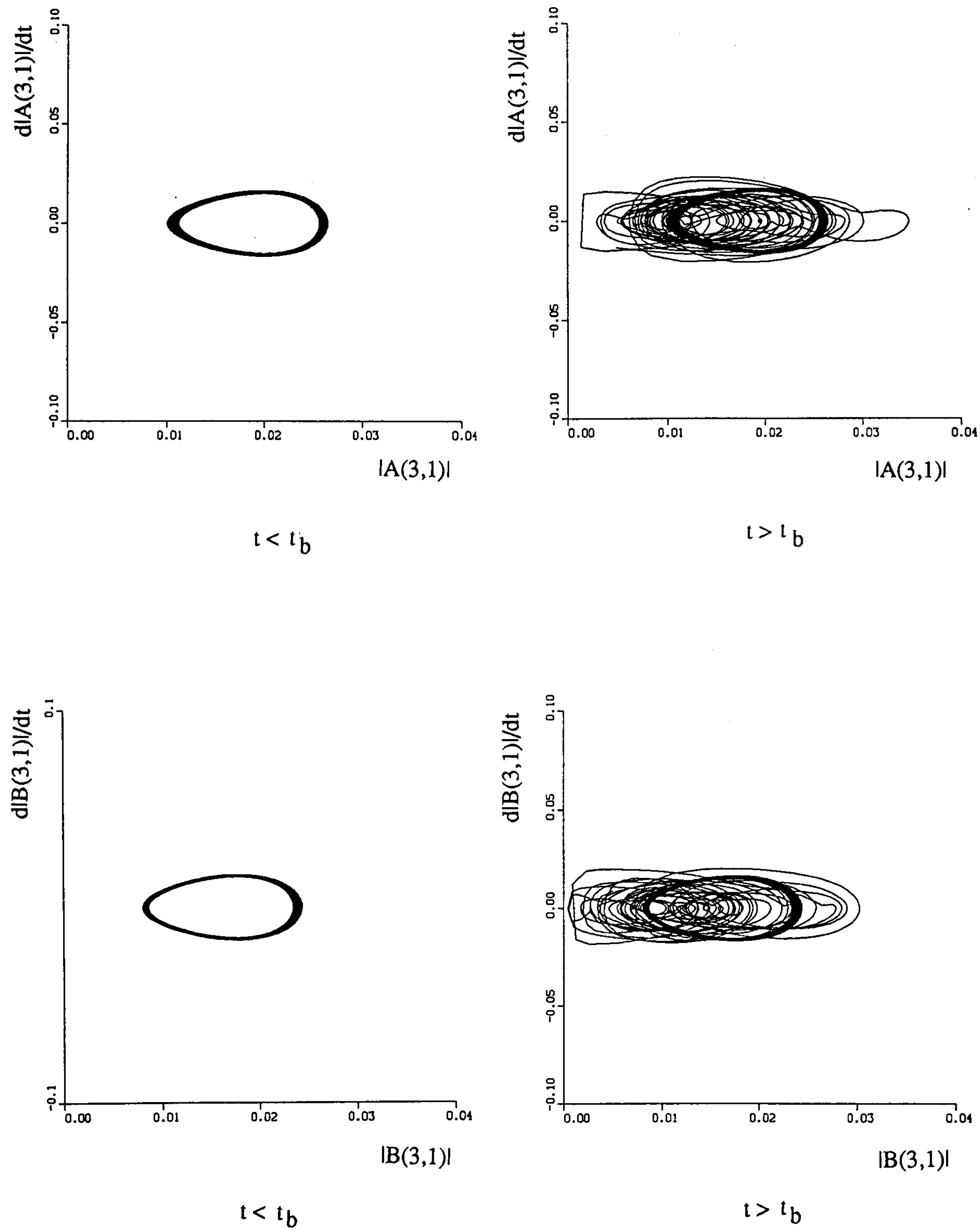

(b) for the case of Fig. 4-7(b)

Fig. 4-8. Continue

The stream function contour plotting of the wave field at the mid-depth in the x-y plane are shown in Figure 4-9. The contour lines and curves represent a uniform series of pressure, and the difference in pressure between adjacent lines or curves is the contour interval of the given map. Thus, contours represent the shape of the undulation of the flow field on the flat surface map.

We have considered basic zonal flows that are strongly unstable, and found that a zonal flow together with a nonlinear wave which is periodic in space and time exists before t_b. And for different initial disturbances, they develop into irregular motion within different time intervals. It is strongly felt this irregularity is due to numerical break down. However, the main characteristics shown here up to point breakdown are similar to those observed in the annulus experiments and analytic results[24].

4.2.2 Nonlinear baroclinic waves analysis with viscous effect

Next a series of five numerical experiments are seen, labeled A, B, C, D and E, as shown in Figure 4-1, to study the evolution of the nonlinear autonomous system Equations (3.14-3.21) under different parameter settings.

In the series A and B, we change both S and δ such that the following ratio is preserved

$$\frac{S_0}{S} = (\frac{\delta_0}{\delta})^{-4} = (\frac{\Omega}{\Omega_0})^2.$$

This implies that, in each series, the imposed temperature difference and dissipation are fixed, and only the rotation rate is changed. These two sequences are similar to those found in the data collected in the annulus experiments by Pfeffer et al.[10][45]. Computationally, in series A, we consider only one zonal wave with wave number k which is basically a repetation of the weng's work [32]. While in

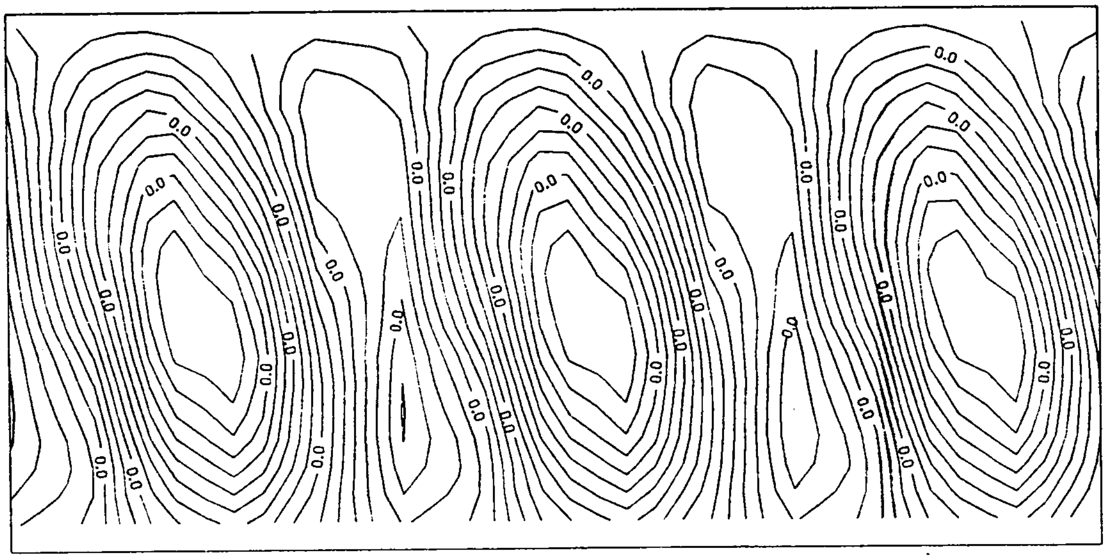

Fig. 4.9. The stream function field of the wave at mid-depth in x-y plane of the case in Fig. 4-7(b).

series B, we consider the first k zonal waves simultaneously. By comparing these two series of results, the difference between the single wave number solution and multi-wave number solution can be analyzed.

Series C and D are calculated for fixed δ, the sequence starting from the upper point to the lower point of the line imply that the imposed temperature difference decreases while the rotation rate is held fixed. These sequences are similar to those found in the data for the annulus experiments conducted by Koschmider and White[9]. In that work, the radial temperature differences at which the transition from one wave number to the next occur was measured with either increasing or decreasing positive radial temperature gradients, at five different rotation rates, while the fluid being always in thermal equilibrium and in contact with an upper rigid lid.

In series E, several cases with different dissipation rates, i.e. δ, are examined in order to investigate the effect of the Ekman dissipation on the evolution of nonlinear baroclinic waves.

4.2.2.1 Evolution of the nonlinear system in experiment of series A

In these series, only one zonal wave with wave number k, with two meridional modes sinπy and sin2πy and four meridional modes for the mean flow correction are considered. The initial values chosen in all of these series are : $A_{k,1}(0)$=0.01, $A_{k,2}(0)$=0.01, $B_{k,1}(0)$ and $B_{k,2}(0)$ are calculated from Equation (4.2) and (4.3) so that the initial wave state is described by the linear dynamics, all the whole of the rest of the components $A_{0,l}(0)$ and $B_{0,l}(0)$ (l=1, 2, 3, 4) are set at zero.

i) Axisymmetric flow

The parameter setting for the case (A0) is k=3, S=0.65, $\delta = 0.01$, which lies in the stable region in the $\delta - S$ plane for the linear stability (see Figure 4-1). The growth rates from the linear theory for both sinπy- and sin2π y- modes are negative: i.e. $kc_{i1} = -0.00$, $kc_{i2} = -0.01$. From Figure 4-10 we can see that all the wave amplitudes and mean flow correction components decay to zero with time. Thus, an axisymmetric flow prevails.

ii) Steady waves

Linear theory predicts there is no region of steady waves in parameter space even when dissipation exists. Yet, when we consider the nonlinearity, steady waves may exist in what was the unstable region of the parameter space in the linear problem with dissipation.

Case(A1) (shown in Figure 4-11) is an example of such a class of steady waves. The parameter setting for A1 is k=3, S=0.30, $\delta = 0.008$. The growth rates from the linear theory for this case is $kc_{i1} = 0.23$ and $kci2 = -0.01$. From Figure 4-11, we can see that after an initial period of adjustment, the wave and the mean flow correction components attain equilibrium values. While the sin$2\pi y$-mode decay to zero with time.

iii) Amplitude vacillation

Case (A2) (shown in Figure 4-12) is an example of amplitude vacillation. The parameter setting is k=4, S=0.15 and $\delta = 0.0067$. The growth rates from the linear theory of the sinπy- and sin$2\pi y$- modes are $kc_{i1} = 0.48$ and $kc_{i2} = 0.00$, respectively. After the initial adjustment, the wave and the mean flow correction components exhibits a limit cycle behavior (Figure 4-12). Figure 4-13 shows the streamfunction of the wave field at the mid-depth in the x-y plane for this code.

From these three cases, namely, A0, A1 and A2, it is found that the present results are in agreement with Weng's [32], in which as the parameter sets are varied

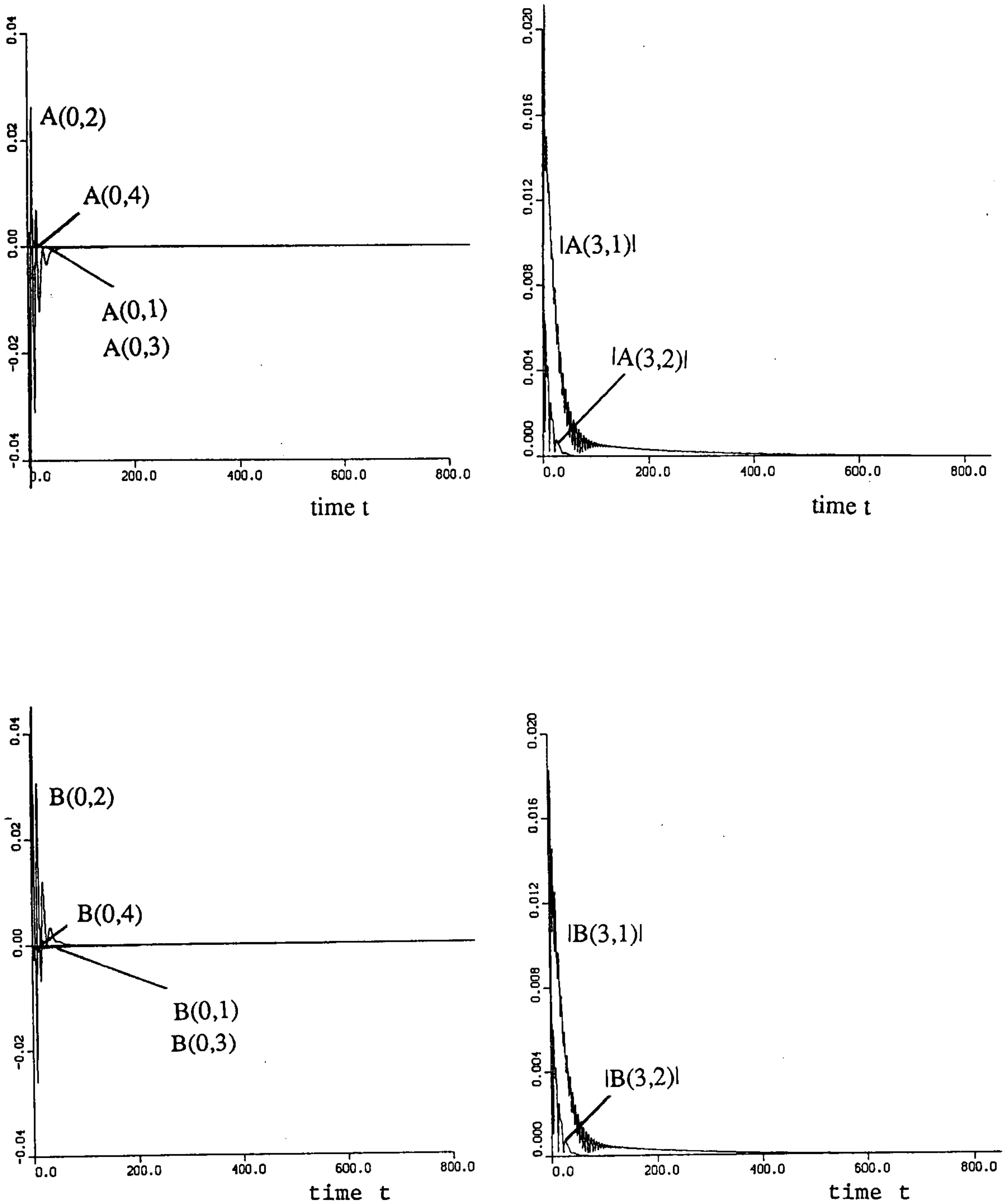

Fig. 4-10. The evolution of the wave components in the case A0,

k=3, S=0.65, δ=0.01, γ=0.1

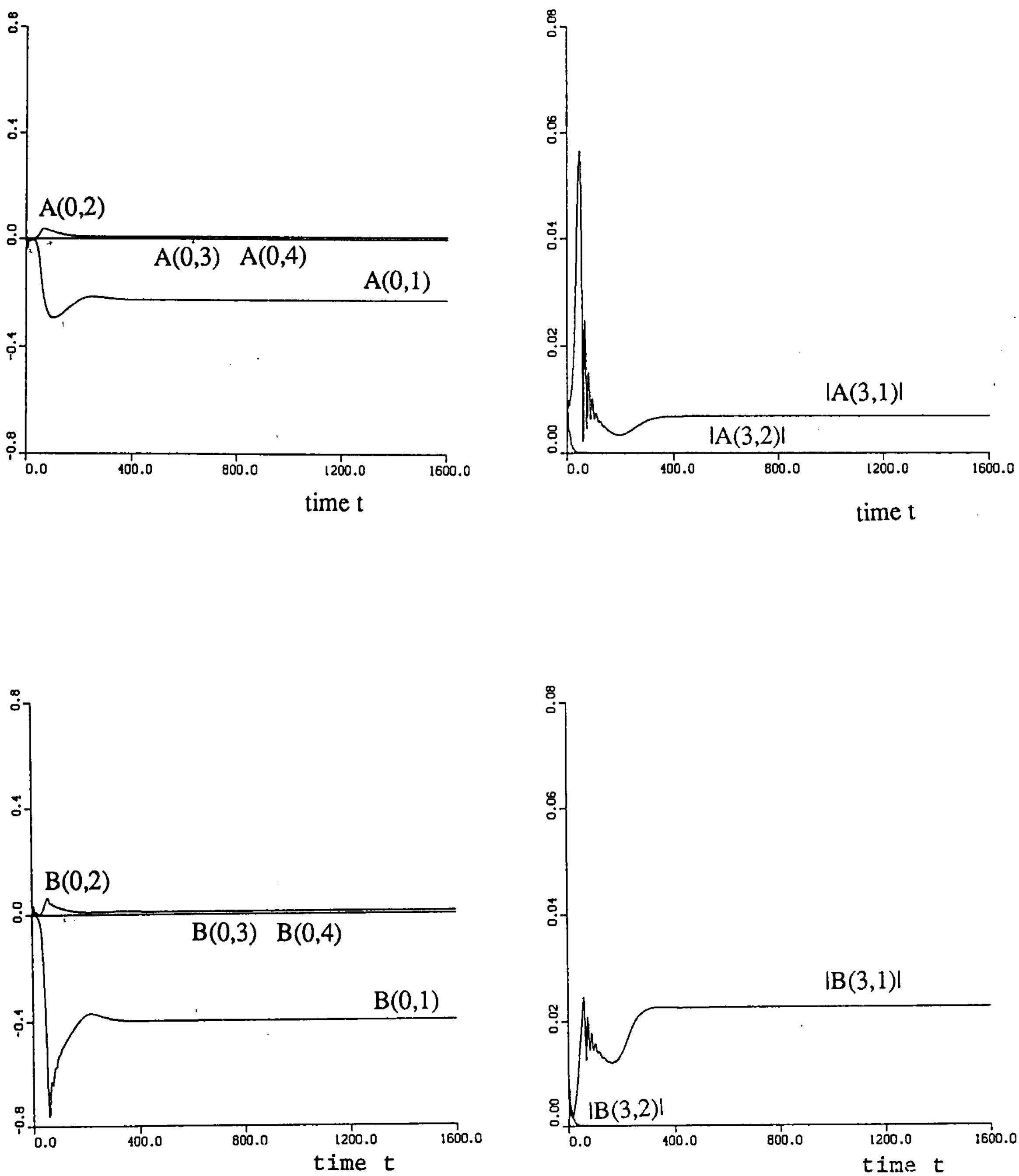

Fig. 4-11. The evolution of the wave components in the case A1

k=3, S=0.30, δ=0.008, γ=0.1

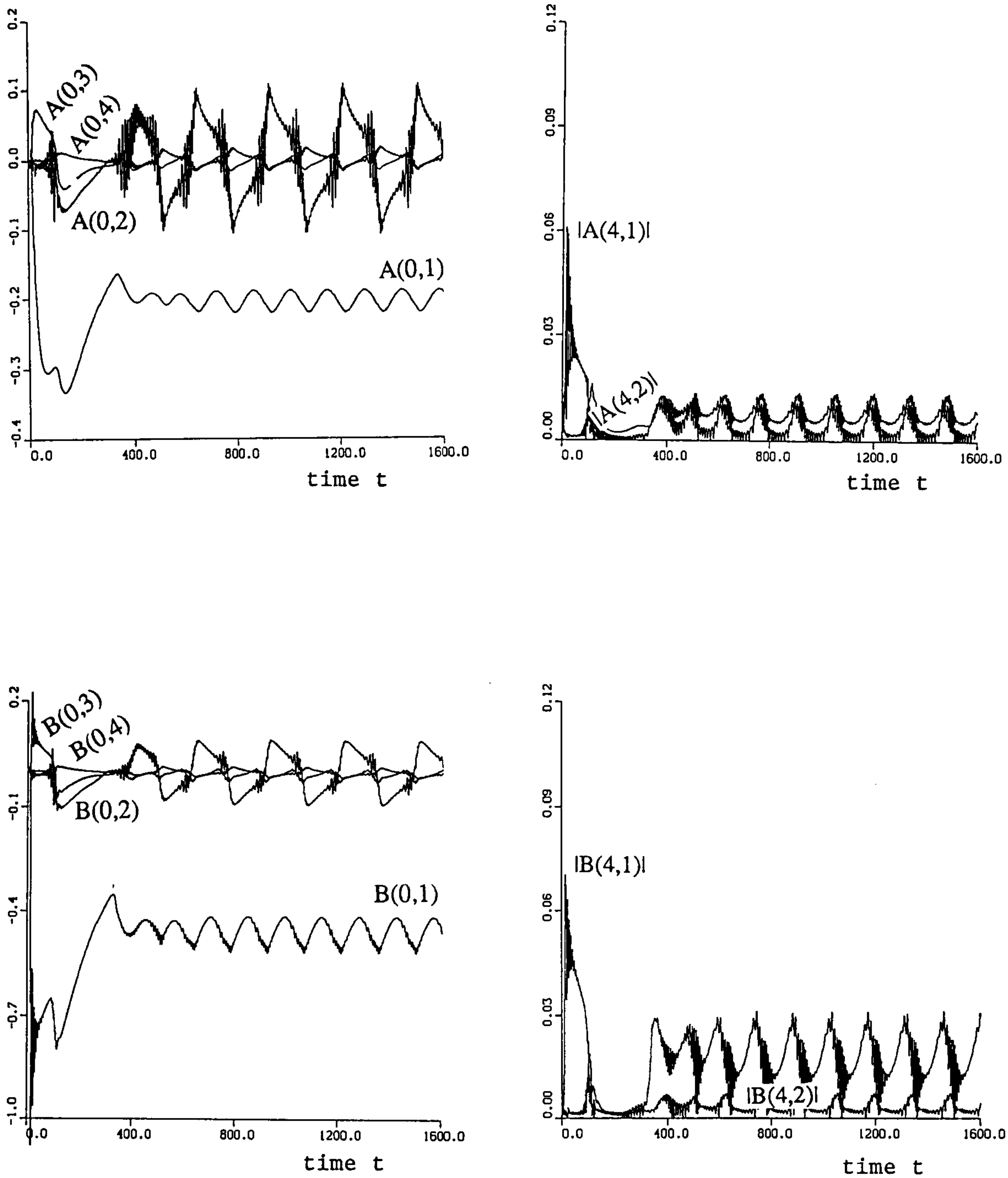

Fig. 4-12. The evolution of the wave components in the case A2

k=4, S=0.15, δ=0.0067, γ=0.1

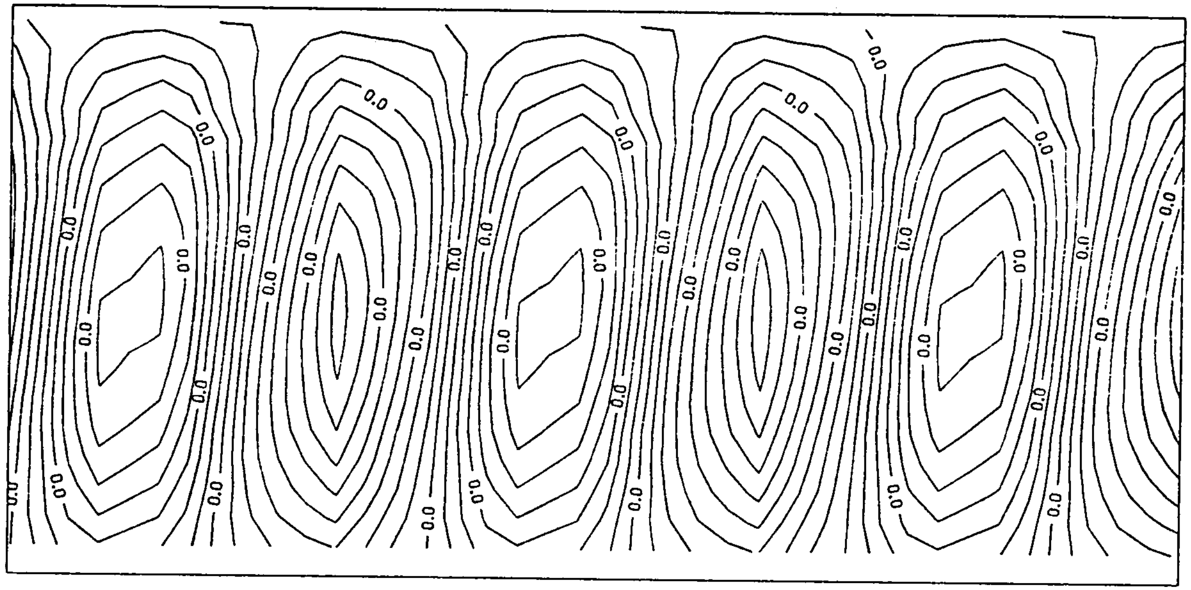

Fig. 4-13. The stream function field of the wave at mid-depth in x-y plane of the case A2

along the line AA' in the S-δ plane, three flow states are predicted. The main characteristics shown here are similar to those observed in the annulus experiments [10][45]. Based on the above comparisons with Weng's analytical and numerical results and the annulus experiments, it is concluded the code developed for this work is validated.

2. Evolution of the nonlinear system in experiments of series B

This sequence of numerical experiments is similar to series A, in which the same parameter settings are used as in series A. The only difference is we deal here with the lowest k zonal waves simultaneously instead of considering only one zonal wave with wave number k. The initial values chosen here are : $A_{k,l}(0)$=0.01, where l=1,2, $A_{kk,l}(0)$=0, where kk=1,2,...(k-1), l=1,2, and all the mean flow correction components being set to zero.

From Figure 4-14(a), it can be seen that, for the case (B0) where k=1, 2, 3, S=0.65, and $\delta = 0.01$, the wave amplitude with wave number k=3 and mean flow correction components approach zero at the final state and the waves amplitude with wave number k=1,2 are zero. Figure 4-14(b) are the phase diagrame for the components A(3,1) and B(3,1). Comparing the case (B0) with the case (A0), we can see that, for this setting, the solution of the multi-wave number model is similar to that of a single wave number.

The parameter setting for B1 (shown in Figure 4-15) is k=1, 2, 3, S=0.30, δ=0.008 and B2 (shown in Fig. 4.16) is k=1, 2, 3, 4, S=0.15, δ=0.0067, which corresponds to the case A1 and A2, respectively. From Figure 4-15 and 4-16, we can see, when $t < 400$ (for case B1) and $t < 450$ (for case B2), the wave component with wave number k=3 (for B1) and k=4 (for B2) and mean flow correction are similar to those in case A1 and A2, and the value of the wave components with

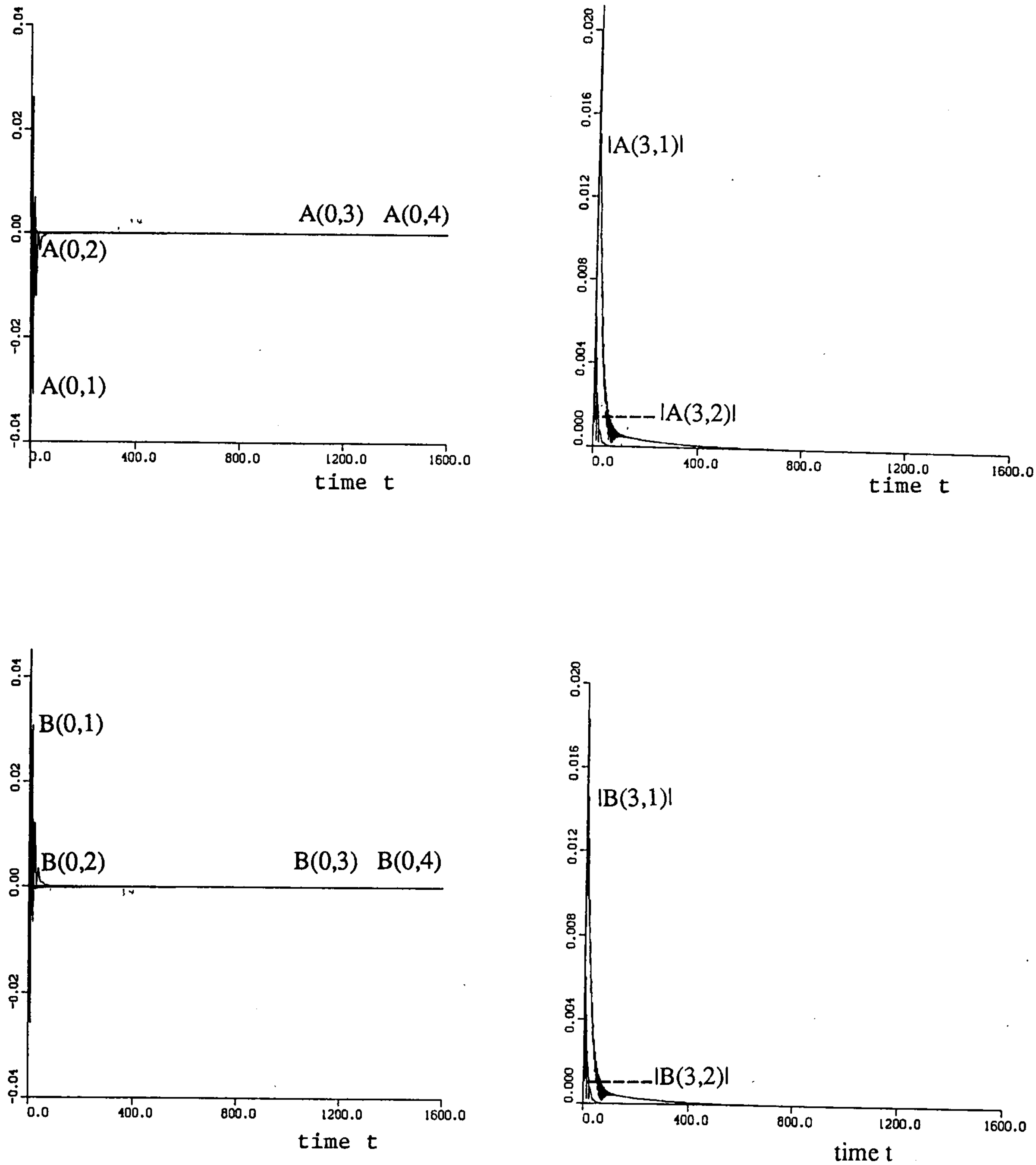

Fig. 4-14(a). The evolution of the wave components in the case B0

k=1,2,3, S=0.65, δ=0.01, γ=0.1

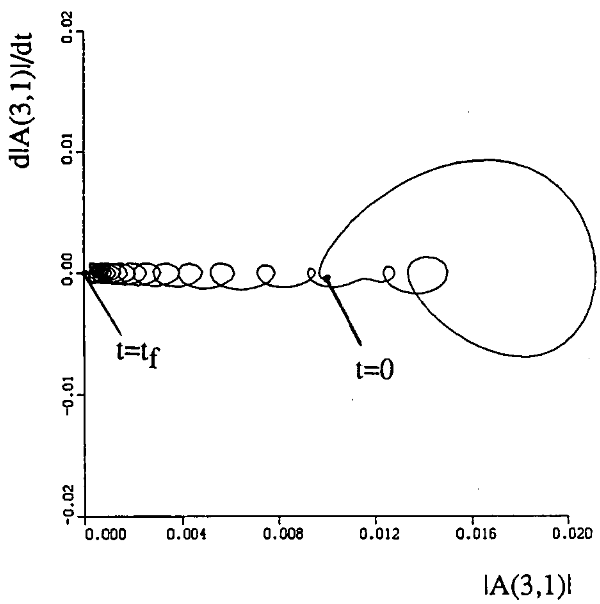

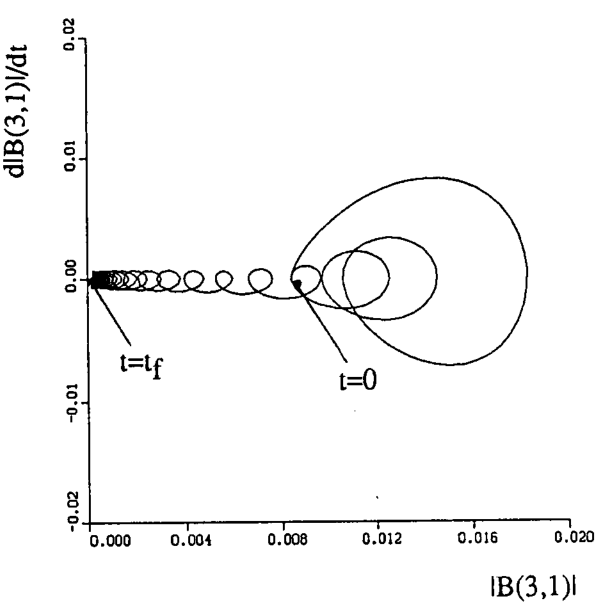

Fig. 4-14(b). Phases diagram for the case of Fig. 4.14(a).

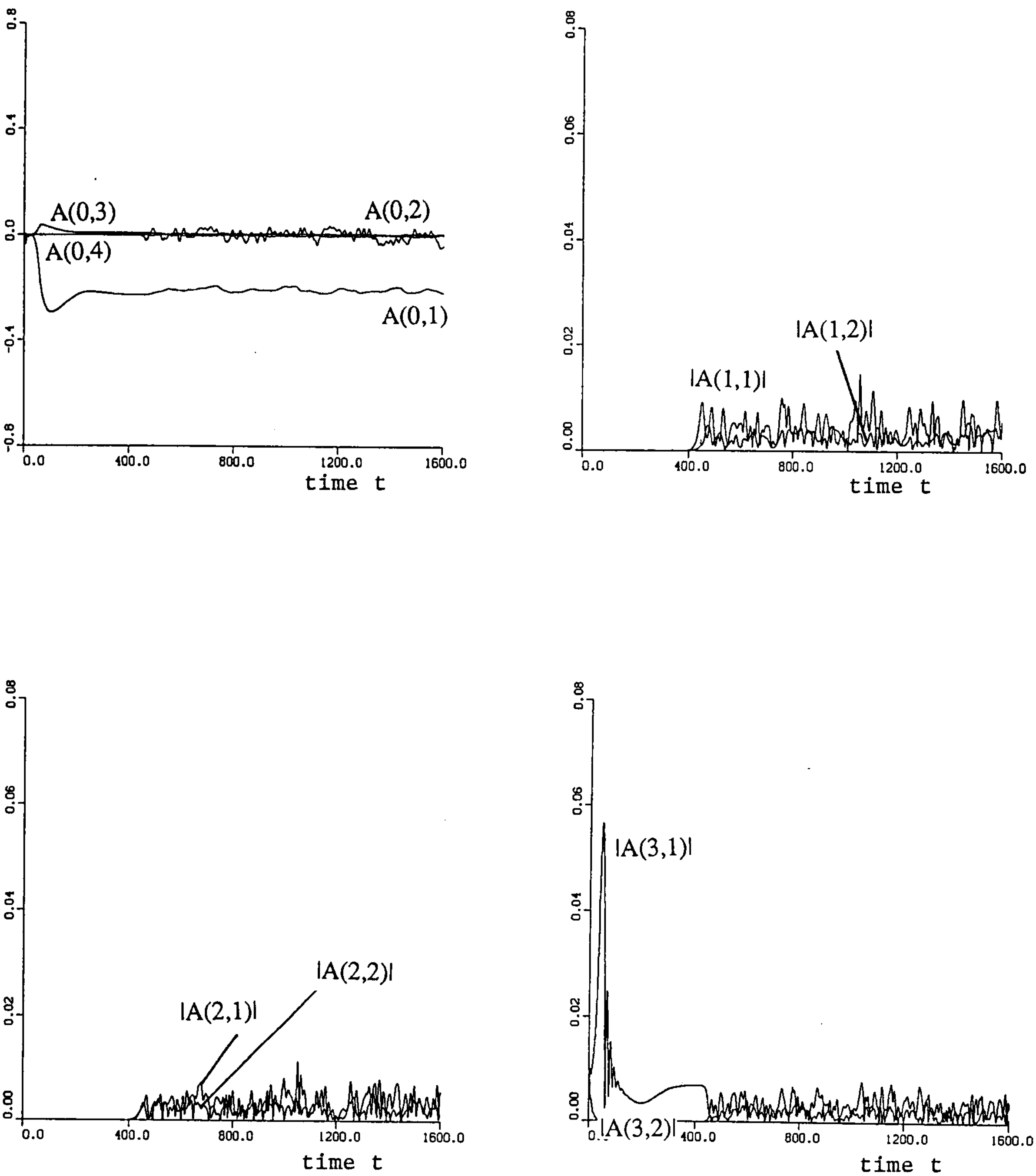

Fig. 4-15. The evolution of the wave components in the case B1

k=1,2,3, S=0.30, δ=0.08, γ=0.1

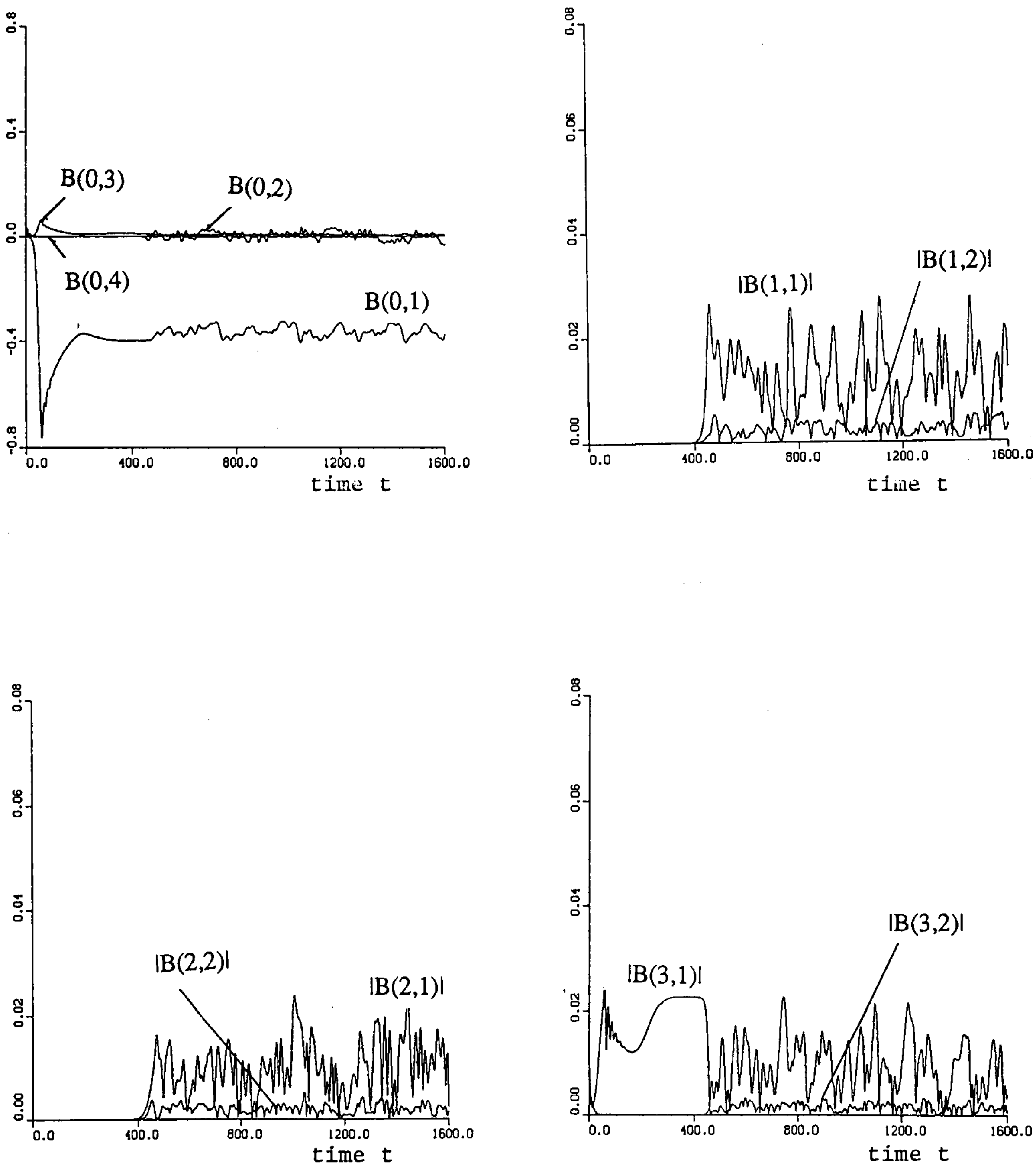

Fig. 4-15. continue

S=0.30, δ=0.08, γ=0.1

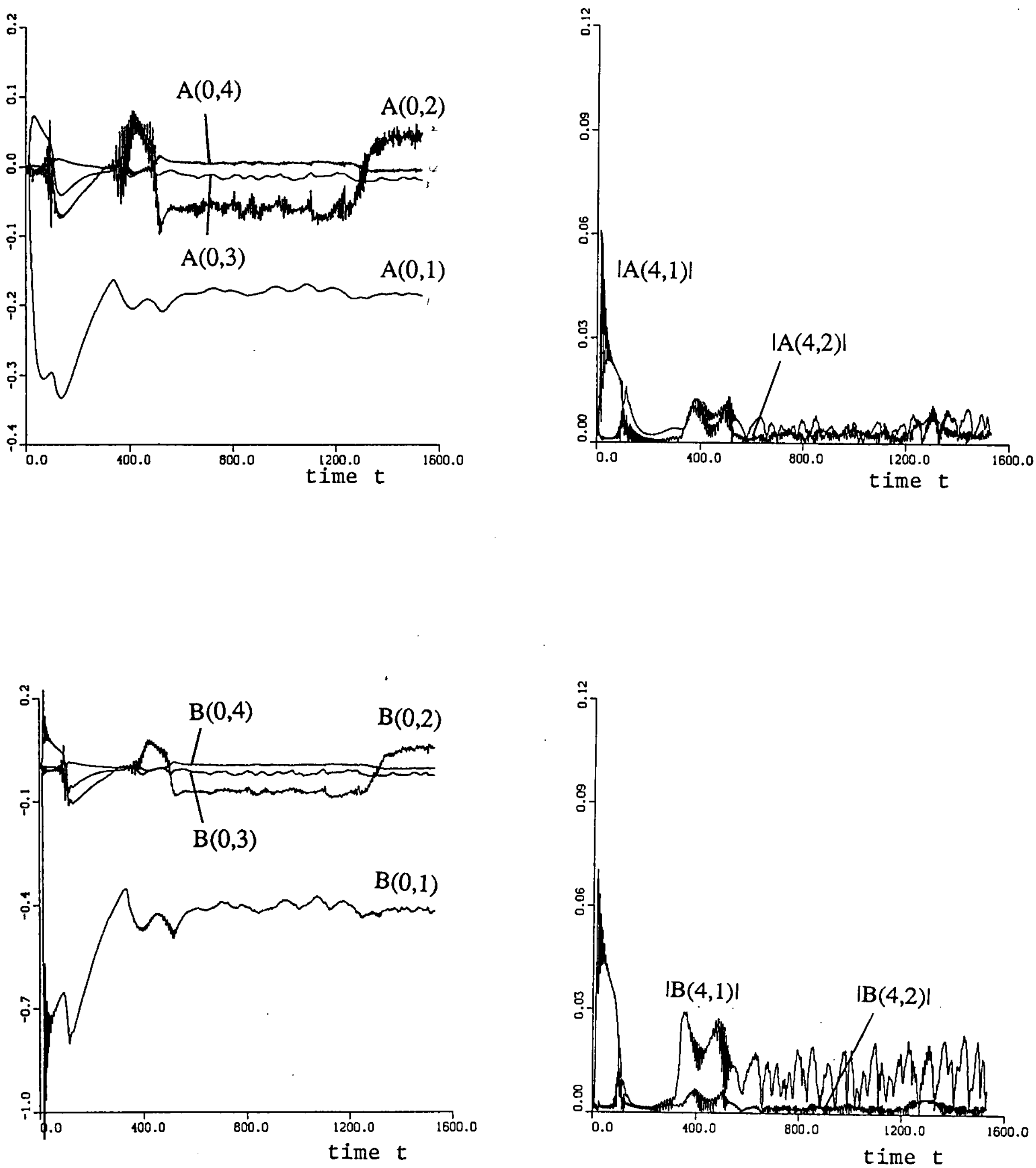

Fig. 4-16. The evolution of the wave components in the case B2

k=1,2,3,4, S=0.15, δ=0.0067, γ=0.1

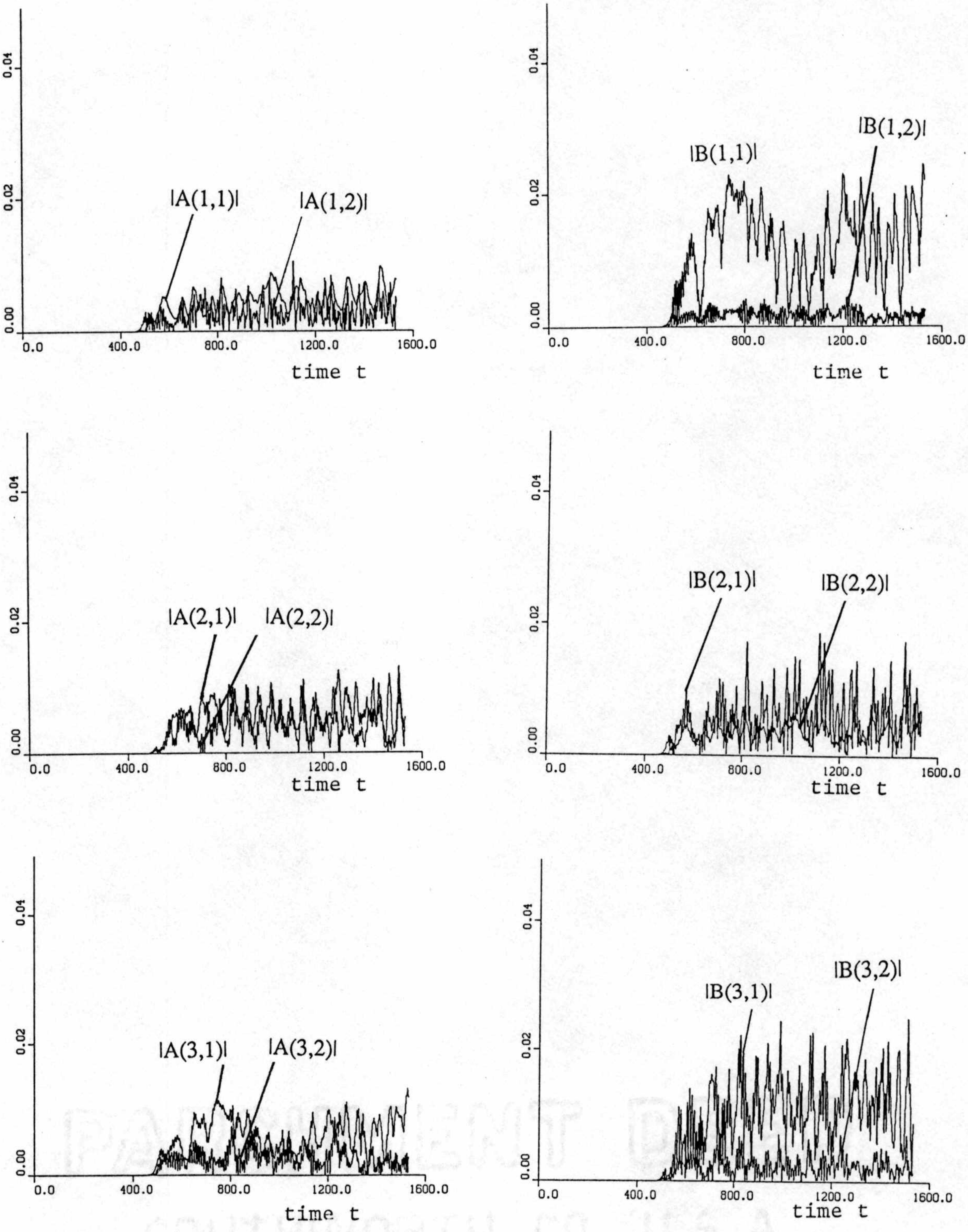

Fig. 4-16. continue

S=0.15, δ=0.0067, γ=0.1

wave number k=1, 2 (for B1) and k=1, 2, 3 (for B2) are zero, i.e. unperturbed. But, as time increases beyond 400 (for B1) or 450 (for B2), the wave component with wave number k=1, 2 (for B1) and k=1, 2, 3 (for B2) have some finite value, and the wave component with a wave number k=3 (for B1) and k=4 (for B2)and the mean flow corrections are different from that in the case A1 and A2. This means for these two cases, the solutions of multi-wave number are different from that of the single wave number. Mathematically, the model of multi-wave number should represent a better approximation to the practical problem than that of the single wave number. Thus, it is necessary to study and develop the multi-wave number model to get more accurate result.

3. Evolution of the nonlinear system in experiments of series C

This sequence of experiments is performed along the line $\delta = 0.001$ in the $S - \delta$ plane. Here, the three lowest wave numbers, i.e. wave number k=1, 2, 3, with two meridional modes $\sin\pi y$ and $\sin 2\pi y$ and four meridional modes for mean flow correction are considered. The initial values chosen are A(k,1)=0.005 and A(k,2)=0.005 for k=1, 2, 3. That means the lowest three zonal waves are considered and the same initial perturbation for each wave component are forced. The only parameter that changes for different cases is S. The sequence of numerical experiments is performed from upper to lower along the line CC' as S decreases.

Figures 4-17, 4-18, and 4-19 show the wave component development for S=0.65, S=0.35, and S=0.20, respectively. It can be seen that when S=0.65, wavenumber k=1 is clearly dominant; but, while S decreases, the wavenumber k=1 decays and wave number k=2 and k=3 becomes stronger than before. For S=0.35 (see Figure 4-18), the values of the amplitude for wave numbers k=1, k=2 and k=3 components are in the same range. When S=0.20 (see Figure 4-19), the amplitude

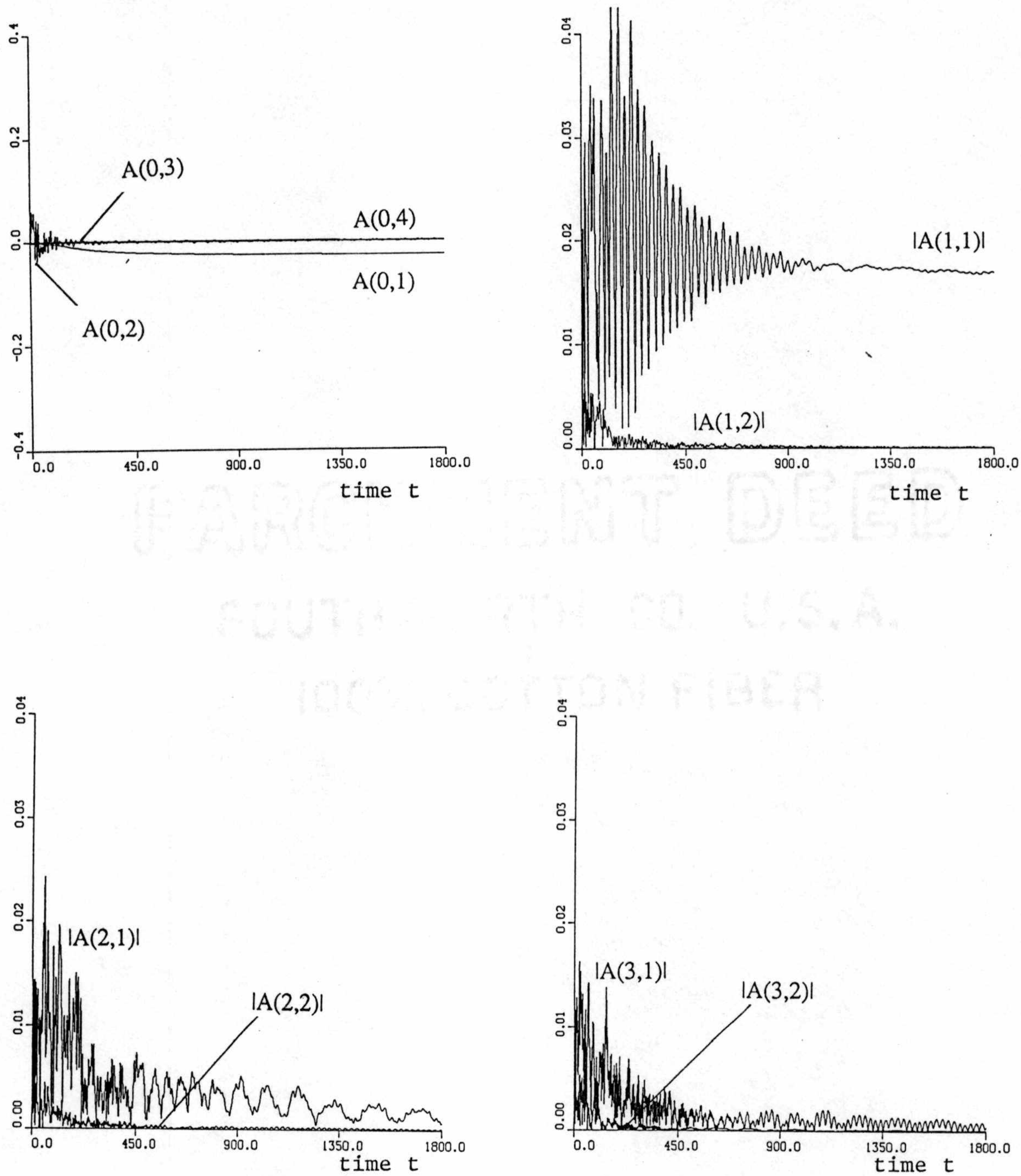

Fig. 4-17. The evolution of the wave components in the case C0

k=1,2,3, S=0.65, δ=0.001, γ=0.1

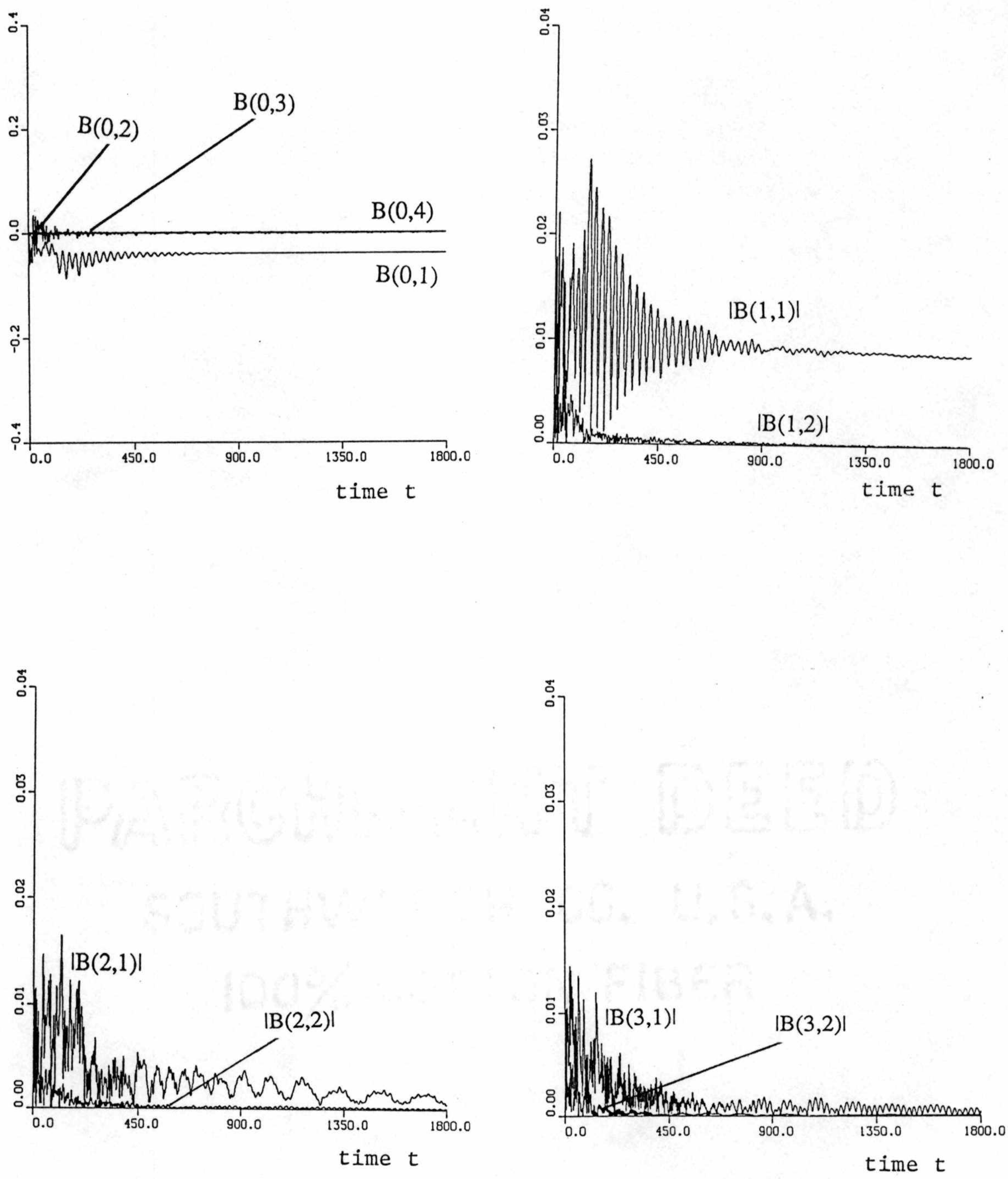

Fig. 4-17. Continue

k=1,2,3, S=0.65, δ=0.001, γ=0.1

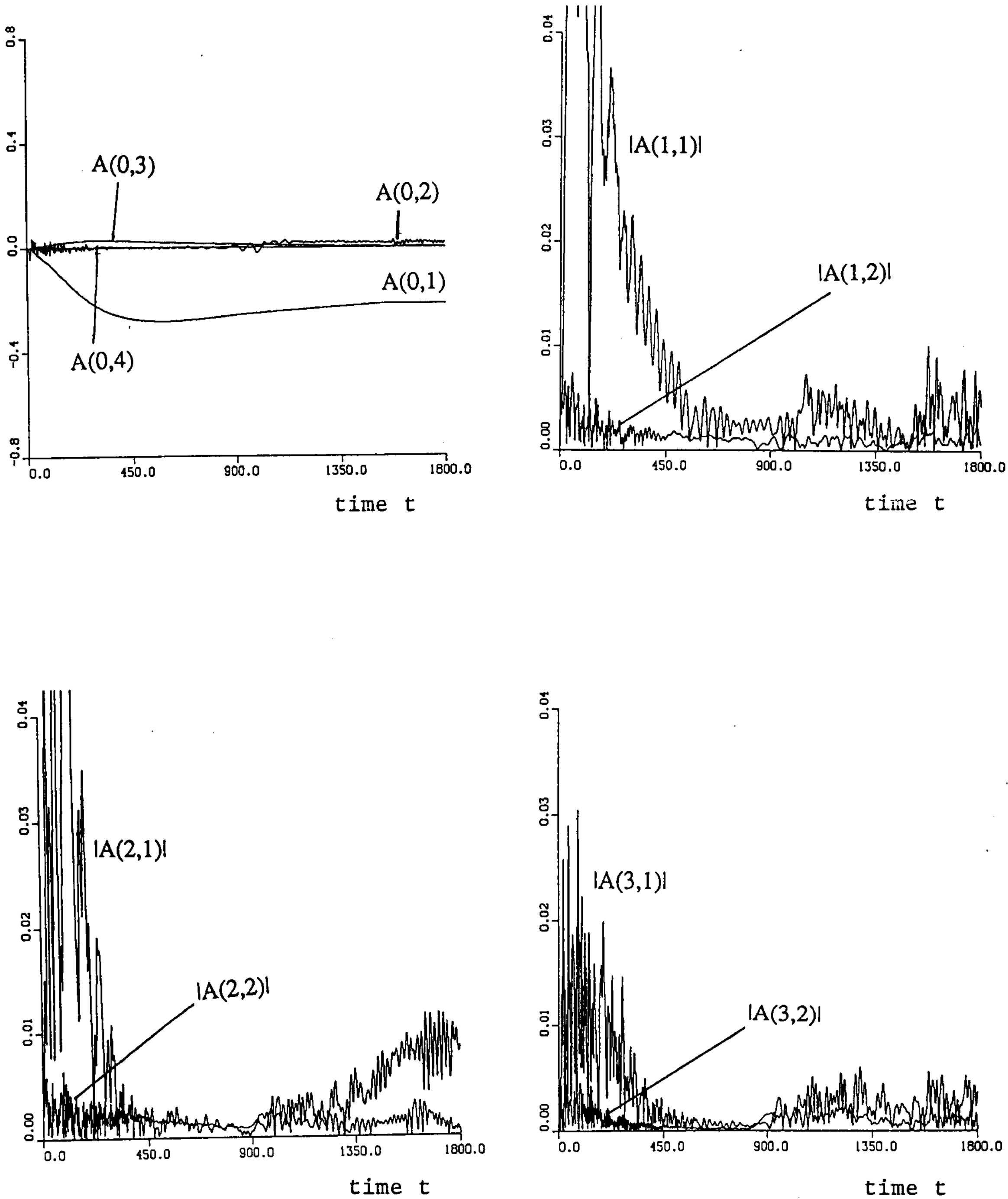

Fig. 4-18. The evolution of the wave components in the case C1

k=1,2,3, S=0.35, δ=0.001, γ=0.1

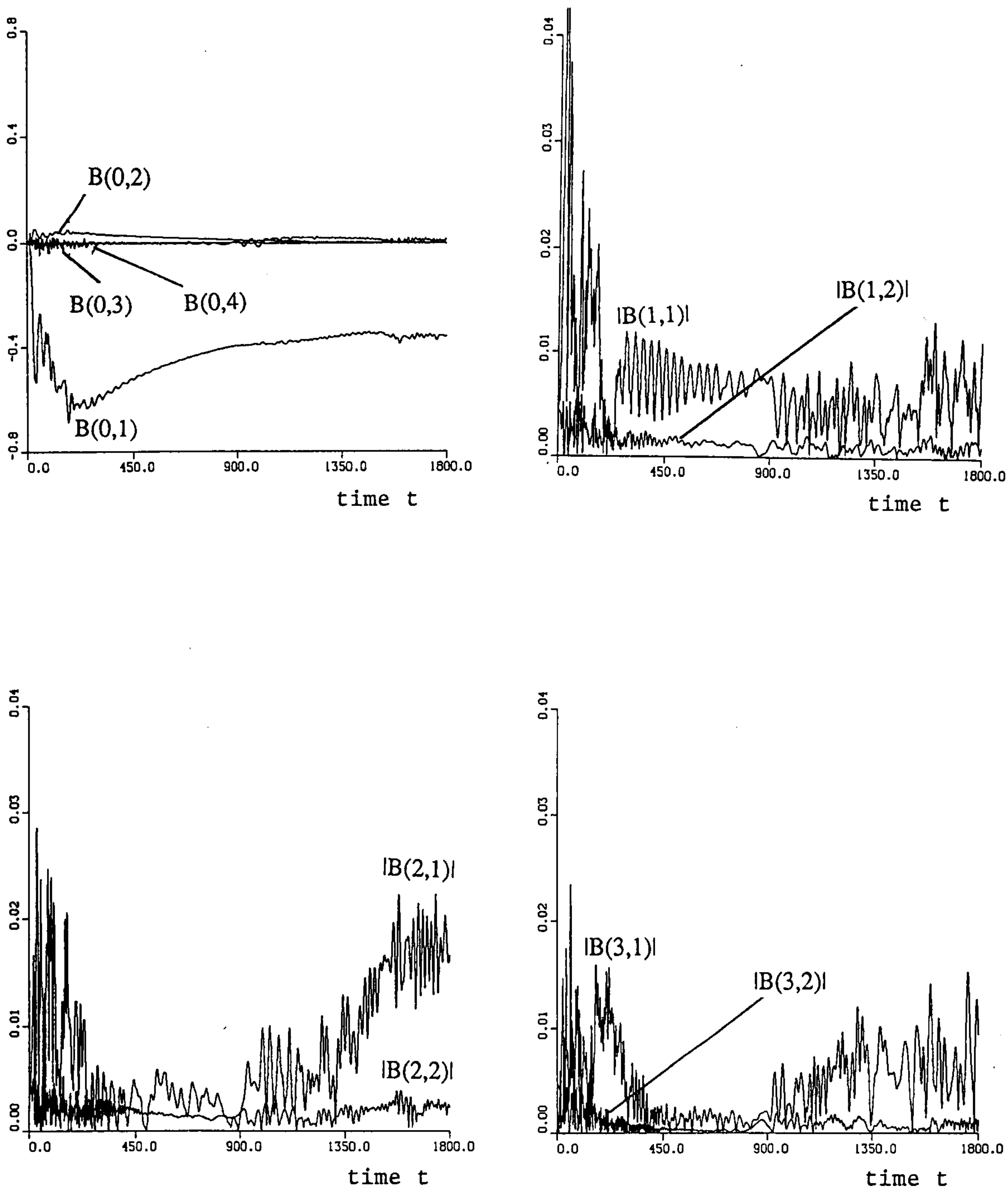

Fig. 4-18. Continue

k=1,2,3, S=0.35, δ=0.001, γ=0.1

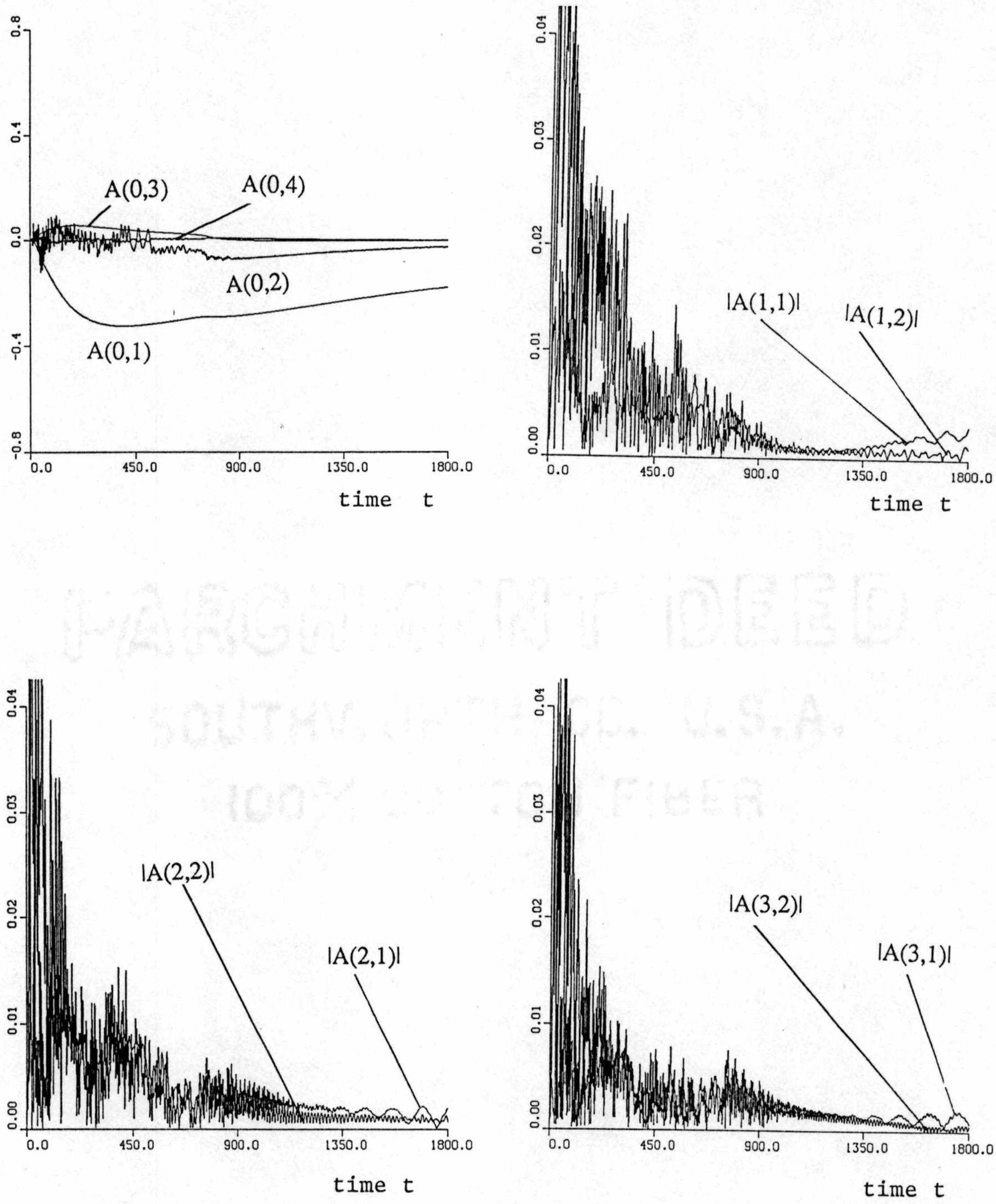

Fig. 4-19. The evolution of the wave components in the case C2

k=1,2,3, S=0.20, δ=0.001, γ=0.1

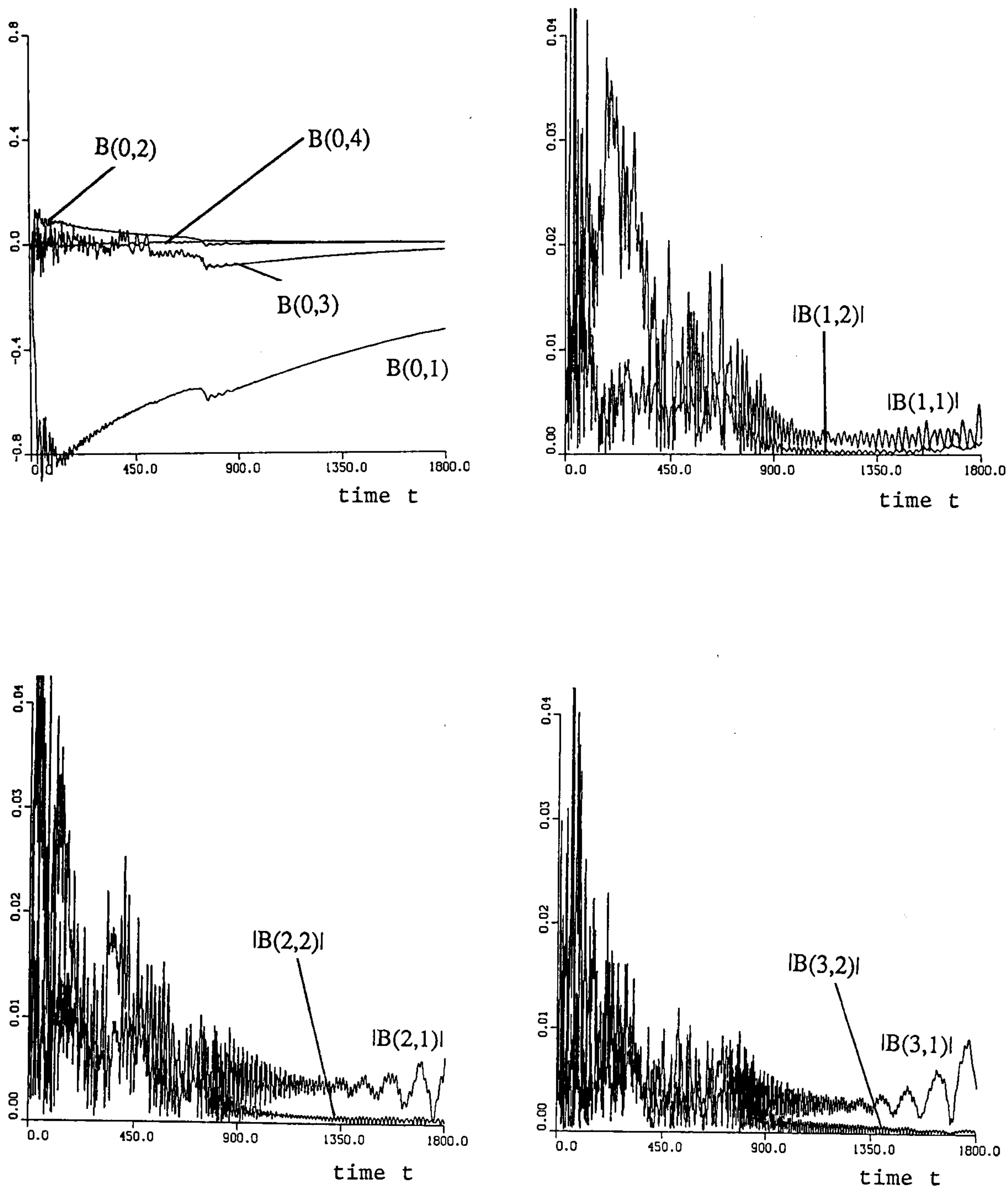

Fig. 4-19. continue

k=1,2,3, S=0.20, δ=0.001, γ=0.1

of wave number k=2 and wave number k=3 are stronger than that of wave number k=1 , and wave number k=2 is stronger than wave number k=3, that is, at this time, the wave number k=2 becomes dominant.

The above result shows that when S decreases, i.e., the imposed radial temperature difference decreases while the rotation rate is fixed, wave number transition occurs and the dominant wave number changes from low to larger, which agree with those observed in the annuals experiments of Koschmider and White[9].

Figures 4-17, 4-18, 4-19, 4-20 and 4-21 are a set of example of meridional mode number transition. Comparing the Figures 4-20 and 4-21 with Figures 4-17, 4-18 and 4-19, we can see that for larger S (i.e. S=0.65, 0.35, 0.20) meridional mode number 1 is dominant. But in the first two cases where S is smaller (i.e., S=0.15, S=0.10) the meridional mode number 2 become more dominant than mode number 1. That means, for lower supercriticality, the meridional mode number 1 with the sinπy structure is the most unstable, the second y-mode with the sin2πy structure becoming unstable when the supercriticality is increased beyond a certain value. This characteristic is similar to those observed in the annulus experiments of Pfeffer et al [45] and agree with linear predictions (see Figure 4-1), i.e., for some zonal wave number, the second y-mode with the sin2πy becomes unstable for the smaller stratification parameter S when compared with the first y-mode for the sinπy structure.

4. Evolution of the nonlinear system in experiments of series D.

This sequence of experiments is similar as in series C, i.e., it is performed along the line $\delta = 0.001$ in the S-δ plane and the only parameter which changes for different cases is the stratification parameter S. The three lowest wave numbers with two meridional modes $\sin\pi y$ and $\sin 2\pi y$ and four meridional modes for the

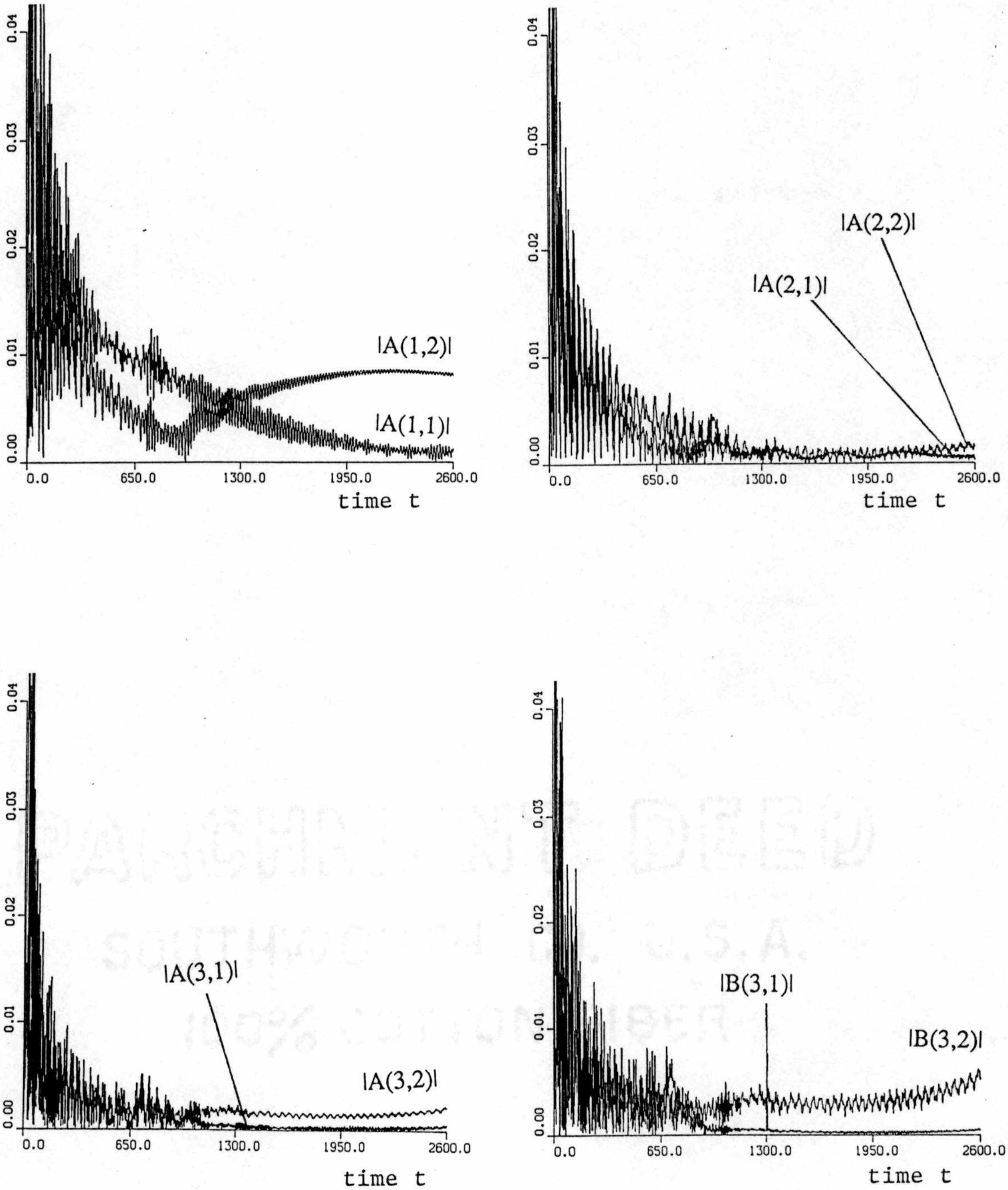

Fig. 4-20. The evolution of the wave components in the case C3

k=1,2,3, S=0.15, δ=0.001, γ=0.1

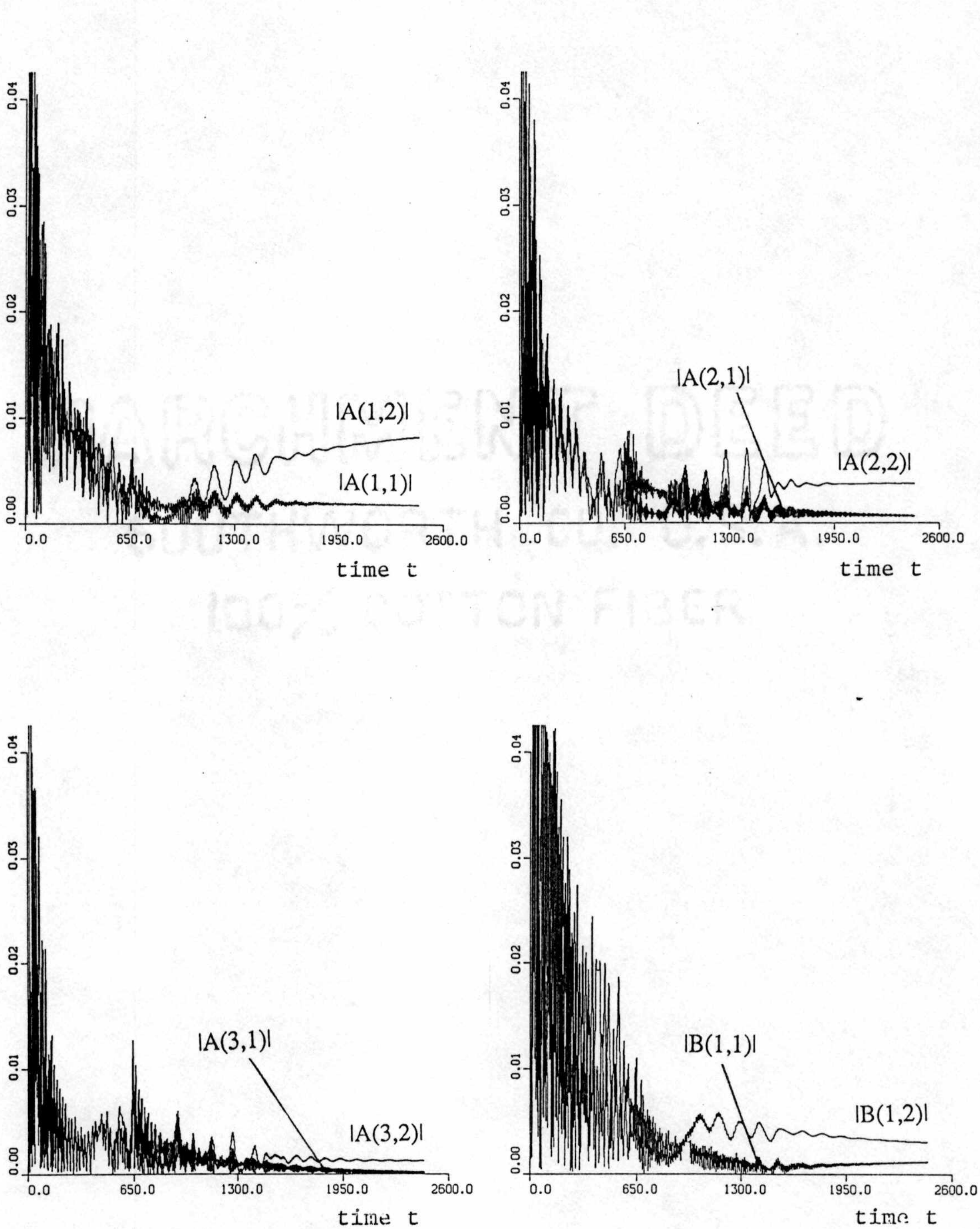

Fig. 4-21. The evolution of the wave components in the case C4

k=1,2,3, S=0.10, δ=0.001, γ=0.1

mean flow correction are considered. But, different initial perturbations are forced to examine the impact of the initial condition on the dominant wavenumber. The initial values chosen are $A_{3,1}(0)$=0.02, $A_{3,2}(0)$=0.01i while all other wave components are set at zero initially. That means we just give wavenumber k=3 a nonzero initial disturbance.

The plot for the wave component development are shown in Figure 4-22, Figure 4-23 and Figure 4-24. As can be seen, the results are similar to those in series C. For S=0.65, the wavenumber k=1 is clearly dominant. While as S decreases, wavenumber k=1 decays, and wavenumbers k=2 and k=3 become stronger, and at S=0.35, the values for these three wavenumber components become almost of the same importance. For S=0.30, the wavenumbers k=2 and 3 become more important and wave number k=2 is dominant.

This result shows that the initial disturbance does not effect the dominant wavenumber, while the character of the flow plays an important role in the determination of the dominant wavenumber.

5. Evolution of the nonlinear system in experiment of E.

In this sequence of experiments, the influence of the dissipation δ on the solution is examined. Figure 4-25 and Figure 4-26 are two examples of different dissipation, δ, for fixed stratification parameter S=0.65, in which $\delta = 0.01$ and $\delta = 0.001$, respectively. As in the series C and D, the three lowest wave numbers with two meridional modes and four meridional modes for the mean flow correction are considered. The initial value are $A_{k,1}(0)$=0.02, $A_{k,2}(0)$=0.01i, k=1, 2, 3; and all the mean flow corrections are set to zero initially.

From Figure 4-25, it can be seen that for higher dissipation, i.e., $\delta = 0.01$, all the wave and mean flow correction components decay very fast and vanish at the

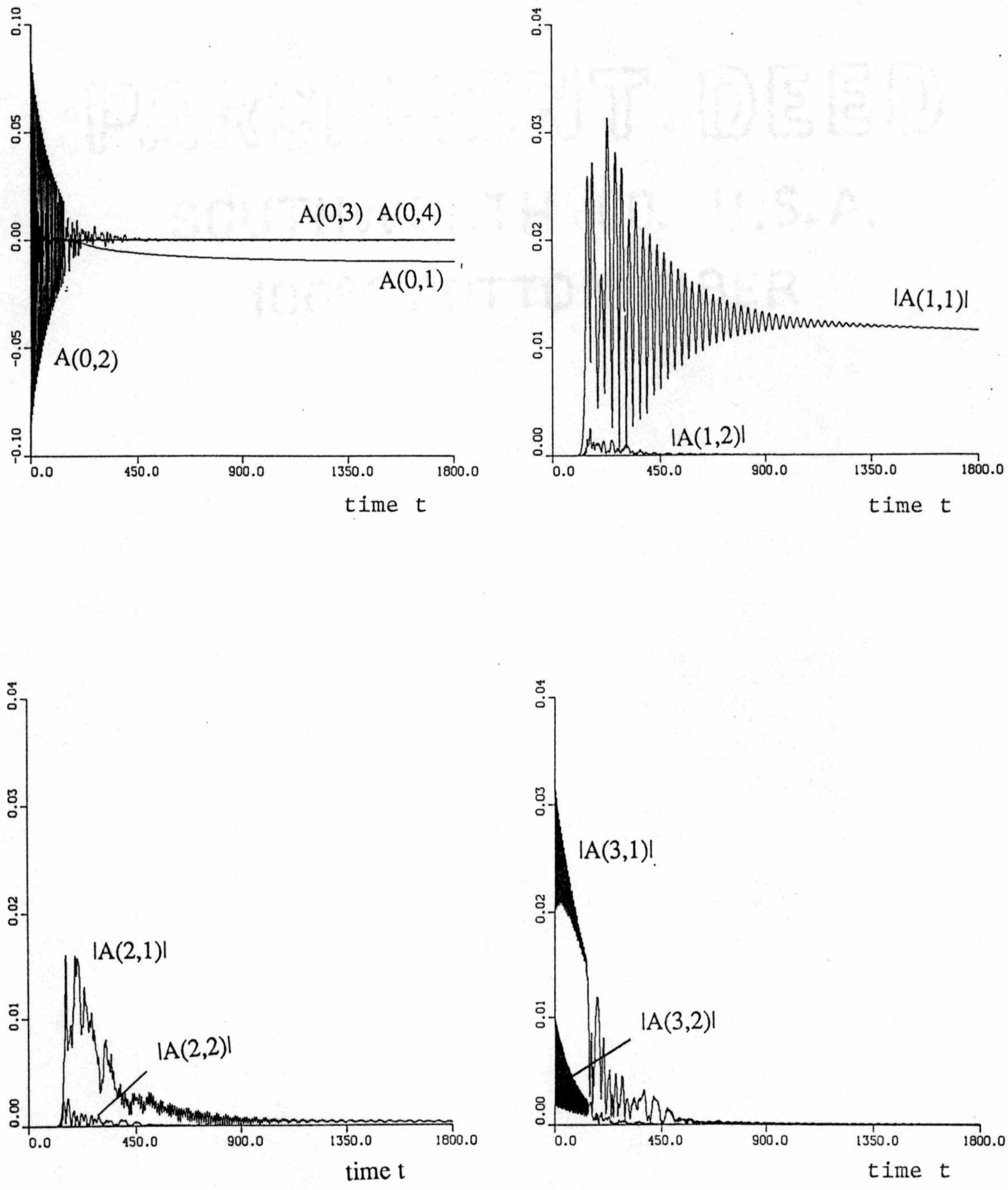

Fig. 4-22. The evolution of the wave components in the case D0

k=1,2,3, S=0.65, δ=0.001, γ=0.1

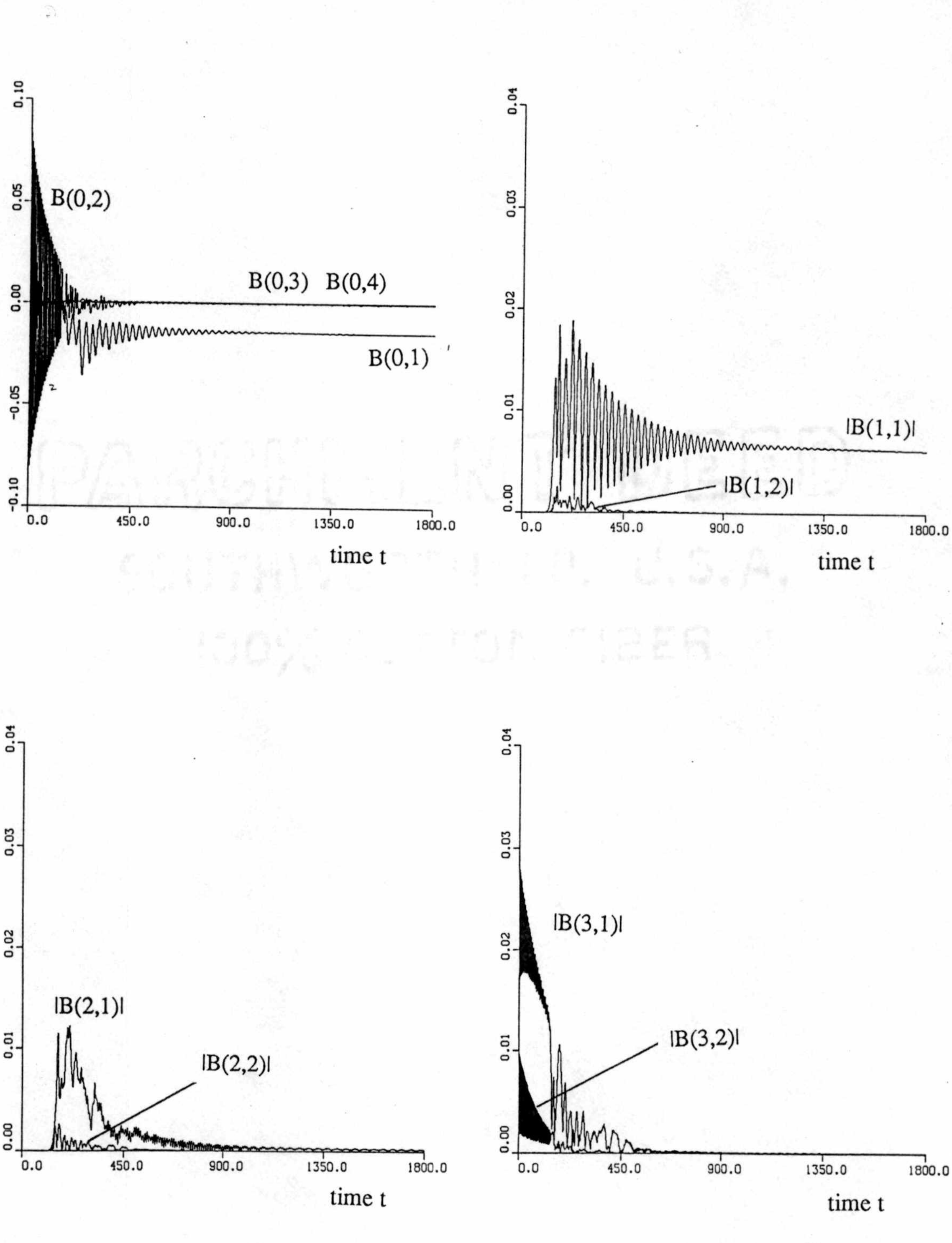

Fig. 4-22. Continue

k=1,2,3, S=0.65, δ=0.001, γ=0.1

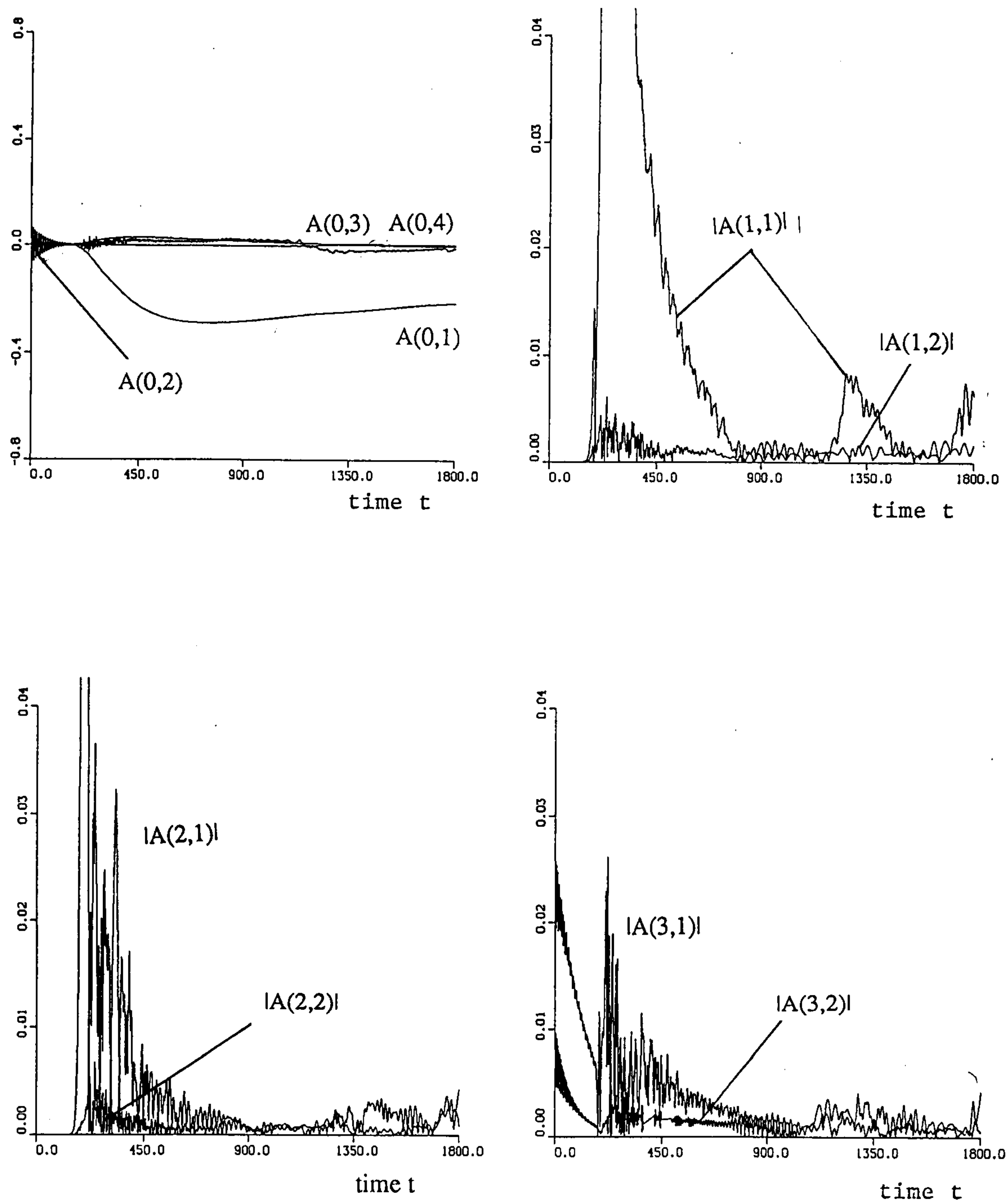

Fig. 4-23. The evolution of the wave components in the case D1

k=1,2,3, S=0.35, δ=0.001, γ=0.1

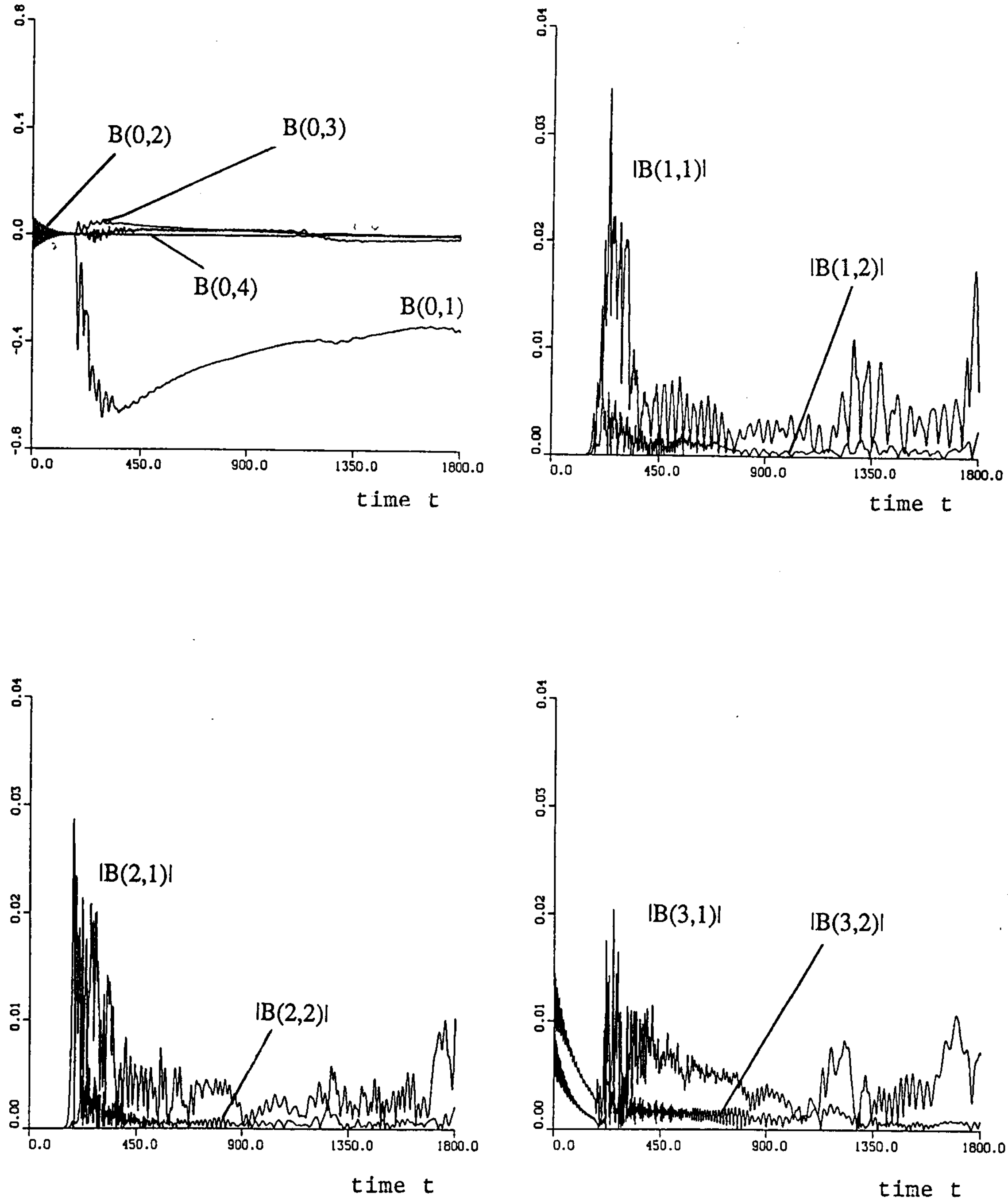

Fig. 4-23. Continue

k=1,2,3, S=0.35, δ=0.001, γ=0.1

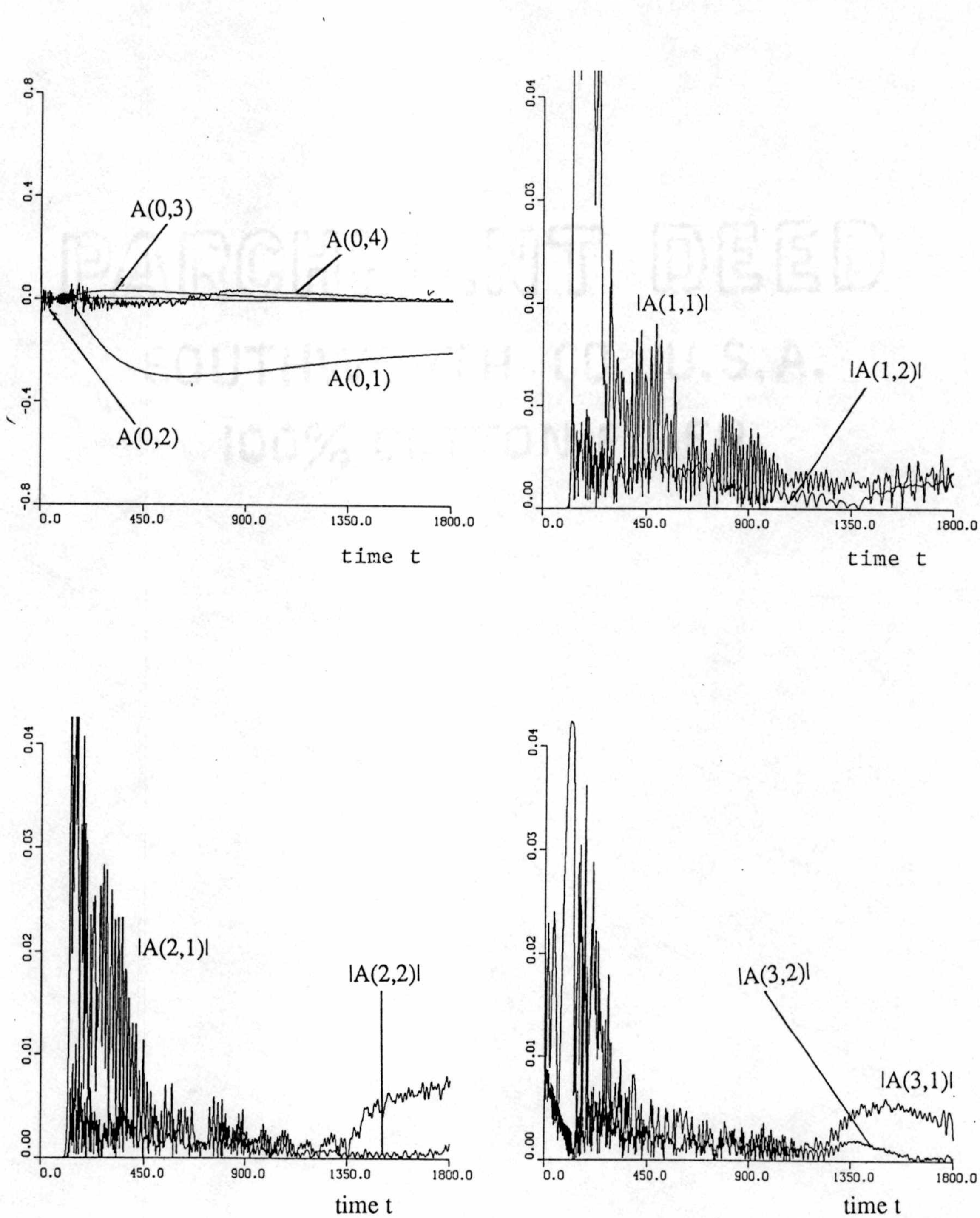

Fig. 4-24. The evolution of the wave components in the case D2

k=1,2,3, S=0.30, δ=0.001, γ=0.1

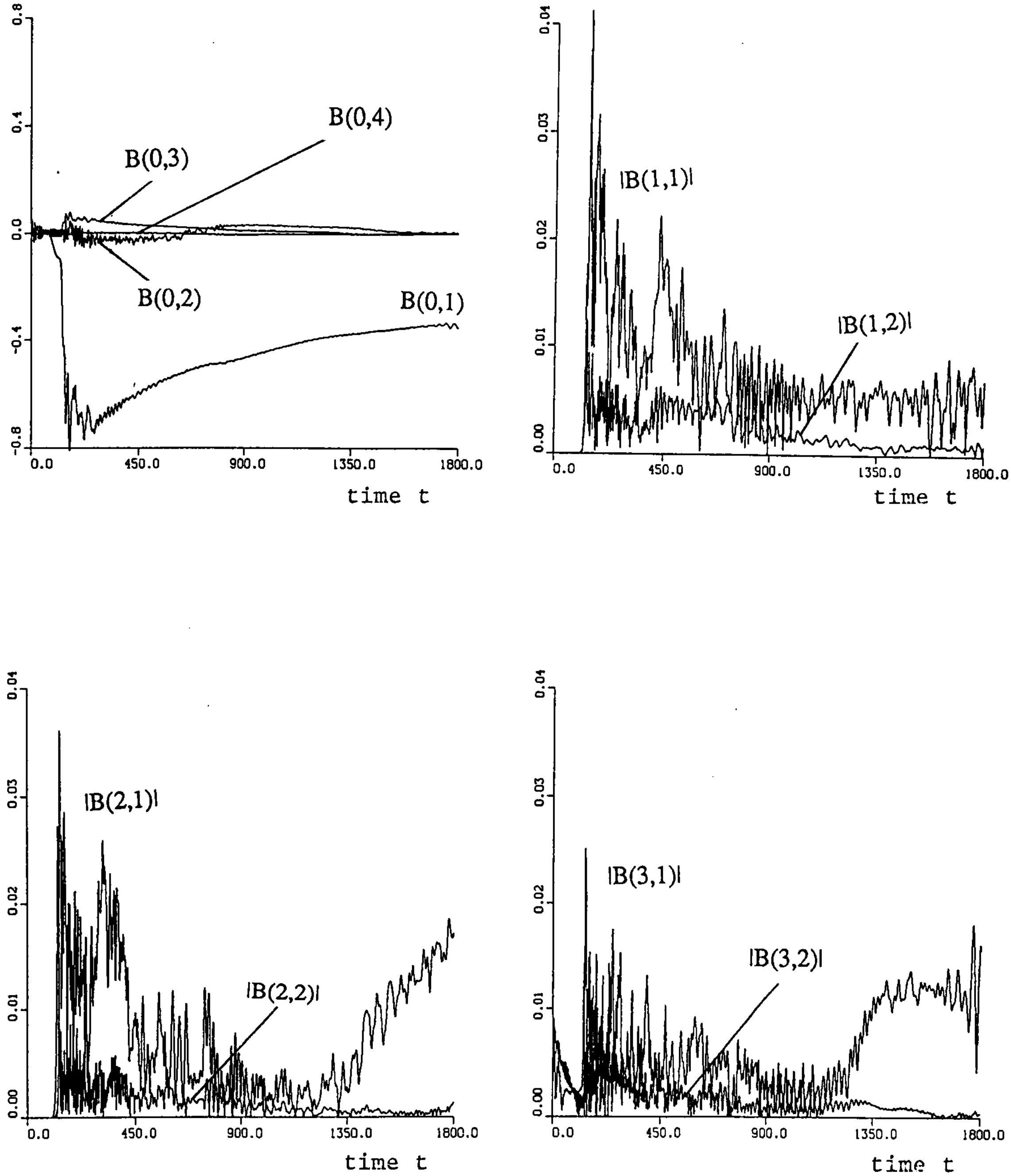

Fig. 4-24. Continue

k=1,2,3, S=0.30, δ=0.001, γ=0.1

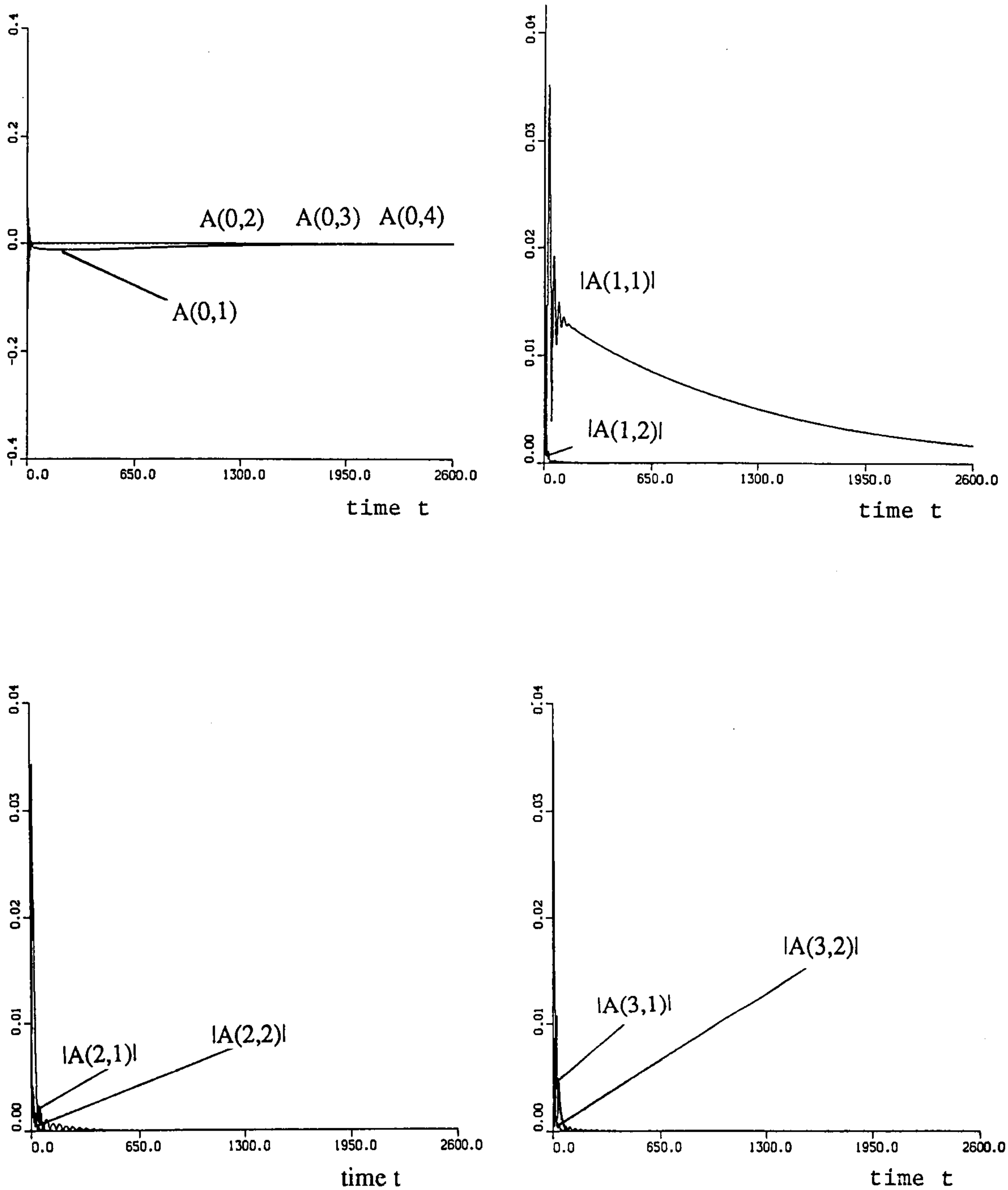

Fig. 4-25. The evolution of the wave components in the case E1

k=1,2,3, S=0.65, δ=0.01, γ=0.1

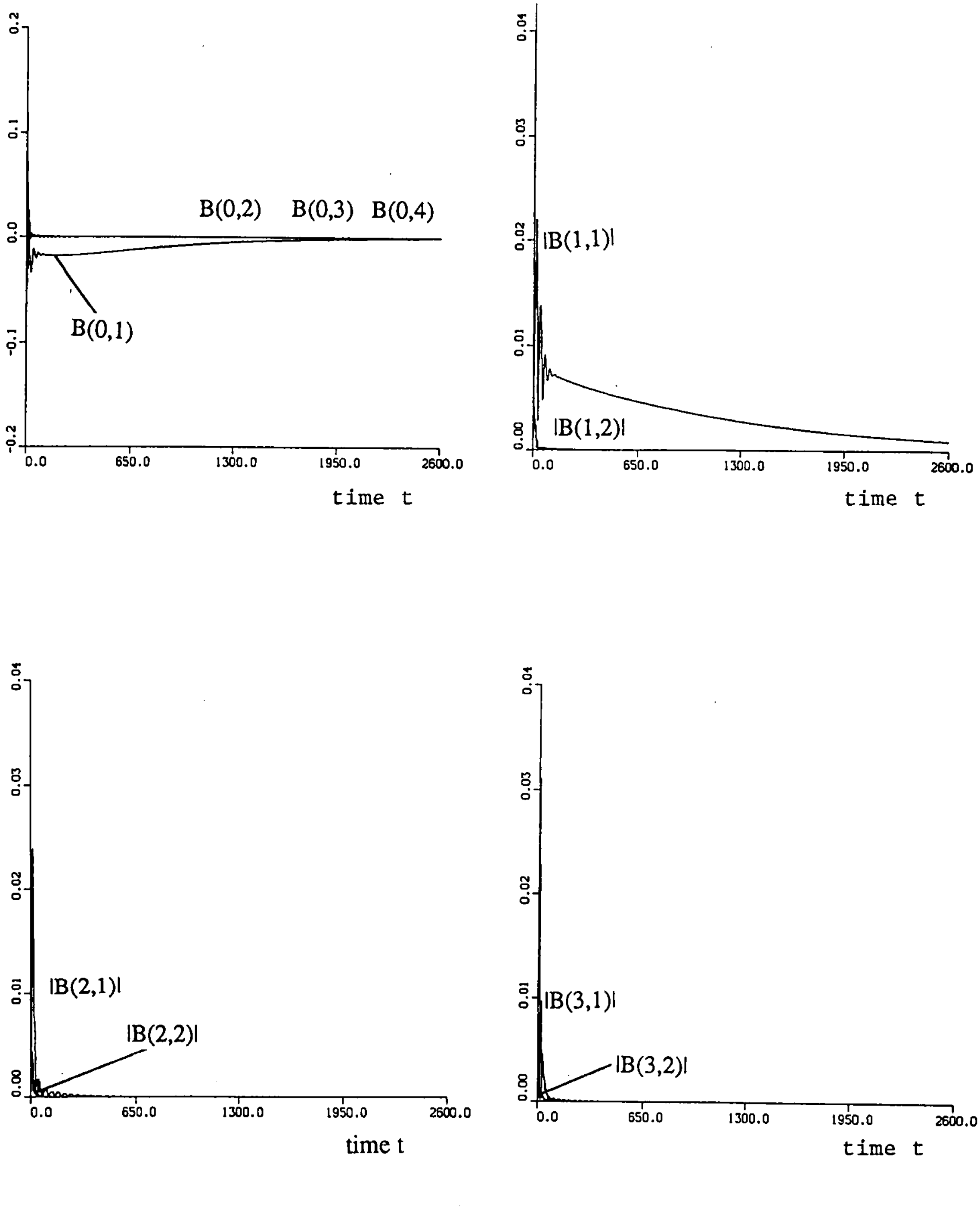

Fig. 4-25 continue

S=0.65, δ=0.01, γ=0.1

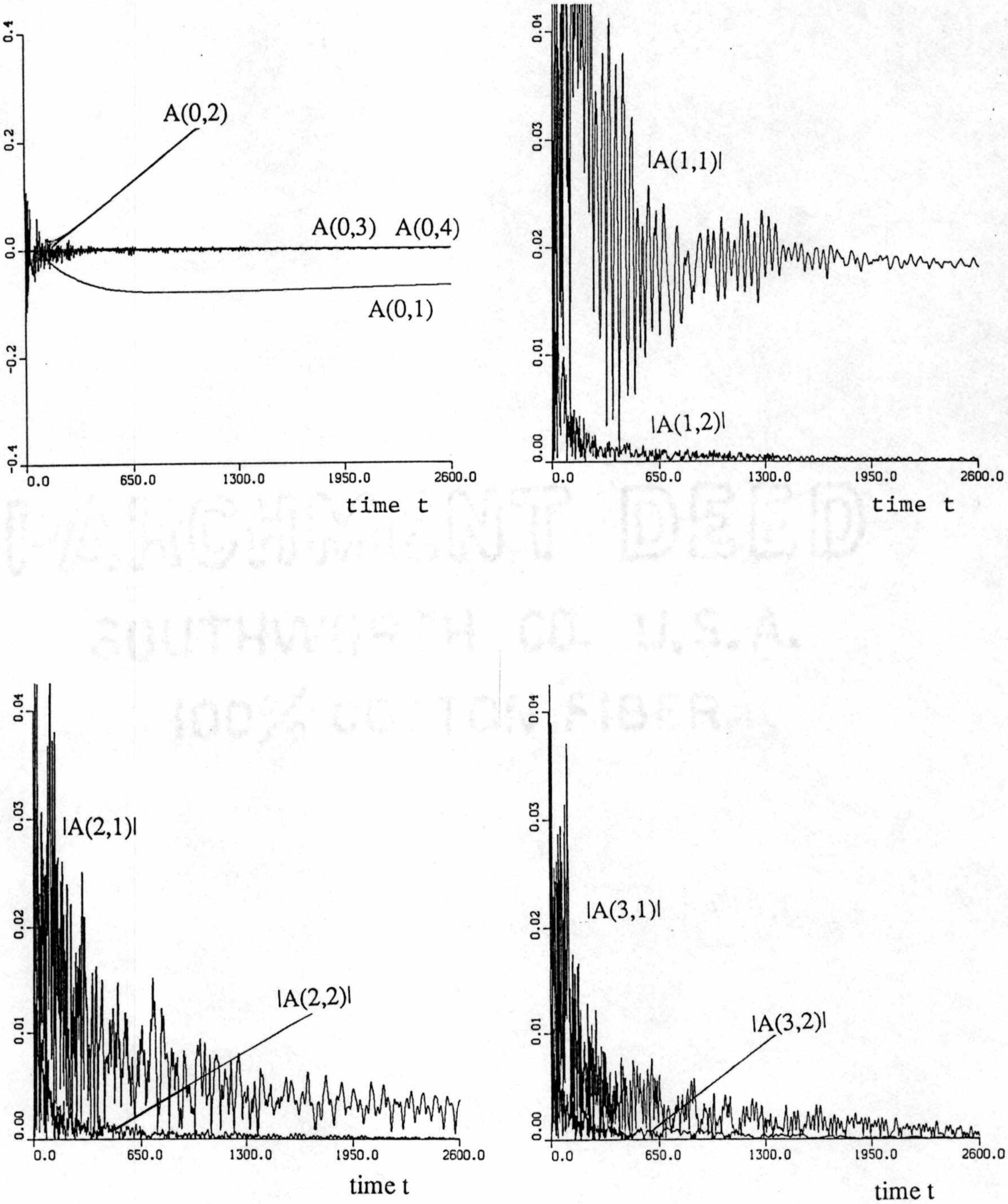

Fig. 4-26. The evolution of the wave components in the case E2

k=1,2,3, S=0.65, δ=0.001, γ=0.1

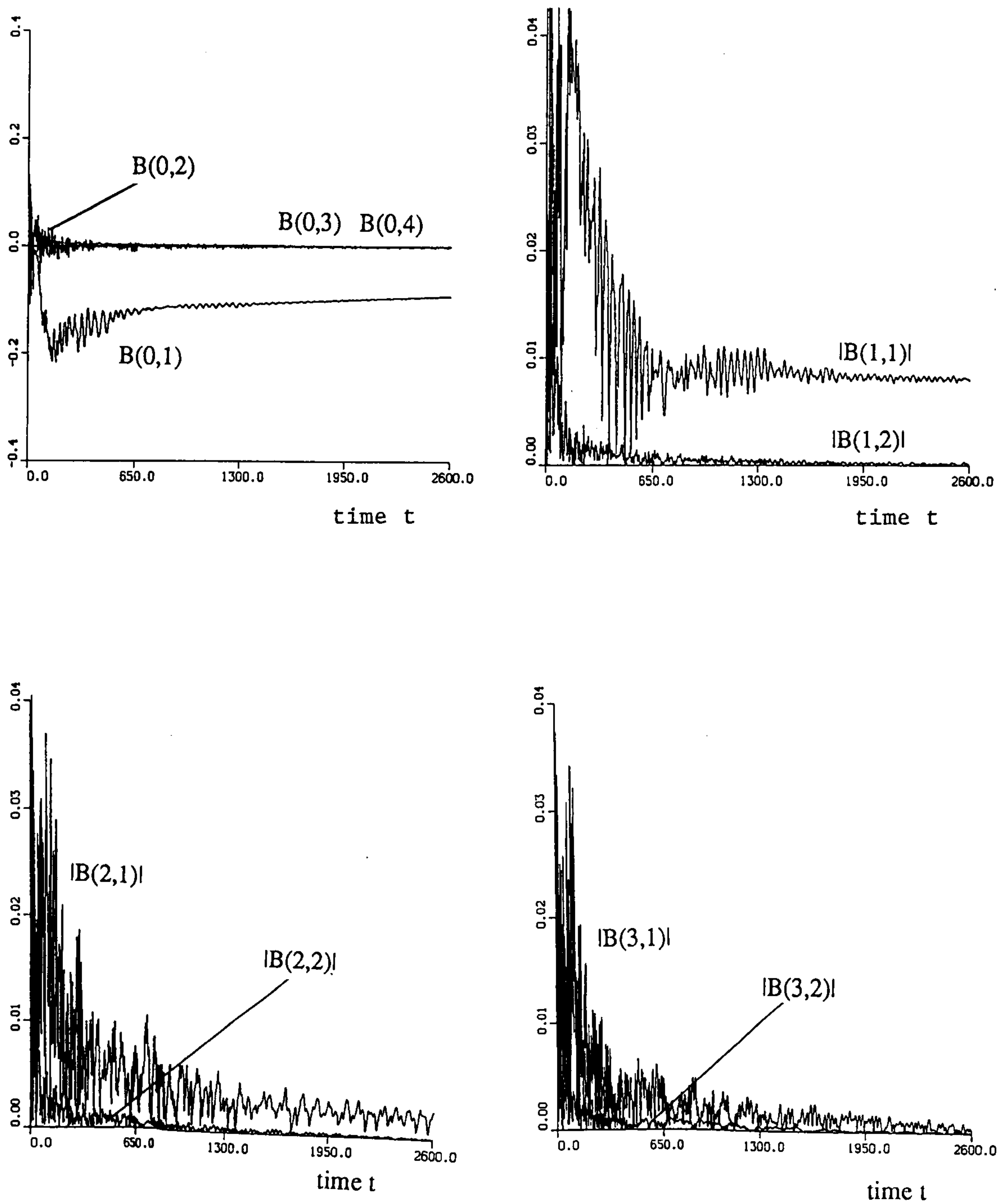

Fig. 4-26. Continue

S=0.65, δ=0.001, γ=0.1

final state. Thus, an axisymmetric flow prevails. In Figure 4-26, the amplitude of the mean flow correction has small nonzero value, and the components of wave number k=2 and 3 decays to zero with time but slower than that in Figure 4-25. The biggest difference between Figure 4-25 and Figure 4-26 is in the component of wavenumber k=1. In the case of Figure 4-26, the amplitude of wave number k=1 approachs a nonzero constant with time.

From the time history, we find that the case in Figure 4-25 damps faster than in Figure 4-26. Comparing Figures 4-25, 4-26 with Figures 4-17, 4-18, we conclude that the larger dissipation seems to damp the disturbance more effectively than the larger stratification does.

CHAPTER V

CONCLUSIONS AND RECOMMENDATIONS

The following conclusions are drawn from the present study.

1. From the linear analysis of the instability:

A. We get the neutral instability curve, it shows the flow regime can be separated into upper stable, lower stable and unstable regime for different S and δ. Only when $\delta < \delta_{cmax}$, there are two critical values of S which correspond to two points on the upper and lower marginal curves, respectively. When $\delta > \delta_{cmax}$, the flow is stable.

B. The Ekman layer asymmetry has a destability effect.

C. For a fixed S, as the Ekman dissipation, δ, changes, the most unstable wave number does not change too much. The Ekman dissipation does not affect the wave selection, but it does affect the growth rates of all the unstable modes.

D. The most unstable wavenumber becomes higher and higher as the stratification parameter, S, decrease.

2. From the inviscid analysis:

A series of numerical experiments for different initial perturbations have been performed. We considered basic zonal flows which are strongly unstable, and found that for different initial disturbance, the wave goes through an amplitude vacillation cycle for different time length, and finally, they develop into irregular motion. We strongly feel this irregularity is the result of numerical break down.

3. From the nonlinear baroclinic wave analysis with viscous effect:

A. Different flow regimes are obtained from this model and based on the series A of numerical experiments, the existence of various flows observed in the annulus experiments may basically depend on whether or not an equilibrium state, or a periodic equilibrium state can be reached when the external parameters are changed. There are three important external parameters: the energy source (ΔT), the energy sink (ν) and the effect of the rotation (Ω), which are expressed in terms of two parameters in the present model, they are S and δ. In the unstable region, the nonlinear interaction between the baroclinic and barotropic patterns of the sinπy-mode and the mean flow results in equilibrium of the flow field, and a steady wave state is observed when the supercriticality is high enough so as to endow the baroclinic and the barotropic patters of the sinπy-mode with different time behavior, but still not high enough to sustain the sin2πy-mode. The nonlinearity results in a periodic or quasi-periodic variation of these two patterns, and amplitude vacillation is observed.

B. Numerical experiment series B shows, for certain parameter setting (case B0), the solution of single wave number (k=3) is similar to that of multi-wave number (k=1,2,3); but not for all parameter settings. For case B1 and B2, the solution of single wave number (k=3 for case A1, k=4 for case A2) is different from that of multi-wave number (k=1,2,3, for case B1, k=1,2,3,4, for case B2) situation. It shows that it is necessary to study and develop the model with several wave number components.

C. Zonal wavenumber transition are found in the numerical experiment series C and D. When we change S from high to low, the dominant wavenumber changes. That means the imposed radial temperature difference decreases if the rotation rate is kept constant, wavenumber transition occurs. Comparing numerical experiment series C and D, we found that the initial disturbance does not influence the dominant wavenumber for a given flow parameter setting, but the characteristics of the flow plays an important role.

D. Meridional mode number transition is displayed in Figures 4-17,4-18,4-19, 4-20 and 4-21. It shows that, for lower supercriticality, the meridional mode number 1 with the sinπy structure is most unstable. The second y-mode with the sin2πy structure becomes unstable when the supercriticality is increased beyond a certain value.

E. From numerical experiment series E for different dissipation δ, we found that the higher dissipation damps faster than lower dissipation; and the large dissipation seems to damp the disturbance more effectively than the large stratification does.

Finally, it should be noted that the wavenumber transition is a primary problem. In here, we obtain some preliminary results. For a deeper understanding and clear interpretation for this phenomena, further work need to be done. A lot of cases need to be run to determine the boundary between different regimes. However,the numerical model constructed in this work appears to be adequate to answer these questions.

BIBLIOGRAPHY

BIBLIOGRAPHY

1. Fultz, D., "A Survey of certain thermally and mechanically driven fluid systems of mrteorological interest." Fluid models in geophysics, Proc. 1st Symposium on the Use of Models in Geophysical Fluid Dynamics, Baltimore, Maryland, 27-63, 1953.

2. Fultz, D., Long, R. R., Owens, G. V., Bohan, W., Kaylor, R. and Weil, J. "Studies of Thermal Convection in a rotating Cylinder with Some Implications for Large-Scale Atmospheric motions." Meteor. Monogr., 4, No. 21, Boston, Mass., Amer. Meteor. Soc., 104pp, 1959.

3. Hide, R., "Some Experiments on Thermal Convection in a Rotating Liquid." Quart. J. R. meteor. Soc., 79, 161, 1953.

4. Hide, R., "An Experimental Study of Thermal Convection in a Rotating Liquid." Phil. Trans. A, 250, 441-478, 1958.

5. Hide, R.,"Experiments on baroclinic instability and "vacillation"." Trans. Amer. Geophys. Union, 45,1,142-143, 1964

6. Pfeffer, R. L. and Chiang, Y., "Two Kind of Vacillations in Rotating Laboratory Experiments," Mon. Wea. Rev., 95, 75-82, 1967.

7. Hart, J. E., "Finite Amplitude Baroclinic Instability," Ann Rev. Fluid Mech., 11, 147-172, 1979.

8. Boville, B. A., "Strongly Nonlinear Vacillation in Baroclinic Waves," J. Atmos. Sci., 39, 1227-1240, 1982.

9. Koschmieder, E. L. and White, H. D., "Convection in a Rotating, Laterally Heated Annulus," Geophys. Astrophys. Fluid Dynamics, Vol. 18, 279-299, 1981.

10. Pfeffer, R. L., Buzyna, G. and Kung, R., "Time-dependent Modes of Behavior of Thermally Driven Rotating Fluids," J. Atmos. Sci., 37, 2129-2149, 1980.

11. Barcilon, V., "Role of the Ekman Layers in the Stability of the Symmetric Regime Obtained in a Rotating Annulus," J. Atmos. Sci., 21, 291-299, 1964.

12. Webster, P. J. and Keller, J. L., "Atmospheric Variations: Vacillation and Index Cycles," J. Atmos. Sci., 32, 1283-1300, 1975.

13. Van Loon, H., Madden, R. A. and Jenne, R. L., "Oscillation in the Winter Stratosphere: Part I. Description," Mon. Wea. Rev., 103, 154-162, 1975.

14. Charney, J. G., "The Dynamics of Long Waves in a Baroclinic Westerly Current," J. Meteor., 4, 135-162, 1947.

15. Eady, E. T.,"Long Waves and Cyclone Waves," Tellus, 1, 33-52, 1949.

16. Antar, B. N., Fowlis, W.W.,"Eiganvalue of a Baroclinic Stability Problem with Ekman Damping," J. Atmos. Sci., 37, No.6, Tune 1980.

17. Phillips, N. A., "Energy Transformations and Meridional Circulations Associated with Simple Baroclinic Waves in a Two-level Quasi-geostrophic model," Tullus, 6, 273-286, 1954.

18. Stuart, J. T., "On the Nonlinear Mechanics of Wave Disturbances in Stable and Unstable Parallel Flows," I. J. Fluid Mech. 9, 353-370, 1960.

19. Watson, J., "On the Nonlinear Mechanics of Wave Disturbances in Stable and Unstable Parallel Flows," II. J. Fluid Mech. 9, 371-389, 1960.

20. Pedlosky, J., "Finite Amplitude Baroclinic Waves," J. Atmos. Sci., 27, 15-30, 1970.

21. Pedlosky, J., "Finite Amplitude Baroclinic Waves with Small Dissipation," J. Atmos. Sci., 28, 587-597, 1971.

22. Pedlosky, J., "Limit Cycles and Unstable Baroclinic Waves," J. Atmos. Sci., 29, 53-63, 1972.

23. Pedlosky, J., "The Effect of β on the Chaotic Behavior of Unstable Baroclinic Waves," J. Atmos. Sci., 38, 717-731, 1981.

24. Drazin, P. G., "Non-linear Baroclinic Instability of a Continuous Zonal Flow," Q. Hart. J. R. Met. Soc., 96, 667-676, 1970.

25. Drazin, P. G., "Non-linear Baroclinic Instability of a Continuous Zonal Flow of a Viscous Fluid," J. Fluid Mech., 55, 577-588, 1972.

26. Barcilon, A. And Drazin, P. G., "A Weakly Non-linear Theory of Amplitude Vacillation and Baroclinic Waves," J. Atoms. Sci., 41, 3314-3330,1984.

27. Chou, S. H. and Loesch, A. Z., "Supercritical Dynamics of Baroclinic Disturbances in a Free-Surface Model," J. Atmos. Sci., 43, 285-301, 1986.

28. Chou, S. H. and Loesch, A. Z., "Supercritical Dynamics of Baroclinic Disturbances in the Presence of Asymmetric Ekman Dissipation," J. Atmos. Sci., 43, 1781-1795, 1986.

29. Boville, B. A., "Amplitude Vacillation on an f-Plane," J. Atmos. Sci., 37, 1413-1423, 1980.

30. Boville, B. A., "Amplitude Vacillation on an β-Plane," J. Atmos. Sci., 38, 609-618, 1981.

31. Boville, B. A., "Strongly Nonlinear Vacillation in Baroclinic Waves," J. Atmos. Sci., 39, 1227-1240, 1982.

32. Weng, H., "Strongly Nonlinear Dynamics of Baroclinic Waves," Ph.D. Dissertation, Florida State University, 1984.

33. Pedlosky, J. Geophysical Fluid Dynamics, New York: Springer Verlag, 1979.

34. Lorenz, E. N., "The Nature and Theory of the General Circulation of the Atmosphere," World Meteorological Organization, 1967.

35. Hess, S. L. Introduction to Theoretical Meteorology, New York: Henry Hort and Company, 1959.

36. Gill, Adrian E., Atmosphere-Ocean Dynamics, New York: Academic Press, 1982.

37. Holton, J. R., An Introduction to Dynamic Meteorology, New York: Academic Press, 1979.

38. Moroz, I. M., Brindley, J., "Evolution of Baroclinic Wave Packets in a Flow with Continuous Shear and Stratification," Pro. R. Soc. London, A 377, 379-404, 1981.

39. Gottlieb, D., Orszag, S. A., "Numerical Analysis of Spectral Methods: Theory and Applications," Society for Industrial and Applied Mathematics, 1977.

40. Pickering,M., "An Introduction to Fast Fourier Transform Methods for Partial Differential Equations,with Application ",Research Studies Press.

41. Burrus.C.S, Parks.T.W., "DFT/FFT and Convolution Algorithms"

42. Lance, G. N., Numerical Methods for High Speed Computers, W. & J. Mackay & Co. Ltd. Fair Row, Chatham, Kent, PP. 56-57, 1960.

43. Fox, L. "Numerical Solution of Ordinary and Partial Differential Equations," London Pergamon Press, pp. 24-25, 1962

44. Christiunsen, J., "Numerical Solution of Ordinary Simultaneous Differential Equations of the 1st Order Using a Method for Automatic Step Change," Numerical Math. 14, 317-324, 1970.

45. Pfeffer, R. L., Buzyna, G. and kung, R., "Relationships among Eddy Fluxes of Heat, Eddy Temperature Variances and Basic State Temperatures in a Thermally Driven Rotating Fluid." J. Atmos. Sci.,37, 2577-2599, 1980.

46. Hide, R., " Fluid Motions in the earth's Core and Some Experiments on Thermal Convection in a Rotating Liquid. Fluid Models in Geophysics," Q. J. R. Meteor. Soc., 19, 161, 1953.

47. Haltiner, G. J., Numerical Weather Prediction, New York: John Wiley and Sons, 1971.

48. Staniforth, A. N. and Daley, R. D., " A Baroclinic Finite Element Model for Regional Forecasting with the Primitive Equations," Mon. Wea. Rev., 107, 107-121, 1979.

49. Aksel, M. H., MacPherson, A. K. and Hilton, P. D., " A Finite Element Study of Frontogenesis," Mon. Wea. Rev., 112, 1053-1066, 1984.

50. Kuiper, G. P., The Earth as a Planet. The University of Chicago Press, 1954.

51. Panchev, S., Dynamic Meteorology. Holland: D. Reidel Pablishing Company, 1985.

APPENDICES

APPENDIX A

MERSON SCHEME

As an improved vision of the classic Runge-Kutta method, Merson scheme uses almost the same idea as Runge-Kutta. Runge-Kutta Method has proved most useful for the solution of ordinary differential equations using high-speed equipment. The process is such that, for initial value problem

$$\frac{dy}{dx} = f(x) \tag{A-1}$$

it is possible to obtain the value of y(x+h) from the knowledge of y(x) and step length h only. Thus, it is obvious that, for the solution of an initial value problem, no special procedure is required to start the integration.

Basically, using Runge-Kutta method, it is extremely easy to program a change of interval size, whereas it is fairly difficult to decrease the step length. Sometimes, it is difficult to make practical use of Runge-Kutta scheme to determine the size of the integration interval which ought to be used to give the required accuracy. An efficient technique was proposed by Merson, which gives an automatic and rapid determination of the interval with a predetermined accuracy.

Basically the Merson scheme is a slight modification of the Range-Kutta scheme as mentioned above. The formulae are

$$y_{n+1} = y_n + \frac{1}{2}(k_1 + 4k_4 + k_5) + o(h^5) \tag{A-2}$$

where

$$k_1 = \frac{1}{3}hf(x_n, y_n)$$

$$k_2 = \frac{1}{3}hf(x_n + \frac{1}{3}h, y_n + k_1)$$

$$k_3 = \frac{1}{3}hf(x_n + \frac{1}{3}h, y_n + \frac{1}{2}k_1 + \frac{1}{2}k_2)$$

$$k_4 = \frac{1}{3}hf(x_n + \frac{1}{2}h, y_n + \frac{3}{8}k_1 + \frac{9}{8}k_3)$$

$$k_5 = \frac{1}{3}hf(x_n + h, y_n + \frac{3}{2}k_1 - \frac{9}{2}k_3 + 6k_3)$$

The advantage of this method is that an estimate of the truncation error, ϵ, is given by

$$5\epsilon = k_1 - \frac{9}{2}k_3 + 4k_4 - \frac{1}{2}k_5 \qquad (A-3)$$

The interval changing criterion is the following:

If the right hand side of (A-3) is greater than five times the preassigned accuracy, the interval h is halved and the computation for the step is begun again.

If the right hand side of (A-3) is less than $\frac{5}{32}$ of the preassigned accuracy, the interval h may be doubled and the calculation for the step is repeated.

Otherwise, the calculation is proceeded to next time step.

At first sight, it might appear to be slower than the Runge-Kutta methods but since, to be on the safe side, the interval length is usually underestimated when it is fixed throughout the calculation, this flowing down is only apparent. In fact, the Merson process is 20 per cent faster than the standard fixed interval procedure.

APPENDIX B

COEFFICIENTS

The coefficients used in Equation (4.1) are listed below:

$\alpha_1 = k(1 - \mu_{k,l} th\mu_{k,l})/2\mu_{k,l}$

$\alpha_2 = -\delta\mu_{k,l}(r_+ - r_-)/S$

$\alpha_3 = k(1 - \mu_{k,l} cth\mu_{k,l})/2\mu_{k,l}$

$\alpha_4 = \delta(r_+ + r_-)\mu_{k,l} th\mu_{k,l}/S$

$\alpha_5 = -\delta\mu_{k,l}(r_+ - r_-)/S = \alpha_2$

$\alpha_6 = k(1 - \mu_{k,l} th\mu_{k,l})/2\mu_{k,l}$

VITA

Yan-Ming Zheng was born on December 5, 1962, in Beijing, People's Republic of China. She attended elementary and high school in Beijing. She entered the Beijing Institute of Aeronautics and Astronautics(BIAA)* in September 1980, majoring in Aerospace Engineering with emphasize on aerodynamics. She received her Bachelor degree in 1984 and Master degree in 1986, respectively.

She entered the UTSI as a graduate student and Research Assistant in January, 1987. In August 1990, she completed her studies with the Doctor of Philosophy degree in Aerospace Engineering.

Ms. Zheng is married to J. D. Mo of Hunan Province of China on November 4, 1985 in Beijing. They have one son: Jack P. Mo, who is sixteen month old.

* Since 1988, the Institute has formally changed its name as The Beijing University of Aeronautics and Astronautics.